

---

Masters Theses

Student Theses and Dissertations

---

Spring 1995

## Effects of specimen size reduction on the transition curve of the Charpy V-notch impact test

Lonnie Eugene Schubert

Follow this and additional works at: [https://scholarsmine.mst.edu/masters\\_theses](https://scholarsmine.mst.edu/masters_theses)

 Part of the [Nuclear Engineering Commons](#)

Department:

---

### Recommended Citation

Schubert, Lonnie Eugene, "Effects of specimen size reduction on the transition curve of the Charpy V-notch impact test" (1995). *Masters Theses*. 1464.  
[https://scholarsmine.mst.edu/masters\\_theses/1464](https://scholarsmine.mst.edu/masters_theses/1464)

This thesis is brought to you by Scholars' Mine, a service of the Curtis Laws Wilson Library at Missouri University of Science and Technology. This work is protected by U. S. Copyright Law. Unauthorized use including reproduction for redistribution requires the permission of the copyright holder. For more information, please contact [scholarsmine@mst.edu](mailto:scholarsmine@mst.edu).

THESIS  
T6960

**EFFECTS OF SPECIMEN SIZE REDUCTION ON  
THE TRANSITION CURVE OF THE  
CHARPY V-NOTCH IMPACT TEST**

by

LONNIE EUGENE SCHUBERT, 1964-

A THESIS

Presented to the Faculty of the Graduate School of the  
UNIVERSITY OF MISSOURI-ROLLA


In Partial Fulfillment of the Requirements for the Degree

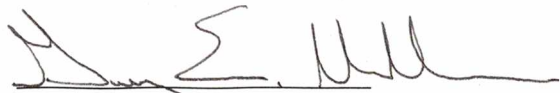
MASTER OF SCIENCE IN NUCLEAR ENGINEERING

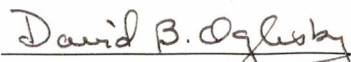
1995

Approved by

T6960  
125 pages

  
Arvind S. Kumar, Advisor

  
Gary E. Mueller

  
David B. Oglesby



8-31-91  
ah

This study continues work begun with Sandia National Laboratories, Battelle Pacific Northwest Laboratory, and the University of Missouri at Rolla, sponsored by the U.S. Department of Energy and in cooperation with the Associated Western Universities.

By acceptance of this article, the publisher and/or recipient acknowledges the U.S. Government's right to retain a non-exclusive, royalty-free license to any copyright covering this paper. This research was supported by the Associated Western Universities, Inc., Northwest Division under Grant DE-FG06-89ER-75522 with the U.S. Department of Energy.

The work was substantially supported by a contract from Sandia National Laboratories (Contract number: 18-0559).

## ABSTRACT

This study was undertaken to correlate the impact properties of ASTM standard full size Charpy V-notch impact specimens to the impact properties of subsize specimens. An ASTM A533-B quenched and tempered plate steel was examined. The fine grained martensitic material had a coarse prior austenite grain size, which resulted in a low upper shelf energy for this material. Three sizes of specimens were included. Specimens were irradiated in the TRIGA Reactor Facility operated by the U. S. Geological Survey in Denver, Colorado, to  $1 \times 10^{19}$  n/cm<sup>2</sup> ( $E > 1$  MeV) at 150°C (302°F). Unirradiated and irradiated specimens were tested at several temperatures in an instrumented drop tower, and the load during impact was recorded as a function of time. Full transition curves of energy versus temperature were determined for the three sizes. The results are presented and compared. A method for correlating the upper shelf energies determined from subsize and full size specimens was developed. The method incorporated a normalizing factor proposed in earlier related studies, and the method is discussed in light of the new data. The estimates of upper shelf energy derived from the correlation agreed with the measured full size values within 10%. The correlation was found to be applicable to the subsize specimen data. The irradiation induced shift in the ductile to brittle transition temperature of the material was found to be independent of specimen size.

## ACKNOWLEDGEMENT

The author would like to specially thank the following people for their assistance, encouragement, support, and patience:

First, my family, especially my wife and daughters. This would not have happened without them.

My adviser, Dr. Arvind Kumar, who provided me with the many opportunities that have culminated in this thesis. Many of these opportunities have lead to new friendships and together have made this arduous task a good one. His out of the limelight efforts did not go unnoticed and are still appreciated. He is responsible for much of what I have learned. Also Dr. Mueller and Dr. Oglesby, who contributed significantly, and also had to endure me.

Dr. Frank Garner, who made himself a friend from our first meeting. His assistance was beyond the technical and will not be forgotten. I thank you, sir.

Scott Cannon, who contributed greatly to this work. He provided me with the base on which to build and the skills and knowledge to accomplish this work.

David Criswell, Elaine Dieffenbacher, Ruby Ermi, and John Keaveney, each assisted immeasurably, particularly with the small details and the day-to-day work.

The staff at the university, particularly Paula Cochran, who tirelessly worked on my behalf as well as on behalf of the many other graduate students at UMR. Also the staff at PNL and AWU who made my work possible.

Dr. Danny Edwards, David Reinhart, Scott Sidener, and Mychailo Toloczko; friends whose value could not be estimated.

Finally, Peggy Hamilton. I could not begin to express my appreciation. A superlative boss, she listened and treated me with respect, was ever ready with helpful suggestions, and, despite her adamant protestations, a part-time surrogate mother. Also, she is a friend.

## TABLE OF CONTENTS

	Page
ABSTRACT .....	iii
ACKNOWLEDGEMENT .....	iv
LIST OF ILLUSTRATIONS .....	vii
LIST OF TABLES .....	ix
LIST OF ABBREVIATIONS .....	x
GLOSSARY .....	xi
I. INTRODUCTION .....	1
II. BACKGROUND OF NOTCHED-BAR IMPACT TESTING .....	6
III. LITERATURE REVIEW .....	9
A. SUBSIZE EXPERIENCE AND CORRELATION EFFORTS .....	9
B. ANALYSIS TECHNIQUES IN INSTRUMENTED CHARPY IM- PACT TESTING .....	19
C. GENERAL ASPECTS OF DATA ACQUISITION AND EVALUA- TION .....	24
IV. EXPERIMENTAL PROCEDURES .....	28
A. MATERIAL .....	28
B. TEST SPECIMENS .....	28
C. TEST EQUIPMENT .....	30
D. TEMPERATURE CONTROL .....	32
V. DATA REDUCTION .....	35
A. CALCULATION OF THE TRUE ENERGY FROM THE APPAR- ENT ENERGY .....	35
B. CURVE FITTING .....	36
C. NORMALIZATION FACTOR .....	37

VI. RESULTS .....	39
VII. DISCUSSION .....	46
VIII. CONCLUSIONS .....	54
APPENDICES	
A. DETAILED PROCEDURE FOR CONDUCTING CVN TESTS WITH THE DROP TOWER .....	55
B. BASIC PROGRAM FOR AUTOMATED CVN TESTING .....	78
C. TEMPERATURE CALIBRATION CHARTS .....	97
D. CURVE FIT STATISTICS .....	104
BIBLIOGRAPHY .....	108
VITA .....	113

## LIST OF ILLUSTRATIONS

Figures	Page
Figure 1. Upper curve represents the temperature dependence of the material yield strength. Lower curve is typical of a series of CVN tests for a steel alloy of moderate toughness. . . . .	2
Figure 2. Portion of a measured load trace. $P_{gy}$ would be chosen as indicated, or perhaps at a slightly higher load. . . . .	11
Figure 3. Generalized relationship between $P_{max}$ , $P_{gy}$ , and the CVN curve. Specimens break before general yield is reached for temperatures below $P_{gy} = P_{max}$ . . . . .	15
Figure 4. Schematic depicting $h$ for a fully ductile specimen which did not break into separate pieces. . . . .	22
Figure 5a. Specimen dimensions in millimeters. . . . .	29
Figure 5b. Dimension Nomenclature. . . . .	29
Figure 6. Schematic of anvil configuration with standard and subsize specimens. . . . .	30
Figure 7. Approximate thermocouple (TC) configuration for the temperature calibration specimens. Full and half size were the same. Third size had only 2. . . . .	33
Figure 8. Comparison of the data of full size, unirradiated and irradiated specimens and the respective best fit curves showing the effect of irradiation. . .	47
Figure 9. Comparison of the data of half size, unirradiated and irradiated specimens and the respective best fit curves showing the effect of irradiation. . .	48
Figure 10. Comparison of the data of third size, unirradiated and irradiated specimens and the respective best fit curves showing the effect of irradiation. . . . .	48

Figure 11. Measured full size specimen data versus normalized half size specimen data. . . . .	53
Figure 12. Measured full size specimen data versus normalized third size specimen data. . . . .	53

## LIST OF TABLES

Tables	Page
Table I Composition by weight percent of the A533-B steel of this study. . . . .	28
Table II Test data for full size, unirradiated specimens.	
(Striker mass 15.35 kg) . . . . .	39
Table III Test data for half size, unirradiated specimens.	
(Striker mass 14.73 kg) . . . . .	40
Table IV Test data for third size, unirradiated specimens.	
(Striker mass 14.73 kg) . . . . .	41
Table V Test data for full size, irradiated specimens.	
(Striker mass 15.35 kg) . . . . .	42
Table VI Test data for half size, irradiated specimens.	
(Striker mass 14.73 kg) . . . . .	42
Table VII Test data for third size, irradiated specimens.	
(Striker mass 14.73 kg) . . . . .	43
Table VIII Upper shelf energy values. . . . .	44
Table IX Ductile to brittle transition temperatures. . . . .	44
Table X Specimen parameters for calculation of the normalization factor. . . . .	50
Table XI Comparison of the normalized USE values. . . . .	50
Table XII Comparison of USE estimate from subsize USE. . . . .	51
Table XIII Predicted USE values obtained from the best fit curves fit to the normalized subsize data. . . . .	52
Table XIV Predicted DBTT values obtained from the best fit curves fit to the normalized subsize data. . . . .	52



## LIST OF ABBREVIATIONS

- a: . . . . . Crack length
- ASTM: . . American Society for Testing and Materials
- b: . . . . . Ligament, length of remaining material under a notch or precrack in a specimen
- B: . . . . . Thickness of a specimen
- COD: . . Crack Opening Displacement
- CVN: . . Charpy V-Notch impact test
- DBTT: . . Ductile to Brittle Transition Temperature
- $E_a$ : . . . . . Apparent absorbed energy
- $E_d$ : . . . . . Actual absorbed energy ("pendulum Dial" energy)
- $E_o$ : . . . . . Kinetic energy
- EPFM: . . Elastic-Plastic Fracture Mechanics
- FATT: . . Fracture Appearance Transition Temperature
- $K_I$ : . . . . . Mode I applied stress intensity factor
- $K_{Ic}$ : . . . . . Mode I plane strain fracture toughness
- $K_t$ : . . . . . Stress concentration factor, a unitless, geometric parameter or multiplier
- $K_{\sigma(p)}$ : . . Plastic stress concentration factor (also Q)
- L: . . . . . Unsupported span of a specimen
- LEFM: . . Linear Elastic Fracture Mechanics
- $P_{gy}$ : . . . . . Load at general yielding
- $P_{max}$ : . . . . . Maximum load recorded
- PWR: . . Pressurized Water Reactor
- RPV: . . Nuclear Reactor Pressure Vessel
- W: . . . . . Width of a specimen
- USE: . . Upper Shelf Energy
- $\sigma_f^*$ : . . . . . Critical fracture stress for cleavage, or microcleavage fracture stress
- $\sigma_y$ : . . . . . Uniaxial tension yield strength
- $\sigma_{yd}$ : . . . . . Dynamic yield strength

## GLOSSARY

Ductile to brittle transition temperature (DBTT): A general term indicating a temperature at which the fracture mode of an alloy changes from ductile (high energy) to brittle (low energy). Typically it is designated in a manner which indicates a prescribed definition. Such as: 41 J—The temperature required to obtain a fracture energy of 41 J. In the text DBTT refers to the midpoint of the best fit hyperbolic-tangent curve, unless otherwise indicated.

Elastic/perfectly-plastic material: Idealized material which does not allow stress to exceed  $\sigma_y$  and does not strain harden.

Ligament ( $b$ ): (or Remaining Ligament) The dimension measured from the notch root or the crack tip to the back edge of the specimen. ( $W - a$ .)

Plane strain: The condition at a stress intensifier when strain is limited to two dimensions. Namely, strain parallel to the crack front approaches zero. A triaxial state of stress exists.

Plane stress: The condition at a stress intensifier when stress is limited to two dimensions, as in a thin sheet under tension. Stress parallel to the crack front (perpendicular to the sheet) approaches zero.

Span ( $L$ ): The unsupported length of a specimen. In the Charpy test, the gap distance between the support anvils.

Thickness ( $B$ ): The dimension of the specimen measured along the notch or crack.

Upper shelf energy (USE): The maximum energy achieved in a standard Charpy V-notch impact test series. Either the average of the test data in which the fracture appearance indicated >95% ductile shear, or the maximum value of the best fit hyperbolic-tangent curve.

Width ( $W$ ): The dimension of the specimen measured in line with the propagation path of the crack. Sometimes referred to as depth.

**Yield Strength ( $\sigma_y$ ):** The stress at which a specimen begins to deform plastically. Typically determined with a smooth cross section test specimen in uniaxial tension and quasi-static strain rates. Yield strength is a temperature and strain rate dependant material property.

**Dynamic Yield Strength ( $\sigma_{yd}$ ):** The yield strength determined at high strain rates.

**Cleavage Fracture Strength ( $\sigma_f^*$ ):** The stress at which brittle fracture initiates in a material.

It is assumed to be more or less temperature and strain rate independent. A crack propagates in a brittle manner if this stress is reached at the crack tip. Plastic deformation and/or ductile rupture may precede brittle fracture and will even prevent mean cross section stresses from reaching this level in a ductile material. The term, "cohesive strength" is often used for  $\sigma_f^*$ .

## I. INTRODUCTION

The strength and ductility of materials are dependent on temperature. Materials with body centered cubic (bcc) crystal structures, such as structural steels, undergo a transition from a mode of fracture typified by high ductility, relatively high fracture energy, and extensive plastic deformation; to a mode typified by minimal ductility, low fracture energy, and negligible deformation. The transition takes place over a temperature range that is typically well below the potential service temperatures of the material, and the transition results from the absence of close-packed planes in the bcc structure as well as the fact that the yield strength is temperature dependent while the cleavage fracture strength is essentially temperature independent. Several factors affect the characteristics of this ductile to brittle transition. The alloy, microstructure, and non-metallic inclusions are a few of the factors which affect the material response. The type of test also affects the observed test results, with the dimensions of the testing fixture as well as the dimensions of the test specimen being significant.

Brittle fracture was not always a pressing concern. Before steel construction techniques incorporated extensive welding, propagating fractures would arrest at the discontinuous component joints, and damage was limited. When components are welded, however, the structure becomes a continuous unit; a fracture can propagate unimpeded, and if the material is embrittled the structure can break in two. Such was the case with numerous bridges, storage tanks, tankers, and armor of the World War II era. When sufficient loads combined with a sufficiently low temperature, the result was sudden, catastrophic failure. Investigators initially suspected the welds but determined that the cleanliness and the microstructure were the dominant factors controlling the transition behavior in both the welds and the structural components. Data from notched bar impact tests exhibited this same type of behavior, that is, a transition from ductile to brittle failure, and the Charpy V-notch (CVN) impact test has become accepted as a rapid and inexpensive evaluation technique for structural steels. The test consists of impacting (breaking) a notched bar with a square cross section and measuring the energy absorbed by deformation and fracture. Other measurements of a given specimen are the lateral expansion of the specimen opposite the notch at the impact load point and the percentage of ductile shear failure determined from the fracture surface.

The top curve in figure 1 is typical of the relationship between the yield strength and temperature; the bottom curve shows a representative CVN transition curve, which is an indicator

of the relationship between ductility and temperature. When plotting a given CVN test result, the test temperature corresponds to the abscissa, and energy, typically, corresponds to the ordinate. An S-shaped curve is derived from the data of several impact tests conducted over a range of temperatures. CVN

curves developed for different materials can be utilized to evaluate the relative fracture resistance of the materials. The upper region, which flattens into a "shelf," and the upward sloping portion of the transition region of typical CVN curves are of particular interest. The upper shelf is defined as the maximum energy calculated from the average curve fitted to the data. The average energy obtained from at least three specimens tested on the upper shelf and at the

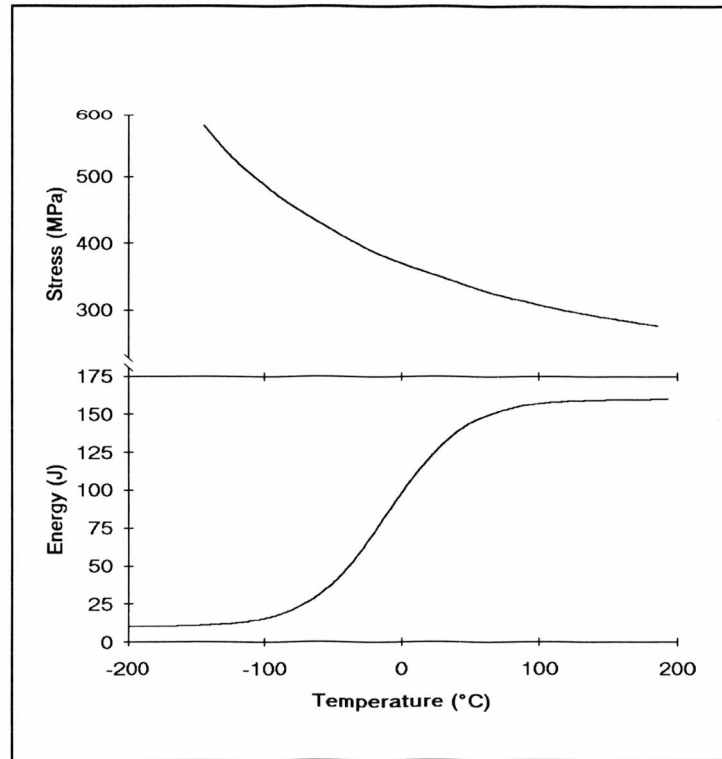


**Figure 1.** Upper curve represents the temperature dependence of the material yield strength. Lower curve is typical of a series of CVN tests for a steel alloy of moderate toughness.

same temperature provides an alternative method of determining the upper shelf energy (USE). A test is considered to have been conducted on the upper shelf if the fracture surface exhibits greater than 95% dull fibrous, or shear, fracture. Large values for the USE indicate high fracture resistance. The transition region is typically denoted by a temperature within the region which corresponds to a predetermined value of energy, percent fracture surface appearance, or lateral expansion. It is generally termed the ductile to brittle transition temperature, or DBTT. An example would be the temperature corresponding to 41 J of absorbed energy. The DBTT must be lower than the lowest expected service temperature.

The CVN test is statistical in nature. That is, variations in most of the dimensions of the specimens and in the testing equipment affect the test results to a greater or lesser extent.

A four-parameter hyperbolic tangent function is often fit to the data, and a best fit to results from as few as six tests conducted at temperatures ranging from the lower shelf to the upper shelf can result in a moderate statistical confidence level. Increasing the number of tests conducted at the appropriate temperatures increases statistical confidence qualitatively, but the confidence intervals, or quantitative confidence, remain roughly unchanged due to the significant scatter in the individual tests. Typical Charpy results display significant scatter even under the most controlled conditions. For example, in a study of weld metals, Nanstad and coworkers [1] conducted several CVN tests at each of several selected temperatures. They show best fit curves with the corresponding data points which indicate no less than  $\pm 10\%$  scatter in the energy values obtained at a given temperature.

Quality assurance programs in steel manufacture and construction generally include the CVN test. Inspectors cut specimens from representative material and test these samples at a predetermined temperature. Empirical correlations based on extensive practical experience in service establish a minimum criterion for acceptance of the steel. The average of the test results of three specimens tested at the specified temperature must be greater than or equal to the criterion. Such measures are typically specified contractually. Standard specifications for CVN testing methods are described in ASTM Standards A 370 [2] and E 23 [3].

Electric power supply companies which utilize light water moderated nuclear reactors have a specific interest in CVN testing. During the operation of light water reactors, neutrons radiate from the core and penetrate the reactor pressure vessel (RPV). A neutron which collides with an atom will cause the atom to dislodge within the material. The displaced atom in turn displaces other atoms. These displacements cause damage and alter the microstructure of the material. The changes result in hardening of the material that is comparable to the hardening induced by cold working of the steel. Both processes result in an increase in the stress required to move dislocations within the material and a corresponding increase in the strength of the steel, as well as a decrease in the ductility and an increase in the notch sensitivity. For CVN data, the representative curve shifts down and to the right with increasing neutron exposure. For RPV steels, the USE decreases, and the transition region shifts to higher temperatures. Since the transition behavior represented by the CVN data is qualitatively similar to the fracture toughness behavior of the RPV material, before and after neutron exposure, it is not surprising

that the ASTM Standard Practice E 185 - 82<sup>e</sup> *Conducting Surveillance Tests for Light-Water Cooled Nuclear Power Reactor Vessels* establishes the Charpy test as the method of monitoring the RPV embrittlement. Since the level of RPV embrittlement increases with the neutron exposure, the design criteria for the vessels must be based on the expected material properties at the end of the design life, with the goal that after decades of power generation the vessel will still exhibit a substantial safety margin. Owners must demonstrate RPV safety throughout the operational life of the plant.

U. S. federal regulations [4] require that the beltline region, which is the portion of the RPV subject to significant neutron irradiation, be constructed of material exhibiting a minimum USE of 102 J (75 ft-lbf). The regulations further stipulate that the vessel materials must retain a minimum USE of 68 J throughout the reactor lifetime, and that the shift in the DBTT, which is used to adjust the nil-ductility reference temperature (defined in ASTM E 185 and the ASME *Boiler and Pressure Vessel Code* [5]), must not raise this reference temperature above 132°C (270°F). If the CVN test results of the irradiated surveillance specimens indicate that either of these criteria is not met, or if the projections stipulated in U. S. Regulatory Guide 1.99 (Revision 2) [6] indicate that the criteria will not be met in the future, then the power plant owners must either discontinue reactor operations or demonstrate the current and continued safety of the RPV by conducting an extensive analysis of the vessel.

In light of the applicable regulations and the potential cost associated with failing to meet the stipulated criteria, one can see the importance of irradiating and testing many surveillance specimens in order to maximize confidence in the test results. Nevertheless, the number of specimens is limited primarily by the limited space inside the RPV. Aside from extracting material directly from the in-service vessel, which would be difficult and potentially detrimental to it, the only apparent means of obtaining significantly larger numbers of surveillance specimens is to reduce the specimen size. Small specimens are potentially more homogeneous than large specimens. The gradients in the environment, such as the temperature and the neutron flux, are less significant for the smaller specimens, and individual specimens are more likely to comprise homogeneous material throughout.

Material properties are affected by the microstructure since the bulk response represents an aggregate of many grains. Specimen dimensions must not approach the dimensions of any

microstructural features in order for the specimen response to represent the bulk response of structural components. Smaller specimen dimensions will increase the statistical scatter associated with imperfections, and the likelihood of a smaller specimen being homogeneous does not rule out the possibility of it being extracted from a portion of the material which is atypical of the whole. Thus, careful selection of representative material for small specimen fabrication is essential. The major obstacle to direct substitution of subsize specimens for standard sizes is that smaller specimens are less susceptible to brittle fracture due to the change in the stress state from near plane strain to near plane stress with reduced bulk constraint that accompanies the size reduction.

This study addresses the effect of loss of constraint by examining the CVN response of an RPV material as a function of specimen size. The specimens were the ASTM E 23 Type A geometry with the following exceptions. Three sizes were incorporated. One size was of standard dimensions, the second, half size in all dimensions, and the third, one-third size in cross section but half size in length; the two subsize configurations have an identical notch geometry, which is sharper than the standard geometry. The sharper notch promotes brittle fracture and thus compensates somewhat for the constraint loss. The objective of this work is to develop a method of utilizing the data collected from tests on subsize specimens, both before and after irradiation, to calculate the shifts in USE and DBTT values that would be expected of standard specimens.

The material utilized in this study is A533-B, Class I, quenched and tempered steel plate, a common RPV alloy. The microstructure of the material was atypical in that it had a coarse prior austenite grain size. The prior austenite grains for this material were determined to correspond to an ASTM grain size number in the range of 0 to 1. The ASTM specification for A533-B [7] stipulates that the prior austenite grains should be "fine", and ASTM A 20 [8] defines "fine" as having a "grain size number of 5 or higher (finer)." This microstructure variant makes the steel prone to brittle fracture in notched impact tests. The beltline steel of RPVs at the end of the operational design life is likewise expected to be prone to brittle fracture in notched impact. The large prior austenite grain size did not alter the tensile properties or macro-hardness of this material from values typically expected of A533-B Class 1 steel plate. This study includes specimens irradiated to  $1 \times 10^{19}$  n/cm<sup>2</sup> at an average temperature of 150°C.



## II. BACKGROUND OF NOTCHED-BAR IMPACT TESTING

ASTM Standard Test Method E 23 describes the standard Charpy impact test. The description includes a pendulum-type test machine only and makes no reference to strain gauge instrumentation that is capable of measuring the load during fracture as a function of time. The original test and apparatus design was based on the principle of conservation of energy. A pendulum dropped from a given height through a given angle will rise through nearly the same angle, reduced only by the friction of its mechanism and windage. ASTM E 23 specifies that the maximum for such losses for a pendulum-type CVN test machine be less than 0.75% of the rated scale capacity. Thus a properly calibrated and maintained machine will register the energy lost while breaking through a specimen placed at the bottom of the arc. The energy registered is a composite measurement in that it includes all energy expended during the pendulum swing except the inherent friction losses for which the calibration compensates. ASTM E 23 specifies several factors and precautions for minimizing energy losses to other than specimen deformation and fracture. The newer drop tower type of impact testers are also common. The configuration does not allow an analog determination of the fracture energy as does the pendulum machine. Drop tower striking tups are configured with electronic load cells strain gauged to record the load during the event as a millivolt signal versus time. This record is subsequently converted to load versus displacement by assuming a constant calibration factor for the strain gauge and a constant velocity throughout the event. The area under the load trace, force times distance, represents the fracture energy, but it is exaggerated somewhat by the constant velocity assumption. The true fracture energy is calculated by applying a correction factor. These calculations and the validity of the assumptions are treated thoroughly in Section III-B.

The ASTM standard addresses the Charpy test primarily in regard to its original purpose, namely, as a proof test or pass/fail criterion. It defines three specimen geometries, and also defines standard size variations, specifically: a reduction of thickness or a reduction of both width and notch depth, but not both thickness and width, with one exception. Half-width specimens are allowed to be half, standard, or double thickness. Further, the standard discourages the use of subsize specimens and asserts, correctly, that the results from different

sizes or geometries cannot be compared directly. The appendix for ASTM E 23 discusses several relevant considerations such as notch effects and size effects. In section X1.3.3, while discussing size effects, the following assertion appears, "General correlation between the energy values obtained with specimens of different size or shape is not feasible, but limited correlations may be established." The assertion has not inhibited research efforts, at least in the nuclear materials field, attempting to develop a general correlation between impact test results of standard Charpy specimens and the results obtained from miniaturized impact specimens of approximate Charpy geometry.

Specimen size is problematic. Linear elastic fracture mechanics (LEFM) is based on linear elastic material properties, and test specimens must be large enough to ensure that nonlinear response in the material is negligible, or LEFM theory cannot be applied. LEFM theories are well established, and LEFM values can be utilized as material properties for design and safety considerations. For instance, the plane strain fracture toughness,  $K_{Ic}$ , is a lower bound critical value for a given material. It is an indicator of the minimum stress required to cause the growth of an existing crack or other sharp flaw in a defined geometry and configuration. Engineers can utilize it in design calculations as long as temperature conditions and loading conditions are appropriately characterized for the structural component.  $K_{Ic}$  is determined from specimens which contain fatigue induced precracks. For high strength, low toughness materials, standard CVN specimens provide valid  $K_{Ic}$  measurements, when these specimens are precracked and tested in quasi-static bending. High toughness materials, however, and particularly those with only moderate strength properties, require that specimens be large for the application of LEFM. So large, in fact, that testing is impractical. Elastic-plastic fracture mechanics (EPFM) takes into account the significant plastic deformation of tough materials; the specimen size requirements are smaller than those for LEFM testing but are still relatively large.

Sharp cracks in thick walls are by definition in a state of plane strain; so a  $K_{Ic}$  value for the material of a thick walled RPV is desirable for design considerations and for monitoring the embrittlement of the material. Since it is not possible to incorporate massive specimens into RPV surveillance programs, a substitute test which utilizes significantly smaller specimens is required. Results from the CVN impact test are qualitatively similar, and the test utilizes specimens which are of a practical size.  $K_{Ic}$  data exhibit a transition equivalent to the CVN

transition, and as indicated, the CVN test is required by government regulation. The empirically-based calculations specified in the regulations are generally considered to be conservative. Equally conservative calculations could be based on the test results of miniature CVN specimens, but the database of subsize geometries, while substantial, is not extensive. A correlation between subsize and full size specimen data could potentially allow substitution of the subsize test results into the current or slightly modified regulations.

### III. LITERATURE REVIEW

The sections in this review describe the various aspects of the CVN test and particularly the instrumented test. The first subsection traces the development of the instrumented test and theory pertaining to it from early efforts to the present work. It also deals with miniature test specimens and the data derived from their use. The second subsection reviews work dealing primarily with the instrumented CVN test. Equations for the various calculations are developed and discussed. The third subsection reviews work dealing specifically with test instrumentation and data acquisition.

#### A. SUBSIZE EXPERIENCE AND CORRELATION EFFORTS

Swedish researchers have successfully employed subsize specimens in their nuclear materials programs from as early as the late 1950s. M. Grounes' review of this work on RPV steels [9] is an indication of the considerable experience obtained in subsize specimen testing. His paper presents data on 15 steels in both unirradiated and irradiated conditions (irradiation dose range:  $0.2 - 3.3 \times 10^{19}$  n/cm<sup>2</sup>,  $E > 1$  MeV). The irradiation temperatures ranged from 40°C to 550°C (105°F to 1020°F). He describes the several irradiations involved and summarized previous work that had included irradiations to as high as  $2 \times 10^{20}$  n/cm<sup>2</sup> ( $E > 1$  MeV). The Swedish efforts included hardness measurements, tensile properties, and Charpy impact data from both standard size and subsize specimens, which were apparently tested on modified pendulum-type machines. The dimensions of the subsize impact specimens were 3.33 x 3.33 x 27.5 mm, with a 0.8 mm deep notch, a 45° included angle, and a 0.11 mm root radius (which is relatively deep and blunt). Experience with the transition curves derived from the subsize specimens indicated 1.6 J was an appropriate substitute reference index for the 41 J transition temperature. The transition temperature obtained using this energy value did not correspond to the same temperature for subsize specimen data as did the 41 J index for the full size specimen data, but it produced approximately the same radiation-induced temperature shift. In regard to the one-third size specimens Grounes remarked, "These miniature specimens have been thoroughly tested and found suitable for comparing the impact properties of steels, and are extremely valuable in irradiation studies."

McConnell et al. [10] reviewed several small specimen test techniques including size reduction of standard tests and reconstitution of specimens from tested fragments, and they summarize the work of Grounes and the Swedish program. Their paper stated that after testing more than ten thousand of the third size specimens on over fifty steels, the Swedish investigators concluded that:

1. Miniature Charpys are suitable for comparing impact properties of steels.
2. Although subsized specimens do not give the same transition temperatures as normal Charpy specimens, the irradiation-induced shifts in an arbitrarily defined transition temperature are approximately the same.
3. Properties of steels are ranked in the same order for both subsized and standard Charpy specimens.
4. Variation (scatter) in impact properties for a given steel was no greater with miniature specimens than with standard CVNs.
5. Subsize specimens were very useful in obtaining data in material with a wide variation in metallurgical state (e.g., welds).

Lucas et al. [11] described their experience with subsize CVN specimens. They chose to reduce all dimensions of both the specimens and the components of the testing apparatus to 1/3 the values specified in ASTM E 23. They retained the measurements of all angles stipulated in the ASTM specifications. Tests at other than ambient temperature required a reduced interval between removal from the temperature bath and impact, to less than three seconds. The tests were conducted on an instrumented drop tower. The drop weight was monitored optically to measure velocity at impact. To ensure that inertial effects did not mask the mechanical response, they increased the test duration by reducing the impact velocity to 1 m/sec. Despite the consistent dimensional conversion, a simple volume normalization proved inadequate for relating subsize and full size specimen data. That is, the relationship of the normalized values of energy per unit volume [with the fracture volume approximated by the square of the ligament times the thickness ( $Bb^2$ )] between full size and third size specimen data was not consistent from one material to another. The values from the subsize specimen tests exceeded those from the standard specimen tests for a material with a low USE, but the inverse was true for materials with a relatively high USE. Nonetheless, the results from third size specimens were qualitatively the same as those from full size specimens.

Further in the same study Lucas and coworkers developed a method for determining the critical fracture stress for cleavage,  $\sigma_f^*$ , based on the value of  $P_{gy}$ , the load at general yield

in the instrumented impact test. Their analysis was successful for the HT-9 examined in the study, but they did incorporate a correction factor for the  $P_{gy}$  values determined from the subsize specimen tests. The correction factor was necessitated by the fact that the measured yield stress and general yield load of the impact test did not fit the predictions of slip-line field theory for the small specimens. Lucas and coworkers did not attempt to explain this deviation. The  $\sigma_f^*$  values calculated for the HT-9 from different test methods including standard and third size CVN specimens were approximately equal and temperature independent. The drawback to utilizing  $P_{gy}$  from the impact load record for this calculation is that the determination of  $P_{gy}$  can be rather subjective. Various problems associated with proper analysis of load versus time (or displacement) curves obtained from electronic instrumentation of the Charpy impact test will be discussed further in subsequent sections, but considering here  $P_{gy}$  and the calculation of  $\sigma_f^*$ ,  $P_{gy}$  is defined as the point in the loading where the plastically deforming region extends through the entire cross section of the specimen under the notch. This condition is defined as the location on the load-time curve where the rate of increase in the load declines significantly (see Figure 2). The assumption is that until the entire cross section has deformed plastically the overall response will be elastic and load will rise linearly, which is correct in a general sense. That is, the average load does increase monotonically until the point of general yield, but the increase is not

strictly linear since some of the material is deforming plastically. Also, the average load is derived from the record of the measured load applied to the specimen superimposed with a variety of elastic oscillations, including inertial effects at the beginning of the impact and electronic noise.

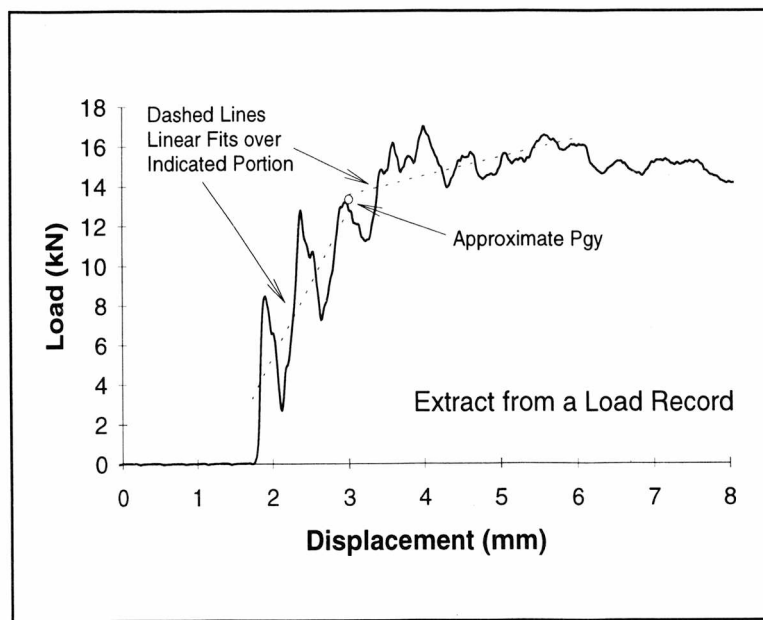


**Figure 2.** Portion of a measured load trace.  $P_{gy}$  would be chosen as indicated, or perhaps at a slightly higher load.

This superposition of waves combined with the variability in the load-time record (or deviation from an idealized response) make the selection of the point on the curve coincident with the load at general yield ( $P_{gy}$ ) subjective.

The impetus for determining  $\sigma_f^*$  for a material lies in the potential for identifying a transition temperature often referred to as  $T_d$ .  $\sigma_f^*$  is considered to be generally independent of temperature and strain rate. The yield strength,  $\sigma_y$ , is both temperature and strain rate dependent, and when plotted against temperature, the  $\sigma_f^*$  and  $\sigma_y$  curves intersect at  $T_d$ , which is defined simply as the temperature below which a smooth bar tension test will exhibit no readily discernible plastic deformation before fracture. Since  $T_d$  depends on  $\sigma_y$ , it is affected by notch effects and strain rates. If  $\sigma_f^*$  can be calculated directly from  $P_{gy}$  values for a given specimen geometry and  $T_d$  determined, then the procedure can be used as a means of correlating results from different size specimens in the transition region. The shift in  $T_d$  due to irradiation could prove to be an appropriate substitute for the DBTT shift used in the calculation of the nil-ductility reference temperature stipulated in the federal regulations pertaining to RPV surveillance.

The concept of utilizing various points on the impact load record for calculations has perhaps been advanced most by R. A. Wullaert. Wullaert [12], and later, Wullaert, Ireland, and Tetelman [13] built on work begun by Wilshaw and Pratt [14]. With the objective, ideally, of defining the CVN test in terms of fundamental properties, Wilshaw and Pratt examined a low carbon, high nitrogen, manganese steel at quasi-static, intermediate, and impact loading rates. Using standard size specimens in accordance with the British standard they recorded the load versus time data for each test. They utilized a pendulum-type tester which had been fitted with strain gauges for the impact tests, and the two slower rate tests were carried out in a constant strain rate configuration. They had chosen the alloy for its property of reacting with Fry's reagent ( $\text{HCl} \& \text{CuCl}_2$ ) to reveal the plastically strained material. They also characterized the deformation zone near the notch at several stages of the test with microhardness measurements and microscopy. Their findings verified that the plastic zone in standard CVN specimens is closely predicted by slip-line field theory. A slow bend test generated a load versus deflection plot similar to a standard uniaxial tension test for a low carbon, low alloy steel with obvious upper and lower yield points. They identify the lower yield point as  $P_{gy}$ .

The paper included photomicrographs of the etched plastic zones associated with several points on the diagram. Comparison of the straining patterns of specimens loaded in pure bending, or four point loading (Knott [15]), to these loaded in the more complex three point loading, reveals that the deformation zone is smaller and sharper in the three point loading of the CVN test. Thus, analysis of the CVN test utilizing theory and calculations based on pure bending is not entirely accurate. Likewise, calculations and analysis generally assume plane strain conditions in the specimen, and for materials like RPV steels, CVN specimens do not satisfy plane strain criteria, even for precracked specimens, except at very low temperatures.

Wullaert, Ireland, and Tetelman [13] noted that Wilshaw and Pratt experimentally determined the plastic zone size and, with equations 1 and 2, the longitudinal stress distribution,  $\sigma_x$ , in the plastic zone.

$$\sigma_x = 2 \tau^* K_{\sigma(\rho)} \quad (1)$$

$$K_{\sigma(\rho)} = 1 + \ln(1 + R/\rho) \quad (2)$$

Where  $\tau^*$  is the shear strength of the material,  $R$  is distance within the plastic zone below the notch, and  $\rho$  is the root radius: the plastic stress concentration factor,  $K_{\sigma(\rho)}$ , is maximum when  $R$  is equal to the radius of the plastic zone (after Hill [16]). Wullaert, Ireland, and Tetelman stated that  $K_{\sigma(\rho)}$  rises to a value of 2.18 and remains constant once the maximum load is 80% of the load required for general yielding. More specifically, however, Wilshaw and Pratt found that beyond the elastic limit of 18% of the general yield load, initial yielding spread inward from the notch root, toward the center load point, greatly reducing the elastic stress concentration,  $K_t$  (which they calculated as 3.25 after Neuber [17]), but then the enlarging plastic zone acted as a stress concentrator and increased stress intensification up to  $2.05 \pm 0.05$  (rather than 2.18, which is a value calculated from the theory) once the maximum load was 80% of the general yield load. This load corresponds to the point at which the slow bend load trace deviates significantly from linearity. Wilshaw and Pratt claimed that "complementary" slip, or internal deformation, began in the material adjacent to the zone that coincided with the slip field analysis, and thus, the stress remained constant in the specimen even though the applied load was still increasing. Accordingly,  $K_{\sigma(\rho)}$  is constant for tests conducted at temperatures where the



maximum load observed is between  $0.8P_{gy}$  and  $P_{gy}$ . Wilshaw and Pratt also noted that once the maximum load exceeds  $P_{gy}$ ,  $K_{\sigma(p)}$  began to increase further to a maximum value of approximately 2.5.

A crack will begin to propagate, or initiate and grow from a stress concentrator such as a notch, either when the shear stress at the tip reaches the shear strength of the material,  $\tau^*$ , or when the normal stress reaches the cleavage fracture strength of the material,  $\sigma_f^*$ . As noted, at sufficiently low temperatures,  $\tau^*$  exceeds  $\sigma_f^*$ , and the crack will propagate in a brittle manner when the normal stress at the tip reaches  $\sigma_f^*$ . At higher temperatures, the shear stress reaches  $\tau^*$  first, and the material deforms appreciably. As the specimen deforms, the plastic zone constrains the material near the crack tip and increases the normal stress, such that after initial yielding and ductile propagation, the crack completes its propagation in a brittle manner. At still higher test temperatures where the maximum load exceeds  $0.8P_{gy}$ , strain hardening combines with the plastic constraint to increase stress intensification and to eventually initiate brittle fracture after increasing plastic deformation. Thus, as the test temperature increases, the proportion of ductile fracture increases. Finally, at sufficiently high temperatures, the plastic strain exceeds the fracture strain limits before the normal stress reaches  $\sigma_f^*$ , and the entire specimen fractures by ductile rupture. Referring to figure 3, first note that the point labeled  $P_{gy} = P_{max}$  is the lowest temperature for which a specimen will exhibit general yield. For lower test temperatures,  $P_{gy}$  must be estimated by extrapolation, since it exceeds the maximum load recorded during the impact. The material behaves elastically when tested at temperatures where the maximum load is less than 18% of the extrapolated  $P_{gy}$  value for the temperature. At test temperatures above where the maximum load reaches 80% of  $P_{gy}$ , a material model must account for strain hardening. In the intermediate temperature region, the material behaves in an elastic-perfectly plastic manner which is readily modeled. In this region, plastic constraint alone raises the normal stress above the cleavage fracture strength, and as the test temperature increases, the plastic zone size and  $K_{\sigma(p)}$  increase together.

Tetelman and McEvily [18] first proposed that, in the region where the increasing but small plastic zone accounted for adequate constraint to initiate brittle fracture, the cleavage fracture strength was equal to the plastic constraint times the dynamic yield strength.

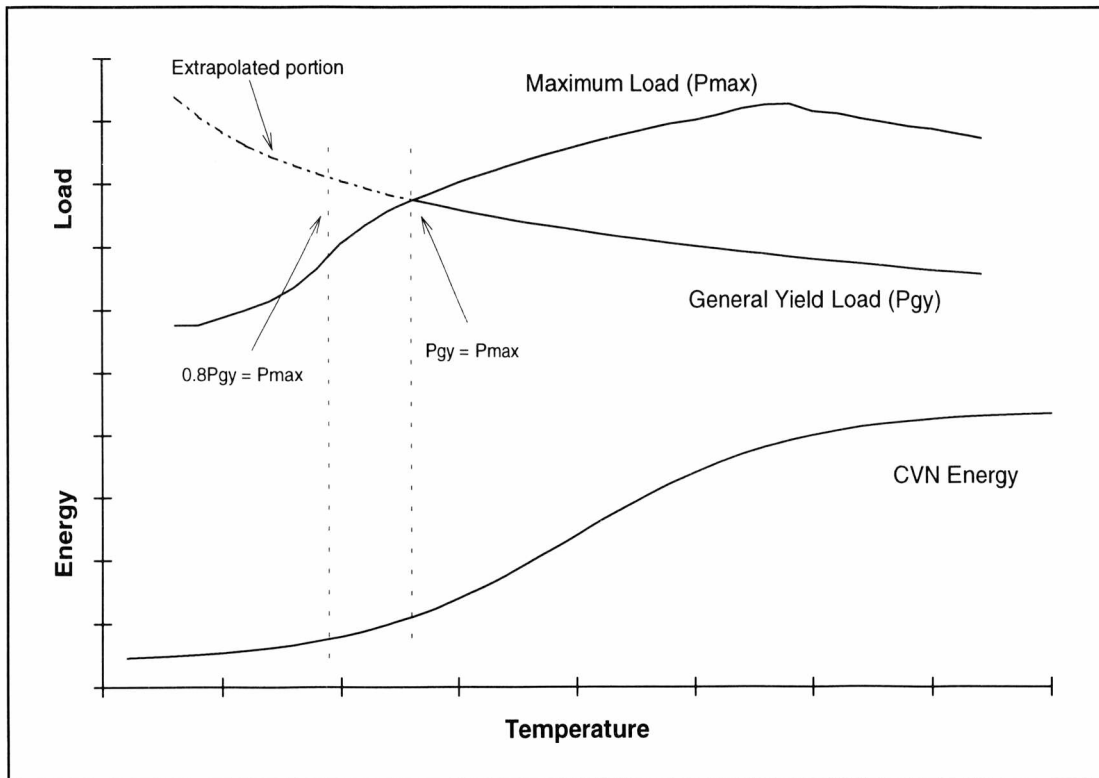


**Figure 3.** Generalized relationship between  $P_{max}$ ,  $P_{gy}$ , and the CVN curve. Specimens break before general yield is reached for temperatures below  $P_{gy} = P_{max}$ .

That is,  $\sigma_f^* = K_{\sigma(p)} \times \sigma_{yd}$ . Since the yield strength is strain rate dependent, the dynamic stipulation is appropriate for impact loading. Also, Green and Hundy [19] employed a plane strain, slip line analysis of an elastic-perfectly plastic material to show that for the standard Charpy test, the dynamic yield strength was directly proportional to the load at general yield, or specifically,  $\sigma_{yd} = 33.3P_{gy}$ . Combining these two equations allows calculation of  $\sigma_f^*$  from  $P_{gy}$ . D. Ewing [20] conducted a similar analysis that included the effects of the tup indentation at the center load point. W. L. Server [21] extrapolated from Ewing's results to derive a more general equation for  $\sigma_{yd}$  for a standard specimen, namely,

$$\sigma_{yd} = 2.99P_{gy} \frac{W}{Bb^2} \quad (3)$$

where  $W$  is the specimen width,  $B$  is the specimen thickness, and  $b$  is the ligament (the width minus either the notch depth or the combined notch and crack depth). Server suggests the constant 2.99 should be reduced to 2.85 for precracked specimens. With standard English units, Ewing's/Server's factor for  $\sigma_{yd}$  is 30.14 compared to Green and Hundy's 33.3.

Assuming  $W$  is equal to  $B$ , as in square cross section CVN specimens, and taking  $K_{\sigma(p)}$  equal to 2.05, the relationship between  $P_{gy}$  and  $\sigma_f^*$  becomes

$$\sigma_f^* = \frac{6.13}{b^2} P_{gy}. \quad (4)$$

The assumptions made to derive this equation make it specifically applicable only to standard specimens tested at a temperature where the maximum load recorded during the impact is equal to 80% of  $P_{gy}$  extrapolated to that temperature. Still, confidence in the equation is not high since  $P_{gy}$  is extrapolated and is difficult to determine for a given test,  $K_{\sigma(p)}$  does not account for specimen size considerations, and plane strain conditions are not fully satisfied. Also, apparently, the proportionality constant must be adjusted with the specimen cross section and ligament length. Equation 4 is therefore informative and useful in limited application, but it is not promising as an intermediate step in correlating data from specimens of different sizes, nor can it provide a definitive measure of the transition temperature  $T_d$ .

As a continuation of their work, Lucas and coworkers [22] later tested several different materials and microstructural variations in the same manner previously described, and they utilized equation 3 to determine  $\sigma_{yd}$  for these materials from both the standard and third size impact load records. They found that the  $\sigma_{yd}$  values calculated from standard and subsize specimens were not equal. The ratio of these two varied with the materials, from significantly above 1 to significantly below 1. One set of values did exhibit a 1:1 correspondence, but with significant scatter. As noted by the investigators, there must be dependencies unaccounted for in the equation, probably related to both material and size effects.

Corwin and Houglund [23] also examined subsize effects with a ferritic stainless steel for fusion reactor materials development. In addition to testing full, half, and third size specimens equivalent to those used in the present study, they also included a half size geometry of standard length, which offers the advantage of volume reduced to one fourth that of full size specimens, but testing of such specimens does not require modification to standard Charpy impact equipment. As might be expected, the long half size specimens averaged lower USE and DBTT values than the short half size specimens. The longer span reduces the effective strain rate at the notch tip, decreasing the tendency for cleavage. Likewise, the reduced strain

rate affects the response of strain rate sensitive steel. Total specimen deformation is also less with the longer span since the angle of deflection is not as great. The specimen behavior and the test results change due to the span variation. This fact tends to support the incorporation of the span dimension into a normalization factor, rather than a nominal fracture volume alone.

Fatigue precracking CVN specimens is attractive in that test results from both standard and subsize precracked specimens consistently exhibit less scatter than notch-only specimens despite the fact that the lower total fracture energies might be expected to show greater relative error. One possible explanation is that the precrack is relatively more uniform than even precision-machined notch roots. The sharp precrack can significantly affect CVN test results. R. O. Ritchie [24] examined a high strength, low toughness 4340 steel. He found that different heat treatments resulted in opposite effects on the Charpy USE and on the plane strain fracture toughness values, which is surprising since the two tests generally produce qualitatively similar results. In this instance, an excessive austenitizing treatment resulted in a greatly enlarged prior austenite grain size. The final quench and temper was chosen such that the two conditions had identical yield strengths, but the effect of the large prior austenite grain size on the standard Charpy specimens was to lower the USE in both quasi-static and impact loading, while the precracked specimens demonstrated increased (valid)  $K_{Ic}$  and  $K_{IId}$  values. Ritchie concluded that no empirical correlation between Charpy results and plane strain fracture toughness could account for the divergence and asserted that both notched bar tests and sharp crack tests were important for fracture characterization of materials.

A group of Japanese researchers is attempting to systematically determine the relative importance and effect of variations in several specimen dimensions, particularly the notch configuration. Preliminary results of Kurishita and coworkers [25] indicated that it may be possible to select a notch geometry for subsize specimens such that the DBTT determined would be the same for the small specimens as for standard size specimens. However, they have more recently published data [26] from the test results of an initial irradiation to  $3 \times 10^{18}$  n/cm<sup>2</sup> ( $E > 0.1$  MeV) at  $\approx 300^\circ\text{C}$  which has led them to conclude that the dependencies of the DBTT on the notch geometry decrease with increasing DBTT. Based on the findings, they maintain that the DBTT is strongly affected by the dimensions of the notch, with root radius and depth being most significant. Also, they presently hold that the USE of subsize specimens is not

significantly affected by the notch geometry, per say, but by the ligament length only. Accordingly, they suggest that a simple volumetric normalization ( $Bb^2$ ) is most appropriate for USE comparisons.

The initial work related to the present study was conducted by W. L. Hu and D. S. Gelles [27] but was conducted with the goal of evaluating the material for fusion applications rather than for size effect considerations. They examined ferritic stainless steel alloys with half size CVN specimens. The specimen geometry and testing procedure carries through to this work.

Building on Hu and Gelles' work, B. S. Loudon et al. [28] conducted tests with standard, 1/2, and 1/3 size specimens. They proposed a correlation factor which successfully correlated subsize and full size results for materials exhibiting low USE values. Kumar, Garner, and Hamilton [29] subsequently amended the correlation to separate the energy of crack initiation from that of crack propagation. They applied the correlation to the difference between the notched only and precracked USE values,  $\Delta USE$  ( $USE_{\text{Notch}} - USE_{\text{Precrack}}$ ). Here, they found good correlation with the simple volume factor,  $Bb^2$ , and suggested that the crack initiation energy, defined in this manner, may be simply proportional to the volume of material involved in deformation and strain hardening. In another paper, Kumar and coworkers [30] further develop this concept and include the results of irradiated specimens from the work of Hu and Gelles.

Rosinski et al. [31] present the preliminary, that is, unirradiated, testing results of the material of this study. The paper thoroughly describes the material, but to summarize, it is a standard A533-B, Class I plate material with the exception that the prior austenite grain size is excessively large. This fact results in a low CVN USE value for the material based on full size specimens, about 59 J. The large prior austenite grain size may also account for difficulties in the subsize specimens, where the specimen dimensions approach the dimensions of these prior austenite grains. However, the overall microstructure is consistent with that which would be expected in A533-B plate material—a fine grained, tempered structure. The microstructure is nominally martensitic with small ferrite colonies more or less outlining the prior austenite grains. While the overall structure is too fine to be of concern in size effect considerations, these ferrite colonies may provide sufficient inhomogeneity to result in atypical behavior for

the subsize specimens relative to the full size specimens. The volumetric correlation as applied to the  $\Delta USE$  was only moderately successful for this material.

Kumar and coworkers [32] then proposed normalizing the partitioned energies,  $\Delta USE$ , by the factor  $Bb^2/LK_c'$ , where  $B$ ,  $b$ , and  $L$  are the width, ligament, and unsupported span, respectively, and  $K_c'$  is a combined elastic and plastic constraint factor. This method also proved appropriate for a weld metal (an A533-B weld material, designated "72W" in the HSST/HSSI testing program.) [33]

The materials testing community has yet to establish standards for variations in Charpy impact testing, including small specimen geometries, the use of drop tower testing machines, and instrumentation and load trace data interpretation. Only as recently as 1993 did ASTM incorporate fatigue precracking guidelines into the E 23 standard, in spite of the fact that these techniques have been utilized by various investigators since at least the early 1960s.

## **B. ANALYSIS TECHNIQUES IN INSTRUMENTED CHARPY IMPACT TESTING**

The standard pendulum-type CVN test provides only an analog measure of the fracture energy. Incorporating load sensing instrumentation in the testing equipment provides additional information. The most common instrumentation is solid state strain gauges affixed to the striking tup, with an oscilloscope used to record the data. C. E. Turner [34] argued that improvements in CVN testing over the years had not led to a sound theoretical basis which might allow CVN data to be incorporated into engineering applications. In establishing a basis for his arguments, he reviewed the development of instrumented testing. He went on to advocate the use of CVN specimens modified by both fatigue precracks and side grooves to increase the constraint on crack propagation for fracture toughness measurements. One of his stated objectives for the modifications was to raise the observed DBTT to above room temperature. Such results would allow for fracture mechanics based investigations. In his conclusions he noted that the precrack and side grooves may not properly approximate the plane strain conditions of specimens thick enough to satisfy the testing specification requirements. In the portion of his paper which reviews earlier work, he began with R. Yamada [35], who in the late 1920's utilized an optical method to monitor velocity changes in the pendulum. Later, S. Watanabe [36] placed piezoelectric crystals on the anvils and utilized a photocell device

to monitor displacement. Turner stated that B. Augland [37] noticed in 1962 that the energy calculated from the instrumentation data was greater than the energy recorded by the pendulum dial. He was able to demonstrate an empirical relationship. Turner noted without further comment that it was 1969 before a theoretical derivation was published by Grumbach and coworkers [38]. The relation is

$$E_d = E_a \left( 1 - \frac{E_a}{4E_o} \right), \quad (5)$$

where  $E_d$  is the actual absorbed energy during fracture (or the pendulum Dial energy),  $E_a$  is the apparent energy calculated from the instrumentation data, and  $E_o$  is the kinetic energy of the pendulum (or drop weight). Equation 5 can be derived as follows; at impact, the hammer has kinetic energy,  $E_o = 1/2 \cdot m \cdot v_o^2$ , where  $m$  is the mass and  $v_o$  is the velocity at the moment of impact. Assuming that  $E_o > E_d$ , the hammer will have residual energy after fracture, and

$$E_d = E_o - E_{Residual} \quad (6)$$

By definition,

$$E_{Residual} = \frac{1}{2} m v_f^2 \quad (7)$$

where  $v_f$  is the velocity immediately after the fracture event.  $F = ma$ , Newton's second law, and the hammer velocity is reduced during fracture by the acceleration due to the interaction with the specimen. This acceleration is

$$a = \frac{F}{m} = \frac{P}{m} \quad (8)$$

where  $P$  is the load during impact, and the velocity after impact is

$$v_f = v_o - \int_0^{\tau} \frac{P}{m} dt \quad (9)$$

where  $\tau$  is the total time for the fracture event. Substituting equation 9 into equation 7, and the resulting equation 7 into equation 6,

$$E_d = E_o - \frac{1}{2} m \left( v_o - \frac{1}{m} \int_0^{\tau} P dt \right)^2 \quad (10)$$

$$= E_o - \frac{1}{2} m \left[ v_o^2 - \frac{2v_o}{m} \int_0^{\tau} P dt + \frac{1}{m^2} \left( \int_0^{\tau} P dt \right)^2 \right] \quad (11)$$

$$= E_o - \frac{1}{2} m v_o^2 + v_o \int_0^{\tau} P dt - \frac{1}{2m} \left( \int_0^{\tau} P dt \right)^2 \quad (12)$$

$$= v_o \int_0^{\tau} P dt - \frac{v_o^2 \left( \int_0^{\tau} P dt \right)^2}{2m v_o^2} \quad (13)$$

$E_a$ , the apparent energy, is defined as the area under the load versus time record of the fracture event, multiplied by the initial velocity. That is,

$$E_a = v_o \int_0^{\tau} P dt, \quad (14)$$

which allows

$$E_d = E_a - \frac{E_a^2}{4E_o} = E_a \left( 1 - \frac{E_a}{4E_o} \right), \quad (15)$$

the same as equation 5.



Note that these equations apply to drop tower as well as the pendulum-type testing machines. The calculation of  $E_d$ , however, is only exact for pendulum-type machines, for which motion during the test is horizontal.

For a drop weight testing machine, one must add a gravity term,  $E_g$ , to the equation for  $E_d$ .  $E_g$  is the increase in  $E_o$  due to gravity,  $g$ , acting on the drop weight during the vertical motion of the test, and  $E_g = m \cdot g \cdot h$  where  $h$  is the distance traversed by the hammer from the instant of impact until immediately after the fracture process is complete. If the specimen does not break but deforms until it is bent sufficiently to squeeze between the anvils, then  $h$  is at its maximum value. (See figure 4.)

The magnitude of  $h$  depends on the specimen dimensions, anvil spacing, and tup geometry, as well as the amount of deformation involved. For a test on the lower shelf  $h$  will be relatively small. In such cases, the specimen will deform a very small amount required for crack initiation, and then it will break in half, resulting in a very small displacement before the fracture is complete; accordingly,  $E_g$  is very small. On the other hand, a specimen which does not separate into two pieces will be in contact with the tup until it is pushed between the anvils as shown in figure 4. In the absence of direct measurement of the tup displacement during contact,  $h$  can be calculated geometrically, as can be seen from figure 4, to a close approximation from the appropriate measurements of the test components. For the testing of this present study, measurements of the specimen before and after deformation and the gap between the anvils indicated that  $h$  is less than 25 mm for full size specimens which did not break.  $h$  is smaller for subsize specimens.

In this study  $E_g$  is assumed to be negligible. The error associated with this assumption is determined as follows;  $E_t$ , the total change in the kinetic energy of the drop weight

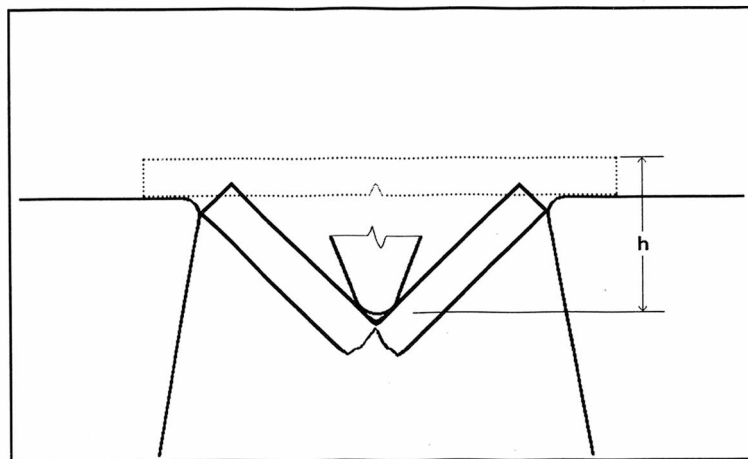


**Figure 4.** Schematic depicting  $h$  for a fully ductile specimen which did not break into separate pieces.

during the fracture event, is given as

$$E_t = E_o - \frac{1}{2} m v_f^2 + mgh, \quad (16)$$

neglecting the friction between the drop weight assembly and both air and the tower guide rails over the distance  $h$ . Gravity must also be included in the calculation of  $v_f$ , and equation 9 can be rewritten as

$$v_f = v_o - \int_0^\tau \left( \frac{P}{m} - g \right) dt. \quad (17)$$

Expanding equation 17 ( $g$  is constant) yields

$$v_f = v_o - \int_0^\tau \frac{P}{m} dt + \int_0^\tau g dt = v_o - \int_0^\tau \frac{P}{m} dt + g\tau. \quad (18)$$

Equation 18 shows that the effect of gravity is to increase  $v_f$  by the quantity  $g\tau$ , as one might intuitively expect. The maximum measured event time interval,  $\tau$ , is less than 0.005 seconds.  $g\tau$  is therefore less than 0.049 m/s, and for  $v_o$  typically greater than 3 m/s, the maximum error in the velocity is less than 1.6%.

Substituting  $E_a$  (equation 14) into equation 18,  $v_f$  becomes

$$v_f = v_o - \frac{E_a}{m v_o} + g\tau. \quad (19)$$

Substituting equation 19 for  $v_f$  in equation 16, the total kinetic energy change becomes

$$E_t = E_o - \frac{1}{2} m v_o^2 + E_a - \frac{E_a^2}{2m v_o^2} + \frac{E_a g \tau}{v_o} - m v_o g \tau - \frac{m}{2} (g\tau)^2 + mgh, \quad (20)$$

which can be reduced to

$$E_t = E_a \left( 1 - \frac{E_a}{4E_o} \right) + \frac{E_a g \tau}{v_o} - m v_o g \tau - \frac{m}{2} (g\tau)^2 + mgh. \quad (21)$$

Since the first term in equation 21 is  $E_d$  as defined in equation 5, the remaining four terms are the difference,  $\Delta E$ , between the kinetic energy of the striker in the pendulum-type machine versus that in the drop tower tester. That is,

$$\Delta E = \frac{E_a g \tau}{v_o} - mg(v_o \tau - h) - \frac{m}{2}(g \tau)^2 \quad (22)$$

The fractional error,  $F$ , associated with neglecting  $\Delta E$  can be defined as  $\Delta E/(E_d + \Delta E)$ , or

$$F = \frac{\frac{g \tau}{v_o} - mg \frac{v_o \tau - h}{E_a} - \frac{m}{2E_a}(g \tau)^2}{\frac{E_d}{E_a} + \frac{g \tau}{v_o} - mg \frac{v_o \tau - h}{E_a} - \frac{m}{2E_a}(g \tau)^2} \quad (23)$$

where each term in the numerator and the denominator has been divided by  $E_a$ . As  $E_a$  approaches zero,  $\tau$  and  $h$  do likewise, and while  $E_d/E_a$  is always less than unity, the ratio approaches unity as  $E_a$  approaches zero. For small values of  $E_a$ , as long as  $v_o$  is significant, it is appropriate to ignore the contribution of gravity, since  $F$  in this case is vanishingly small. Much credit for the derivation of equation 23 is due N. Scott Cannon (personal correspondence).

The value of  $F$  is maximum for full size specimens, tested on the upper shelf, which did not break in two during testing. For the experiments of this study, the value of  $F$  is always less than 0.005.

### C. GENERAL ASPECTS OF DATA ACQUISITION AND EVALUATION

The load data of an instrumented impact test can be recorded digitally by an electronic instrument that samples the output from the tup strain gauge at predetermined time intervals during the impact event and stores the data in consecutive memory registers. Typical instrumentation is limited either by the memory capacity or by the minimum possible time interval. A time interval and a load signal sensitivity range must be selected such that the entire impact event is recorded. For instance, a 12 bit digital oscilloscope provides 4096 ( $2^{12}$ ) data pairs, or divisions of both the x and y scales. The duration of typical CVN tests is less than

4 milliseconds. Thus a time interval of 1 or 2 microseconds per point allows the entire event to be recorded.

M. C. Cheresch and S. McMichael [39] treated various considerations relating to data acquisition and evaluation in the instrumented test. They offered general guidelines for initial estimates of the required voltage range and the time interval for data recording and pointed out the more important potential sources of error, namely, inertial load effects and harmonic oscillations. They discussed triggering the recorder as an important aspect in collecting complete load traces, and Cheresch and McMichael summarized appropriate considerations for both internal (load change) and external (photodetector, typically) triggering methods. They suggested that about 10% of the data points should be devoted to the pre-impact load. This allows accurate calculation of the baseline zero load.

Some data acquisition systems incorporate analog filters for the load trace. Cheresch and McMichael point out that the appropriateness of such filters is limited, and suggest that test data be recorded and stored without any filtering. Digital filtering techniques or curve smoothing (averaging) techniques can be applied subsequently, allowing the original data to be stored in a recoverable condition. The computational capabilities of computers provides investigators with limitless possibilities, contraindicating the use of anything other than the maximum achievable resolution in the raw, unfiltered data.

In offering guidance for data evaluation, Cheresch and McMichael defined inertial effects and harmonic oscillations, or ringing, due to dynamic elastic response. Both can mask the actual mechanical response of the specimen being tested. For medium to high toughness steels, these effects are minimal except in the lower shelf domain. Often the best and most practical method of reducing both effects is to reduce the impact velocity.

D. R. Ireland [40] examined various physical aspects of the instrumented test, including a discussion of the frequency response limit of the instrumentation and how such a limit is determined. Current digital equipment generally has a frequency response of at least 100 kHz, which should be sufficient for impact test applications. Ireland also defined the three primary components of the load signal from the strain gauges on the striker, asserting that the strain gauges and the signal amplifiers and processors in common use at the time were good enough to make high frequency noise (from the 50-60 Hz range upward) irrelevant. This assertion

is even more true today. Ireland indicated that the inertial load is a function of the acoustic impedances of both the striking tup and the specimen, and that the magnitude of the inertial load is dependent upon the velocity of the tup. However, the time increment or period of the inertial loading is not noticeably affected by velocity changes. He asserted that 20 to 30  $\mu$ s is a typical duration for inertial load perturbations in aluminum and steel Charpy specimens, and that the first oscillation in the load trace should be considered to be caused by inertial effects rather than specimen mechanical response.

Ireland suggested that one should calibrate the tup load cell using dynamic loading. He described a method which utilizes specimen compliance and a low energy elastic impact technique (termed "low blow"). A paper by W. L. Server and Ireland [41] included a section detailing the procedure. As a secondary verification technique, Ireland also suggested comparing the dynamic response of a strain-rate-insensitive material to its quasi-static response. That is, the maximum load obtained in the impact test should be less than 110% of the maximum load obtained with an identical specimen using the same load cell in the same configuration loaded in a quasi-static manner; i.e.,

$$P_{\max, \text{impact}} < 1.1 P_{\max, \text{slow-bend}} \quad (24)$$

for a nominally strain-rate-insensitive material. Note that Ireland specified 3%, but later work cited in Server [21] indicated that the dynamic situation will result in nearly 10% higher loads for the typically utilized 6061-T651 aluminum alloy. The technique was recommended as a regular means of checking calibration and is not called out as a means of establishing the initial calibration.

Two papers, one by Venzi, Priest, and May [42] and the other by Saxton, Ireland, and Server [43], examine inertial effects in detail. Venzi, Priest, and May instrumented the tup, the anvils, and specimens; load traces from each of these sets of strain gages revealed significant differences in the loading of each at any given time after impact. They found that a specimen can fail by brittle fracture before any load is registered on the anvils. As a definitive verification, they tested specimens with no restraining anvils and obtained complete cleavage fracture from specimens tested at low temperatures. The inertial loading alone proved sufficient to fracture such specimens. Their results also indicate that fracture initiation cannot be generally

associated with attainment of the maximum load on the load/time record. Rather, fracture initiation occurred coincident with the maximum load for some tests, as well as substantially beyond maximum load for others. Work with an inverted loading geometry pendulum and an optical COD (Crack Opening Displacement) detector by R. Rintamaa and coworkers [44], [45] indicates that crack initiation can also significantly precede the maximum load. Other investigators [46] have reported similar results with the inverted loading geometry testing equipment. Server, Norris, and Prado [47] likewise concluded that crack initiation cannot generally be associated with the maximum load in the load/time record.

## IV. EXPERIMENTAL PROCEDURES

A detailed procedure for conducting the CVN testing is included in Appendix A. The following sections describe the essential aspects of the material and the procedures. Radiation hazard considerations are also discussed.

### A. MATERIAL

The material used was A533-B, Class I pressure vessel steel plate obtained from the Electric Power Research Institute. The composition is given in Table I. The material is representative of a pressure vessel steel often employed in nuclear reactor designs, except that the prior austenite grain size is large. The large size of the pre-quench and temper grains resulted in the steel being atypically notch sensitive. That is, the USE for the material was about half of the value that would normally be expected of A533-B plate. Likewise, the DBTT was higher than typically observed, or  $\approx 100^\circ\text{C}$ . This material was irradiated for one year to  $1 \times 10^{19}$  n/cm<sup>2</sup> at  $150^\circ\text{C}$  in the TRIGA Reactor Facility operated by the U. S. Geological Survey in Denver, Colorado.

**Table I** Composition by weight percent of the A533-B steel of this study.

C	Si	Mn	Mo	Ni	S	P	Cu
0.22	0.18	1.35	0.53	0.62	0.012	0.010	0.14

### B. TEST SPECIMENS

The dimensions of the three sizes of specimens used are given in figure 5. The orientation of the specimens was longitudinal, and the notches were precision cut by electrodischarge methods. As reported in Rosinski, et al. [31], the metallographic examination of this material indicated that it should exhibit essentially isotropic mechanical properties.

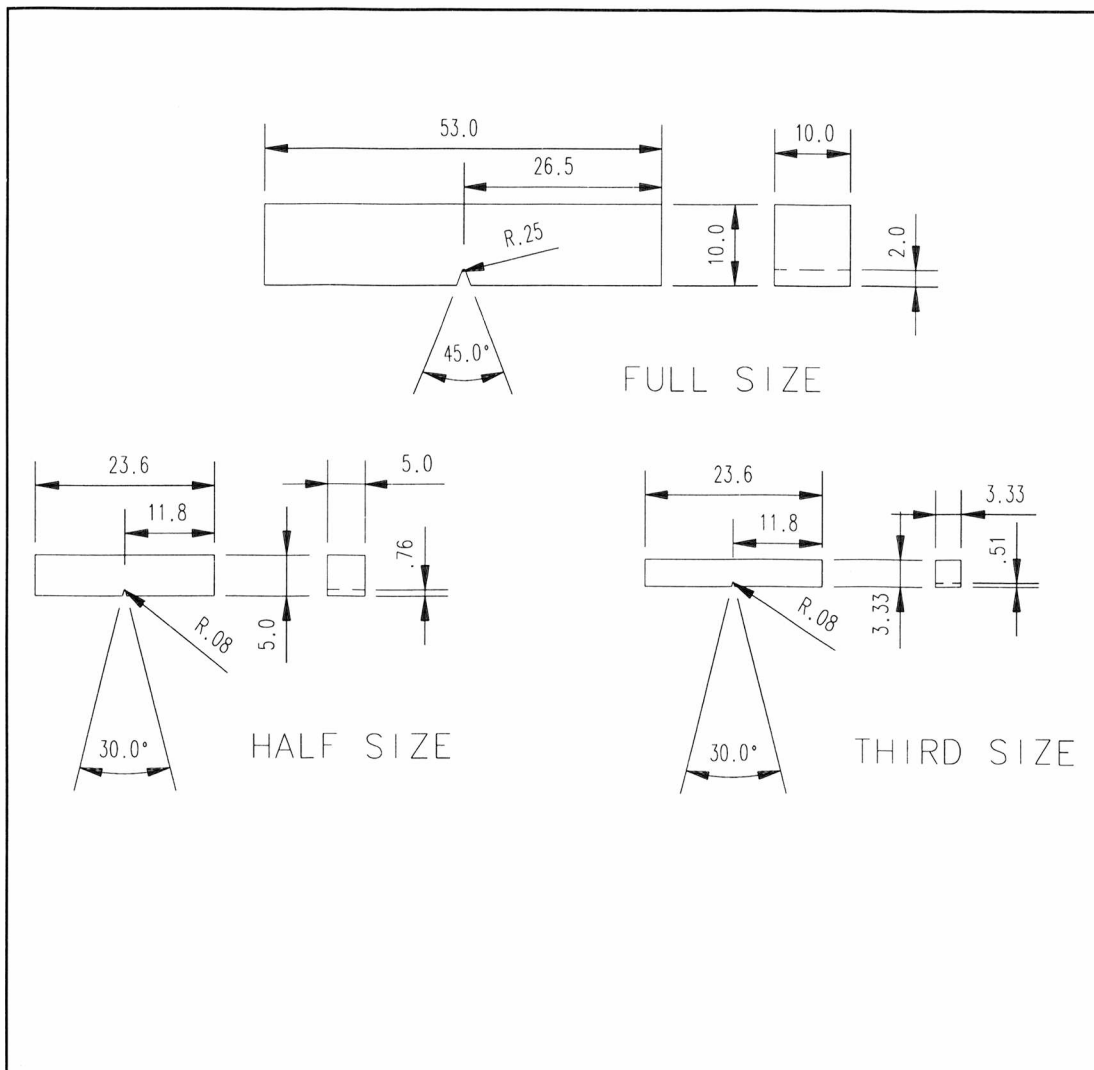


**Figure 5a.** Specimen dimensions in millimeters.

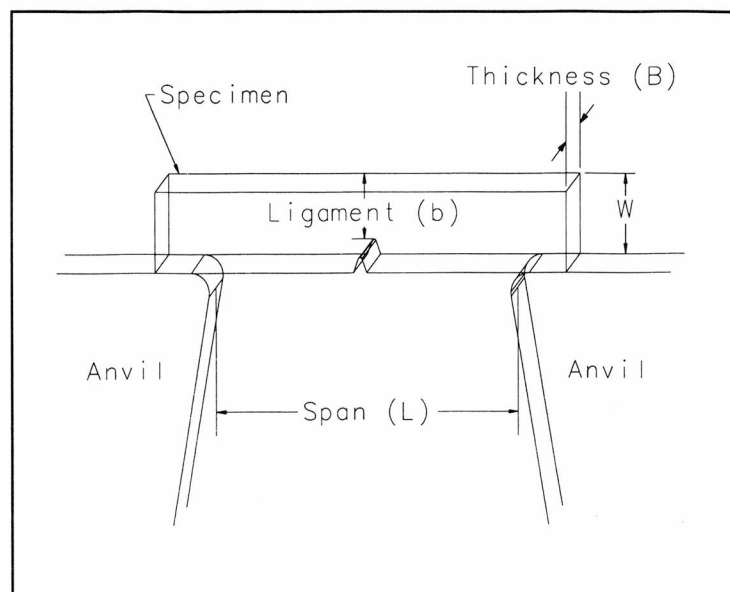


**Figure 5b.** Dimension Nomenclature.



### C. TEST EQUIPMENT

Charpy V-notch impact tests were conducted in an instrumented Dynatup model 8200 - extended height drop tower in compliance, as applicable to the drop tower and subsize specimens, with ASTM Standard Test Methods E 23 and A 370. The drop weight assembly was configured with a 10 kip (44.5 kN) striker/load cell for testing the full size specimens, and with a 3.5 kip (15.6 kN) striker/load cell for testing the subsize geometries. The support anvils were constructed such that there was a 46 mm gap and a 20 mm gap for the full size and subsize specimen geometries, respectively. Standard specimens were placed on the anvils with the longitudinal center line of the specimens centered between the drop tower guide rails. Figure 6 depicts the anvil/specimen configuration. The 10 kip striker was attached centered at the bottom of the drop weight assembly such that it met the specifications of ASTM E 23. The subsize specimens rested on the anvils just to the left of center as indicated in figure 6. The 3.5 kip striker was assembled at the bottom of the drop weight assembly such that it was the same amount to the left of center as the specimen. The center of percussion, thus, remained in the center of the striker. The 10 kip strik-

er was fitted with a removable striking tip. The geometry of the tip conformed to the specifications of ASTM E 23. The 3.5 kip striker also was fitted with a removable striking tip, but this tip was not standard. Its interior angle was  $50^\circ$  with a 3.18 mm ( $1/8^{\text{th}}$  inch) tip radius. A pneumatic triggering mechanism controlled both the position and the release of the drop weight assembly and was adjustable to about two meters. When dropped from the highest position possible, the velocity of the drop weight assembly on impact was

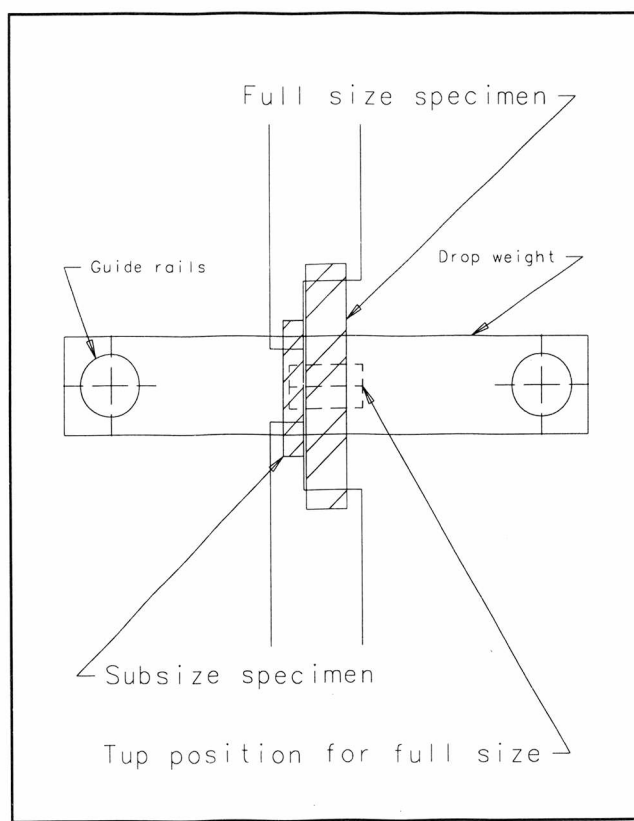


**Figure 6.** Schematic of anvil configuration with standard and subsize specimens.

$\approx 6$  m/s. The striker mass was  $15.353 \pm .007$  kg configured with the 10 kip striker/load cell, and  $14.725 \pm .007$  kg with the 3.5 kip striker/load cell.

Each striker/load cell was mounted in a hydraulic load frame and calibrated under quasi-static conditions to ensure the linearity of the cell response. Each was also used to test a series of 6061-T651 aluminum specimens in quasi-static three-point bend loading. Subsequent impact testing of additional aluminum specimens indicated that the maximum load obtained under impact loading was approximately the same as obtained in slow bend, within 10%, as indicated by Server [21]. The impact tests of aluminum specimens was conducted periodically as testing proceeded. The maximum loads obtained during the aluminum tests stayed approximately constant throughout the testing and indicated that the load cells retained calibration.

For testing, the load cell was attached to a two channel, 2 MHz sampling rate digital oscilloscope, Nicolet Model 2090-III. The frequency response was greater than 100 kHz, and it had 12 bit resolution, providing 4096 data pairs per load trace. The scope included a floppy disk storage drive on which the actual millivolts versus microseconds data were stored. The data were also downloaded to a DOS-based desktop computer.

An infrared device monitored the passage of a rigid flag attached to the drop weight assembly. As the flag passed through the device and interrupted the IR sensor, it triggered the oscilloscope to capture the load trace. A second identical oscilloscope recorded the length of time required for passage of the flag, and this time interval was input into a BASIC program that had been written to calculate the initial impact velocity,  $v_o$ , and subsequently convert the raw data to load versus displacement. The BASIC program established the average zero-load, selected 4000 of the points for eventual input into spreadsheet software, and calculated the apparent energy,  $E_a$ , from the beginning of the impact to the point where the load dropped back to zero. Using equation 5 (Section III-B) the program calculated the fracture energy for the test. The BASIC program is provided in Appendix B. The load traces were inspected and compared with the computer calculations and the selected begin and end points. If the computer calculation selections proved inappropriate, the energies were recalculated with more accurate begin and end points.

As noted, the data capture was triggered by the passage of the velocity flag through the IR sensor. Both the flag and the sensor were mounted rigidly, and both had hardware for

fine adjustment. There was no accommodation, however, for gross adjustment. Since the drop weight fell significantly farther before impact during subsize tests, an electronic timing delay circuit was added to the triggering circuitry. The circuit was adjustable to accommodate the two subsizes and velocity variations. The delay time was monitored from test to test to ensure that the impact data was collected completely. Also, since the velocity measurement was taken significantly before impact with the subsize specimens, the BASIC program calculated the velocity for subsize tests after including the extra fall distance. Friction was neglected over the distance (less than 10 cm).

Personnel in the testing area were shielded from radiation by a lead and steel enclosure approximately one meter cubed with four inch thick walls. There were horizontally rolling doors at the top that could be slid open for relatively easy access to the interior. For tests, the drop weight fell through a hole in the doors, which were closed to minimize the potential for spread of radioactive contamination. There were also small storage compartments that were lead shielded. Irradiated specimens were removed one-at-a-time from the storage, tested, and replaced. During handling, personnel exposure was minimal and was maintained at all times less than 100 mrem/hr measured 30 cm from the specimens. When not transferring specimens between storage and the test position, personnel exposure was below the measurable limit of 0.5 mrem/hr.

#### **D. TEMPERATURE CONTROL**

Test temperatures other than ambient were obtained by directing heated or chilled gas onto the specimen inside an insulated temperature conditioning chamber, or furnace. The specimen would subsequently be transferred to the anvils. Specimens were placed onto a loading track by hand. Full size specimens rested in a groove in the center of the track, subsize specimens rested in a second groove located just to the left of center. A pneumatic ram was utilized to push the specimen into the furnace.

For heating, helium or argon was passed through a flow-through gas heater rated for 760°C maximum outlet temperature. The system can provide stable temperature control of the specimen up to 400°C. When argon was found to provide inadequate cooling for the heater element, testing continued with helium. The argon also did not provide temperatures greater

than 280°C. A continuous readout of the furnace temperature was provided by a digital display of a type-K thermocouple located near the specimen position inside the furnace. The specimen temperature that corresponded to the furnace temperature was determined during repeated calibration runs with instrumented specimens of each size. The calibration procedure also allowed establishment of nominal set points of the gas temperature and flow rate for desired specimen test temperatures. For each specimen size, the instrumented specimen was positioned in the furnace in the same configuration as impact test specimens, and the flow rate and gas temperature were set to the desired levels. Data were collected during heat-up until the temperature had stabilized for three minutes. Further data were collected by repeatedly increasing the gas temperature, flow rate, or both. Plotting the temperature data established the straight line relationships shown in Appendix C between the actual specimen temperature and the furnace temperature.

Type-K thermocouples were spot welded to specimens as shown in figure 7. There were four junctions on the full size specimen and the half size specimen and two on the third size specimen. The thermocouple readings indicated significant gradients during heat-up of the full size and half size specimens, but they converged to within 2°C of the mean after the temperature stabilized. Repeated calibration runs have demonstrated good reproducibility and linearity.

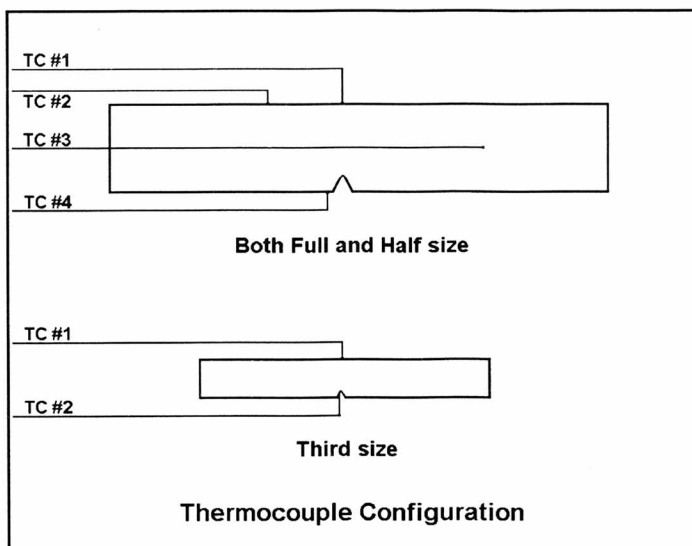


**Figure 7.** Approximate thermocouple (TC) configuration for the temperature calibration specimens. Full and half size were the same. Third size had only 2.

The apparatus for chilling specimens to below room temperature passed nitrogen gas through a heat exchanger filled with liquid nitrogen. The chilled gas then flowed into the furnace, as with heating. The heat exchanger was sufficiently efficient to partially liquefy the nitrogen gas. Thus, specimens could be chilled to approximately -196°C, the nominal gas

temperature. Temperature calibration runs with each of the instrumented specimens again provided the specimen temperature that corresponded to a given furnace temperature, but since the gas temperature could only be controlled at the boiling point, test temperatures were obtained by chilling to at least 50°C below the desired test temperature before allowing the furnace and specimen to warm back up to that temperature for testing. Once the furnace temperature readout indicated the required temperature, the gas flow was cut off, and the system was held in a quasi-static state to ensure equilibrium warming conditions. As shown in Appendix C, the relationships between the actual specimen temperature and the furnace temperature were dependent on how cold the system was driven before warming, and the relationships were not straight lines. Still, repeated calibration runs have demonstrated good reproducibility with this warm-up method.

Once the desired test temperature was achieved, the pneumatic ram would push the specimen out of the furnace and onto a motorized positioning arm that placed the specimen on the anvils in the testing position. The arm was driven by a computer controlled DC stepping motor. Testing personnel observed the positioning and triggered the drop weight release as soon as the specimen was resting on the anvils. The positioning arm in its neutral position closed a fail-safe circuit. Premature release of the drop weight was thus averted while the positioning arm was in motion. The time interval between the exit of the specimen from the temperature conditioning chamber and the impact averaged less than three seconds for all tests.

## V. DATA REDUCTION

The primary data sought in this study are the upper shelf energy (USE) and the ductile to brittle transition temperature (DBTT) for each of the three specimen sizes for the A533-B steel examined. Individual tests consist of a large set of load versus time data. This section describes the method used to reduce these sets of data to absorbed energy values and the subsequent determination of the USE and DBTT.

During the impact test the raw data consists of the output of the load cell mounted on the striker as a function of time. The load cell output was in millivolts. The millivolt signal was recorded as a function of time with the digital oscilloscope described in Section IV-C. The time of passage of a velocity flag of known dimension was recorded. A computer program (Appendix B) was utilized to calculate the velocity and convert the time data to displacement in millimeters. The BASIC program also contained the load cell calibration factor and converted the millivolt data to kilonewtons. The area under the load/displacement curve is the apparent absorbed energy,  $E_a$ , in joules. The program numerically integrated the area by simple rectangular quadrature. The implicit assumption of the method is that the velocity is constant throughout the fracture event. Since the velocity actually decreases throughout the fracture event, the apparent absorbed energy is greater than the actual absorbed energy. The following subsection discusses the equations for calculation of the true absorbed energy. The second subsection discusses the mathematical treatment of the energy versus temperature data and curve fitting.

### A. CALCULATION OF THE TRUE ENERGY FROM THE APPARENT ENERGY

The apparent absorbed energy value,  $E_a$ , derived from the load/time record is related to the actual absorbed energy,  $E_d$ , by

$$E_d = E_a \left( 1 - \frac{E_a}{4E_o} \right). \quad (5)$$

$E_a$  is obtained by integrating the load versus time curve, and  $E_o$  is the kinetic energy of the drop weight at impact,  $1/2 \cdot m \cdot v_o^2$ .  $E_a$  is calculated as

$$E_a = v_o \int_0^{\tau} P dt, \quad (14)$$

where  $v_o$  is the initial striker velocity at impact,  $P$  is the load at time  $t$ , and  $\tau$  is the total time interval of the impact event.  $\tau$  is determined nominally from the load/time record as the time interval between initial loading and the point where the average load returns to zero. Section III-B discusses the relationship between  $E_d$  and  $E_a$  more thoroughly.

The actual energy,  $E_d$ , was calculated from the apparent energy,  $E_a$ , for all tests. Then  $E_d$  as a function of the test temperature was fitted with a hyperbolic tangent function to determine the USE and DBTT as described below.

## **B. CURVE FITTING**

The  $E_d$  values and the corresponding test temperatures were input into a Jandel Scientific curve fitting application, *TableCurve*<sup>TM</sup> (v1.12). The fitting procedure was iterative, and it determined a true least-squares solution. It used the Levenburg-Marquardt procedure [48] for finding the global minimum of the  $\chi^2$  sum of deviations. The Levenburg-Marquardt procedure requires matrix inversion with each iteration, and *TableCurve*<sup>TM</sup> utilized the Gauss-Jordan method [49] for the inversion. For each of the CVN data series, a four parameter hyperbolic tangent function was found to fit well, with an  $r^2$  value near unity and a large *F-statistic* (a measure of the extent to which the equation represents the data). The actual equation fit to the data was

$$E = a + b \cdot \tanh[c(T - d)] \quad (25)$$

where  $E$  is the absorbed energy,  $(a + b)$  is the curve maximum and taken as the USE,  $c$  determines the slope of the transition region,  $d$  is the midpoint (inflection point) of the curve and taken as the DBTT, and  $T$  is temperature. The regression analysis adjusted all four coefficients during the determination of the best fit to the data. If the DBTT of a material approaches the maximum temperature capabilities of the testing equipment, the result may be

a data set with upper shelf tests at temperatures too low to clearly define the shelf portion of the curve. It may appear that the absorbed energy values are still rising with temperature. If, however, the specimens tested at the highest temperatures each exhibit large deformations and 100% ductile tearing, the USE is approximately equal to the average absorbed energy of these specimens.

### C. NORMALIZATION FACTOR

The position presented in this thesis is that the results of tests conducted on subsize specimens are correlated by a normalization factor to the results of tests conducted on full size specimens. The ratio of the normalization factors calculated for the full size and the subsize specimens can be used as a scaling factor. Doing so allows direct prediction of the USE of full size specimens from the data of subsize specimens. Also, the scaling factor can be applied to the individual data points from subsize specimen test sets, and subsequent least-squares regression to the data provides an estimate of the entire full size CVN transition curve.

In developing the normalization factor, it was assumed that this factor should be based on the physical dimensions of the specimen. Various factors have been proposed for comparing USE values from different size specimens, and these factors were discussed in Section III. Dividing the USE by the cross section under the notch tends to consider only the energy required to create the two fracture surfaces and discounts both the three dimensional nature of the fracture process and the triaxial state of stress. Dividing by a volume is appropriate, but a simple volume normalization is applicable only for a narrow range of full size USE values. The unsupported span dimension of the test specimen significantly affects the test results, as indicated by the results of Corwin and Houglund [23]. The geometry of the notch strongly affects the DBTT of a CVN transition curve for a given material, and also the notch depth strongly affects the USE of a CVN transition curve for a given material, but the notch angle and root radius are not as significant, relative to the notch depth, as indicated by the work of Kurishita and coworkers [26]. A successful normalization factor would then be expected to at least include the following physical dimensions:

- a fracture volume determined by  $B$  and  $b$ , e.g.,  $Bb^2$  or  $(Bb)^{3/2}$



- the length of the unsupported span
- some representation of the notch geometry, e.g., a stress concentration factor.

The normalization factor employed was first proposed by Loudon and coworkers [28]. It is modified by a plastic constraint factor,  $K_{\sigma(p)}$ . The normalization factor is

$$N.F. = \frac{Bb^2}{K_t K_{\sigma(p)} L} \quad (26)$$

where  $B$ ,  $b$ , and  $L$  are the specimen thickness, ligament, and span respectively and  $K_t$  is the elastic stress concentration factor.

The nominal fracture volume, the span length, and  $K_t$  are each dependent only on the initial specimen dimensions. According to Tetelman and McEvily [18], for an elastic/perfectly-plastic material with no strain hardening, the maximum value  $K_{\sigma(p)}$  can achieve is dependent only on the initial specimen dimensions, specifically, the notch angle, and

$$K_{\sigma(p)}^{\max} = 1 + \frac{\pi}{2} - \frac{\omega}{2} \quad (27)$$

where  $\omega$  is the interior angle of the notch in radian measure (and  $\pi$  is 3.14...).  $K_{\sigma(p)}$  has been successfully employed in physical calculations of material parameters by Lucas et al. [11].

$K_t$  was calculated with the equations of Neuber [17], and  $R$  is the notch root radius.

$$K_t = \frac{2\left(\frac{b}{R} + 1\right) - f\left(\frac{b}{R} + 1\right)^{1/2}}{\frac{4}{g}\left(\frac{b}{R} + 1\right) - 3f} \quad (28)$$

$$f = \frac{2\left(\frac{b}{R} + 1\right)\left(\frac{b}{R}\right)^{1/2}}{\left(\frac{b}{R} + 1\right)\arctan\left[\left(\frac{b}{R}\right)^{1/2}\right] + \left(\frac{b}{R}\right)^{1/2}} \quad (29)$$

$$g = \frac{4\left(\frac{b}{R}\right)^{1.5}}{3\left(\frac{b}{R}\right)^{1/2} + 3\left(\frac{b}{R} - 1\right)\arctan\left[\left(\frac{b}{R}\right)^{1/2}\right]} \quad (30)$$

## VI. RESULTS

The load record of the impact tests provided the data presented in Tables II - VII. The tables list two energy values: the apparent energy,  $E_a$ , and actual energy,  $E_d$ , absorbed by the specimen in fracture. The test temperature and the striker velocity at impact are also included. The procedure for calculating  $E_d$  from  $E_a$  is explained in Section V-A.

Tables II, III, and IV list the data for unirradiated full, half, and third size specimens, respectively.

**Table II** Test data for full size, unirradiated specimens.  
(Striker mass 15.35 kg)

Temperature (°C)	Apparent Energy ( $E_a$ -- J)	Velocity (m/s)	Actual Energy ( $E_d$ -- J)
-102	1.86	3.61	1.85
-40	2.88	"	2.86
23	11.82	"	11.47
60	32.71	"	30.04
96	32.83	"	30.14
122	43.23	"	38.56
149	50.87	"	44.40
158	69.90	"	57.69
172	81.92	"	65.15
195	75.85	"	61.47
242	65.13	"	54.53

The 158°C test was the first one on the upper shelf for the full size, unirradiated specimens. The 172°C test was the highest energy test at 65.15 J. Comparing the apparent and actual energy columns, it can be seen that  $E_d$  is close to  $E_a$  for low energy tests.  $E_a$  can be substantially larger than  $E_d$ , however, for the large energy values.

**Table III** Test data for half size, unirradiated specimens.  
(Striker mass 14.73 kg)

Temperature (°C)	Apparent Energy ( $E_a$ -- J)	Velocity (m/s)	Actual Energy ( $E_d$ -- J)
-87	1.35	3.73	1.35
24	1.87	3.73	1.86
62	3.19	3.73	3.17
102	5.57	3.73	5.49
152	9.80	3.72	9.56
203	12.55	3.72	12.16
255	13.30	3.72	12.87

The trend of  $E_a$  and  $E_d$  being nearly equal at low energy values but  $E_a$  being larger than  $E_d$  at the higher energy values is seen to hold in each of the data sets. Table III indicates that upper shelf behavior begins with the test at 203°C. The 255°C test is highest for the half size, unirradiated, with an actual energy of 12.87 J. The regression for this set of data is remarkable. The scatter of the data is exceptionally low. The scatter of the other data sets is normal for CVN data.

From table IV, the highest energy test of 4.70 J for the third size, unirradiated specimens was at 184°C. This test was also the lowest temperature test to appear on the upper shelf. The relatively low USE values of this specimen set did not alter the overall trends with respect to temperature.

**Table IV** Test data for third size, unirradiated specimens.  
(Striker mass 14.73 kg)

Temperature (°C)	Apparent Energy ( $E_a$ -- J)	Velocity (m/s)	Actual Energy ( $E_d$ -- J)
-88	0.14	3.74	0.14
-32	0.44	3.74	0.44
25	0.78	3.73	0.78
66	1.84	3.74	1.83
103	2.35	3.74	2.34
159	3.39	3.73	3.36
184	4.76	3.74	4.70
210	4.59	3.73	4.54
259	4.32	3.73	4.27

The data from the specimens irradiated at 150°C to  $1 \times 10^{19}$  n/cm<sup>2</sup> ( $E > 1$  MeV) follow in tables V, VI, and VII, respectively, for the full, half, and third size specimens.

The data presented in table V indicate that the full size specimens, after irradiation, appear to begin the upper shelf behavior with the 212°C test. The highest energy value was obtained at 226°C, specifically, 55.71 J. The tests at 212°C and at 343°C indicate how the constant velocity assumption for determination of  $E_a$  can affect the data.  $E_a$  for the 212°C test was 52.10 J, and  $E_a$  for the 343°C test was 52.00 J. But  $E_d$  was 47.64 J and 49.58 J, respectively, for the two tests. The larger difference between the apparent energies and actual energies at 212°C is due to the reduced impact velocity. The sparse data at lower temperatures is due to the availability constraints of irradiated specimens and the fact that the unirradiated DBTT for this material was relatively high.

**Table V** Test data for full size, irradiated specimens.  
(Striker mass 15.35 kg)

Temperature (°C)	Apparent Energy ( $E_a$ -- J)	Velocity (m/s)	Actual Energy ( $E_d$ -- J)
24	2.89	5.98	2.88
161	33.40	3.68	30.71
181	26.84	4.45	25.66
203	30.88	4.46	29.32
212	52.10	4.45	47.64
226	62.02	4.46	55.71
239	44.30	4.32	40.87
251	49.10	4.47	45.16
294	57.55	4.46	52.12
343	52.00	6.03	49.58

**Table VI** Test data for half size, irradiated specimens.  
(Striker mass 14.73 kg)

Temperature (°C)	Apparent Energy ( $E_a$ -- J)	Velocity (m/s)	Actual Energy ( $E_d$ -- J)
-50	0.43	3.70	0.43
22	0.75	3.71	0.75
100	1.72	3.70	1.71
164	3.85	3.70	3.81
190	6.55	3.70	6.44
221	7.73	3.70	7.58
231	8.26	3.70	8.09
254	10.98	3.71	10.68
267	12.44	3.76	12.07
298	10.73	3.70	10.44
376	10.40	3.73	10.14

The irradiated half size specimen data covers the broadest temperature range. The data cover a 426°C interval. Upper shelf behavior seems to begin with the 254°C test. The 267°C test absorbed a substantially higher energy considering the relatively small temperature difference between the two tests. The fracture surface of the 190°C test comprised very nearly 50% ductile rupture. The steep slope of the transition region of this data set is apparent in the tabulated data.

**Table VII** Test data for third size, irradiated specimens.  
(Striker mass 14.73 kg)

Temperature (°C)	Apparent Energy ( $E_a$ -- J)	Velocity (m/s)	Actual Energy ( $E_d$ -- J)
-50	0.13	3.71	0.13
22	0.46	"	0.46
71	0.53	"	0.53
114	1.54	"	1.53
144	1.43	"	1.42
164	1.78	"	1.77
175	1.87	"	1.86
247	3.14	"	3.12
260	3.81	"	3.77
285	4.14	"	4.10
307	3.77	"	3.73
322	3.88	"	3.84

The table VII data for the third size, irradiated specimens, also spans a large temperature interval, and the absorbed energy values rise relatively linearly with the test temperature. The slope of the data in table VII is much less steep than the slope of the data in table VI. The specimen tested at 247°C was deformed severely and the fracture surface was mostly ductile

rupture, but the 260°C test was the lowest temperature test on the upper shelf. The 285°C test showed the highest absorbed energy at only 4.10 J.

A few data points were excluded as outliers. The exclusions did not greatly alter the coefficients of the best fit equations, with one exception. An excluded point in the transition region of the half size, irradiated data increased the indicated DBTT from 187°C to 202°C. The lower value seems to represent the data better than the higher value.

Curve fitting of the data in each table provided the values of USE and DBTT. Table VIII presents the USE values for the three specimen sizes in both the unirradiated and irradiated conditions. The ligament under the notch is relatively longer in the half and third size specimens. That is, the ratio of the ligament length,  $b$ , to the specimen thickness,  $B$ , is 0.80 for the full size specimens and 0.85 for the subsized specimens. The fact does not appear to be significant in this instance. In the table, the ratio of unirradiated USE to irradiated USE, given in the ratio column, shows that this ratio seems to be independent of specimen size.

**Table VIII** Upper shelf energy values.

Size	Unirradiated USE (J)	Irradiated USE (J)	Ratio	Shift (J)
Full	63.4	52.0	1.22	-11.4
Half	13.2	11.1	1.19	-2.1
Third	4.7	4.0	1.18	-0.7

Table IX presents the DBTT for each specimen condition.

**Table IX** Ductile to brittle transition temperatures.

Size	Unirradiated (°C)	Irradiated (°C)	Shift (°C)
Full	88	164	+76
Half	122	187	+65
Third	100	170	+70

It is noted that the DBTT of the full size, unirradiated specimens is well above room temperature. Also, comparing the full, half, and third size specimens, the difference between full and half is 34°C, and between half and third the difference is -22°C. The trend is the same for the irradiated specimen DBTTs, but the magnitude of the differences is reduced; 23°C and -17°C, respectively. The irradiation induced shift in the DBTT appears to be independent of specimen size and is about +70°C for each of the three sizes.



## VII. DISCUSSION

Figures 8 - 10 present the absorbed energy data graphically. Each figure shows the radiation response of the material by comparing the unirradiated and irradiated specimen data for a given size. Irradiation causes the DBTT to shift to a higher temperature and the USE to shift to a lower energy. Each curve in the figures is the best fit hyperbolic tangent function for the respective data. The regression equations and statistics are provided in Appendix D. The statistical parameters, such as an  $r^2$  value approaching unity and a large value for the *F-statistic*, indicate good fits to the data.

The appearance of the fracture surface of a tested specimen provides information on the mode of failure of the specimen. Examination of the fracture surface readily establishes whether or not a given specimen failed in a fully ductile mode. Test specimens that failed by fully ductile tearing can be definitively placed on the upper shelf. Likewise for the DBTT, tests conducted near the transition temperature will exhibit mixed ductile and brittle fracture in roughly equal proportions. Individual fracture surfaces were compared to a chart from ASTM E 23 to estimate the percentage of the fracture surface which failed in a ductile mode.

The USE values were taken as equal to the sum ( $a + b$ ) in the best fit hyperbolic tangent equation discussed in Section V-B. The USE is also equal to the maximum value of the best fit curves, with one exception. The curves in figures 8 - 10 each appear to establish the upper shelf at approximately the average energy value of the highest temperature tests. The best fit curves represent the first five data sets in all respects. For the sixth data set, the third size, irradiated specimens, the best fit curve rose well above the average energy of the highest temperature tests, which were on the upper shelf. Each of the four specimens failed by either fully ductile tearing or by excessive deformation without breaking apart. Therefore, the USE for the third size, irradiated specimens was taken as 4.0 J, the average value of these highest temperature tests. It appears that the regression would require more data at higher temperatures in order to properly fit the upper shelf in this instance. The lack of additional irradiated specimens precluded this possibility.

Since the energy scales in figures 8 through 10 expand as the specimen sizes decrease, the figures provide a relative comparison. Preliminary examination indicates that each size

had a comparable relative response to irradiation, as was indicated by the data of tables VIII and IX. Examining figure 8 and comparing to figure 9, it is noted that the slope of the curves in the transition region are steeper for the half size data. The increase in the severity of the transition region seems consistent with the increased severity of the notch in the half size specimen. Comparing figure 9 to figure 10, the slope of the curves in the transition region decreases. The elastic stress concentration factor,  $K_t$ , which is different for each of the three specimen sizes, may account, in part, for the observed changes in the slope of the transition region. The values of  $K_t$  for full, half, and third size specimens are 4.81, 6.09, and 5.03, respectively. Other factors that may affect the transition region are span and the degree of constraint. It appears that  $K_t$ , which represents the effects of the notch, is dominant over the other factors.

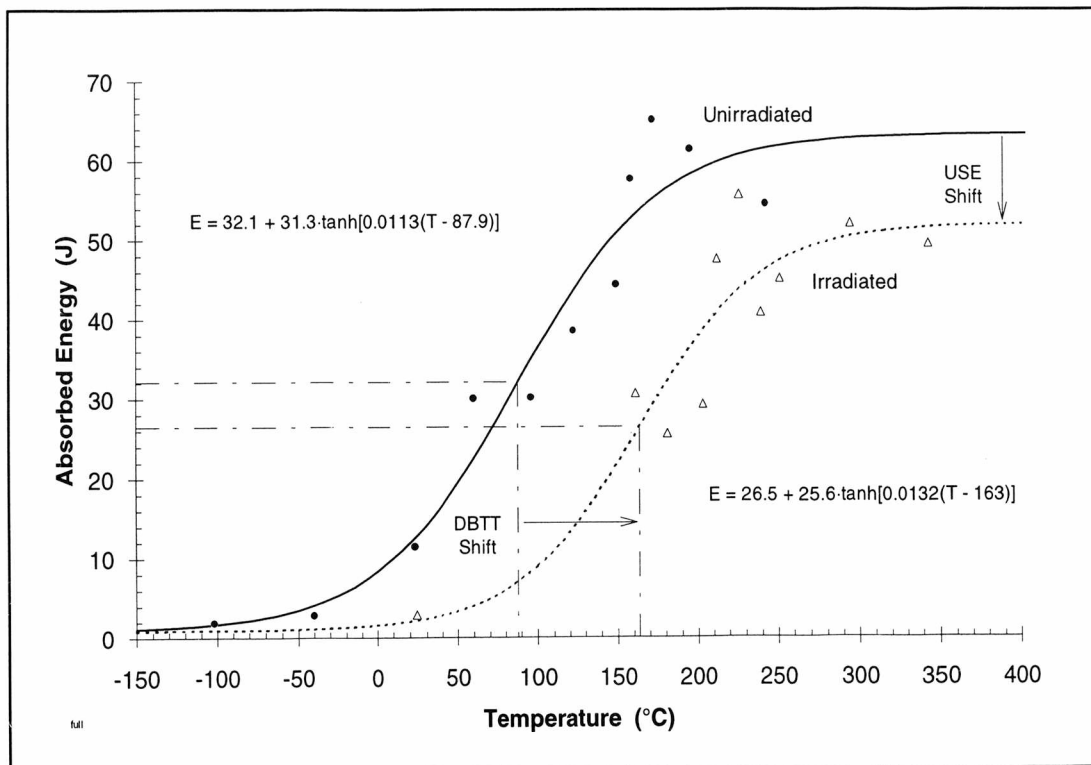


**Figure 8.** Comparison of the data of full size, unirradiated and irradiated specimens and the respective best fit curves showing the effect of irradiation.

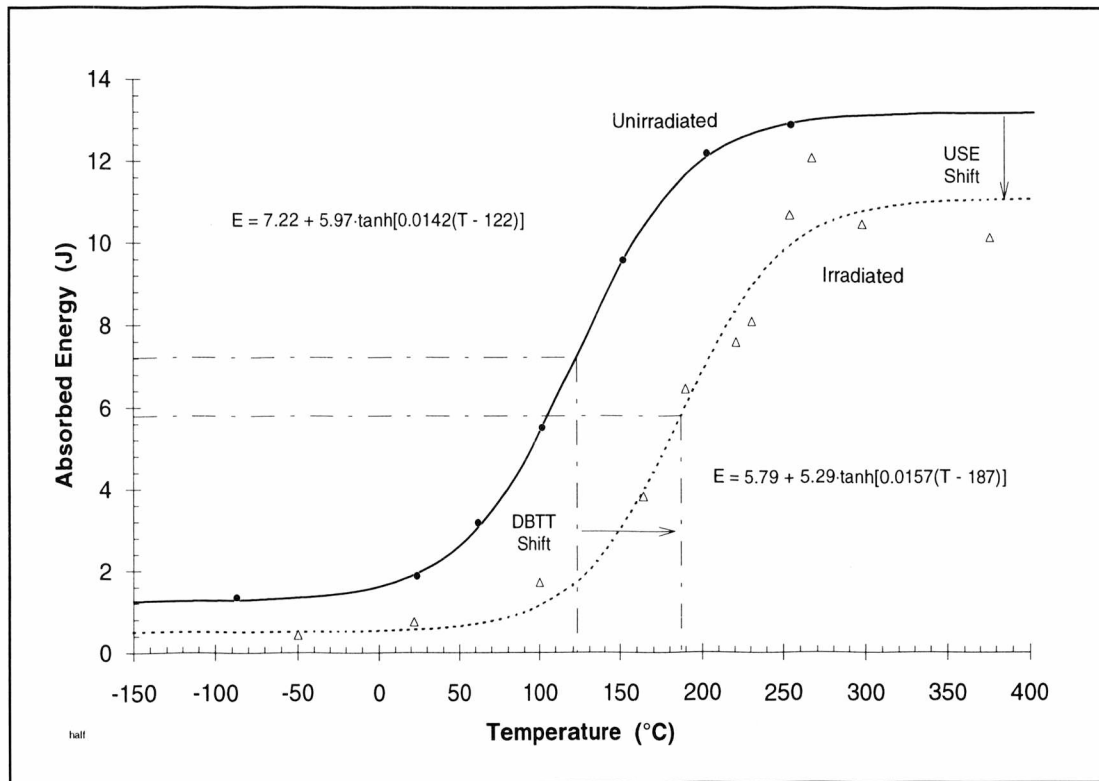


**Figure 9.** Comparison of the data of half size, unirradiated and irradiated specimens and the respective best fit curves showing the effect of irradiation.

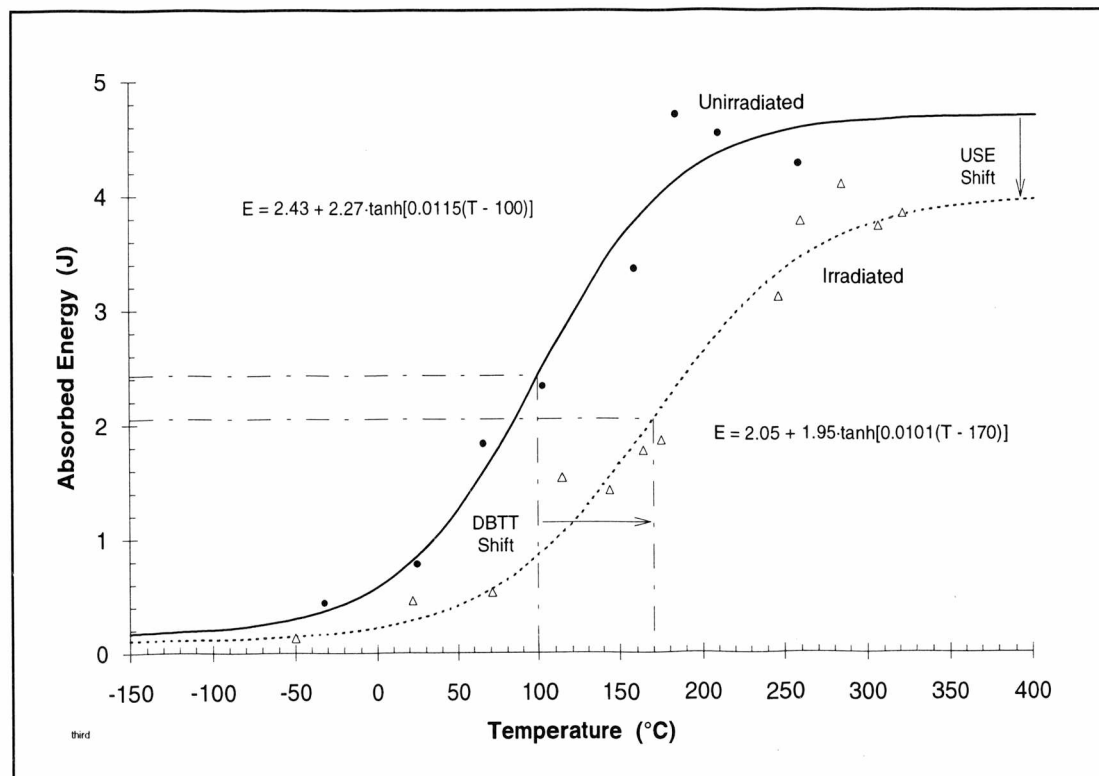


**Figure 10.** Comparison of the data of third size, unirradiated and irradiated specimens and the respective best fit curves showing the effect of irradiation.

The DBTT values were taken as equal to  $d$  in the best fit hyperbolic tangent equation (Section V-B). The DBTT lies at the inflection point of the best fit curves for each size and irradiation condition. Referring again to the third size, irradiated specimen data, adjusting the USE to a lower level affected the DBTT indicated by the best fit curve. Lowering the USE also lowered the DBTT from 186°C to 170°C. Note that the effect is attributable to the shift of the inflection point along the transition portion of the curve with the USE. However, the slope and position of the transition portion of the best fit curve was little affected by the reduction of the upper shelf. The third size, irradiated specimen data points near the curve inflection point were each of mixed ductile and brittle fracture ( $\approx 50/50$ ). Based on fracture appearance criteria the DBTT would be chosen in the neighborhood of 170°C rather than 186°C.

Comparing the DBTTs indicated in figures 8 - 10, the DBTT values of the half size specimens are higher than the full size specimens, but lower than the third size. The trend follows that which was noted regarding the slope of the curves. The indication is that there are two important effects of reduction in specimen size and of increase in notch geometry severity. These two effects tend to counter each other.

To compare the USE values of the different size specimens, the USE values were divided by a normalization factor, discussed in Section V-C, given as

$$N.F. = \frac{Bb^2}{K_t K_{\sigma(p)}^{max} L} \quad (26)$$

where  $B$  and  $b$  are the specimen thickness and ligament length, respectively;  $K_t$  is the elastic stress concentration factor,  $K_{\sigma(p)}^{max}$  is the maximum value of the plastic stress concentration factor (the plastic constraint), and  $L$  is the unsupported span length (the anvil gap). The factor has units of area.

The specimen parameters needed to calculate the normalization factors for each size are summarized in the following table.

**Table X** Specimen parameters for calculation of the normalization factor.

Size	Span, L (mm)	Thickness, B (mm)	Ligament, b (mm)	Notch angle (radian)	Root Radius (mm)	$K_t$	$K_{\sigma(p)}$
Full	46	10	8	0.785	0.25	4.81	2.18
Half	20	5	4.24	0.524	0.08	6.09	2.83
Third	20	3.33	2.82	0.524	0.08	5.03	2.83

In Table X,  $K_t$  was calculated utilizing equations 28 - 30, Section V-C.  $K_{\sigma(p)}$  was calculated by equation 27.

Table XI indicates the closeness of the normalized USE values for the different sizes. The normalized USE values of the half and third size, unirradiated specimens are greater than the full size, unirradiated values by  $\approx 6\%$ . For the irradiated specimens, the half and third size values are 8.7% and 9.7% greater, respectively, compared to the full size values. In each case the estimate is larger than the actual value, but the estimate is well within the general scatter expected for CVN data. The normalization appears to be successful. That is, after normalization the USE is independent of the specimen size.

**Table XI** Comparison of the normalized USE values.

Size	Unirradiated USE (J)	Normalized USE (J/mm <sup>2</sup> )	Irradiated USE (J)	Normalized USE (J/mm <sup>2</sup> )
Full	63.4	47.8	52.0	39.2
Half	13.2	50.6	11.1	42.6
Third	4.7	50.5	4.0	43.0

Assuming that the normalized USE values are independent of size, we have

$$\frac{USE_{Full}}{NF_{Full}} \approx \frac{USE_{Subsize}}{NF_{Subsize}} \quad (31)$$

and

$$USE_{Full} \approx USE_{Subsize} \cdot \frac{NF_{Full}}{NF_{Subsize}} \quad (32)$$

Thus the ratio of the normalization factors can be utilized as a scaling factor. With this scaling factor, the USE of full size specimens can be predicted from the USE determined for subsize specimens. Table XII includes the predicted full size USE values compared to the measured full size USE. The percent deviation is included also.

**Table XII** Comparison of USE estimate from subsize USE.

Size	Predicted Unirradiated USE (J)	Actual Unirradiated USE (J)	Deviation of Estimate from Actual Value
Half	67.1	63.4	+ 5.8%
Third	67.1	63.4	+ 5.8%
	Predicted Irradiated USE (J)	Actual Irradiated USE (J)	Deviation of Estimate from Actual Value
Half	56.5	52.0	+ 8.7%
Third	57.1	52.0	+ 9.8%

The scaling factor can be applied to the individual data points as well. Figures 11 and 12 reproduce the full size specimen data from figure 8, but with the addition of the normalized half size and third size data, respectively. The open data points in these two figures represent the subsize data multiplied by the appropriate scaling factor. That is, each energy value was scaled by the ratio of normalization factors (full-size/half-size, or full-size/third-size). The curves for the full size specimen data (thin lines) are the same as in figure 8, and the curves fit to the normalized subsize data were fit in the same manner as the other best fit curves presented.

These best fits to the normalized data provide another means of predicting the response of full size specimens from the data of subsize specimens.

Tables XIII and XIV summarize the values taken from the normalized data best fit curves in figures 11 and 12. Comparing table XIII to table XII indicates that the predictions of both methods are essentially the same. The predictions based on the half and third size, unirradiated data are the same in the two tables. The predictions based on the data from the half and third size, irradiated specimens from table XIII are 0.5% and 3.7% less, respectively, than the corresponding values listed in table XII. The measured irradiation induced shift of the USE from the full size specimens of -11.4 J is matched favorably by the predicted values. The shift predicted from the half size specimen data is  $\approx 5\%$  less than the measured shift. The shift predicted from the third size specimen data is  $\approx 5\%$  greater than the measured shift.

**Table XIII** Predicted USE values obtained from the best fit curves fit to the normalized subsize data.

Size Basis	Predicted Unirradiated USE (J)	Predicted Irradiated USE (J)	USE Shift Based on Predictions (J)
Half	67.0	56.2	- 10.8
Third	67.0	55.0	- 12.0

The data normalization and subsequent regression did not alter the DBTT values. Examining table XIV and comparing to table IX, the DBTT for each size and irradiation condition is seen to be the same within one or two degrees.

**Table XIV** Predicted DBTT values obtained from the best fit curves fit to the normalized subsize data.

Size Basis	Predicted Unirradiated DBTT ( $^{\circ}\text{C}$ )	Predicted Irradiated DBTT ( $^{\circ}\text{C}$ )	DBTT Shift Based on Predictions ( $^{\circ}\text{C}$ )
Half	123	189	+ 66
Third	100	168	+ 68

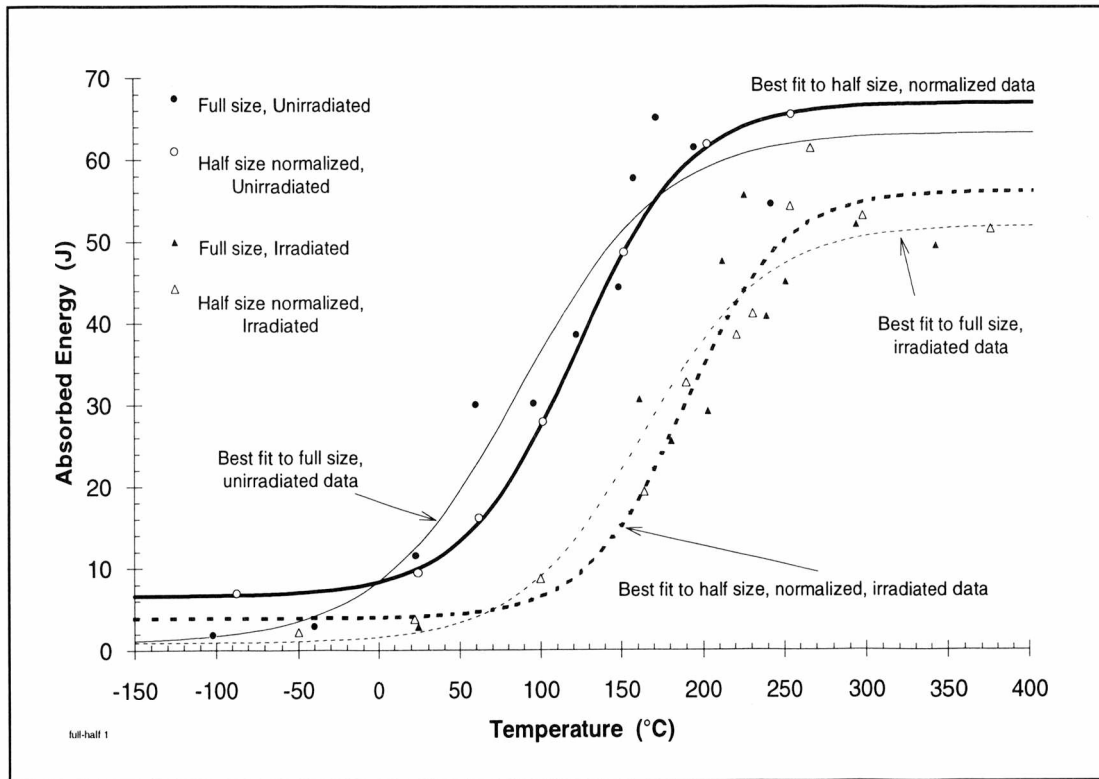


Figure 11. Measured full size specimen data versus normalized half size specimen data.

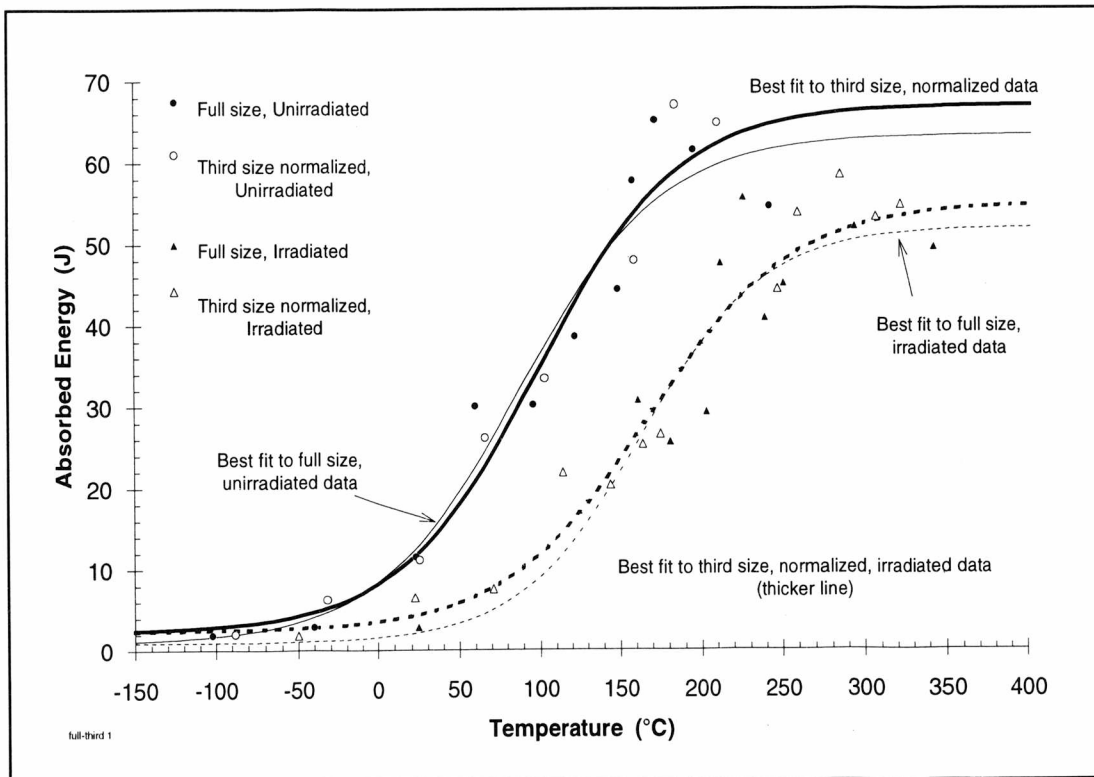


Figure 12. Measured full size specimen data versus normalized third size specimen data.



## VIII. CONCLUSIONS

The Charpy V-notch impact test has been utilized to examine a notch sensitive A533-B steel plate material. The tests were conducted to study size effects and to investigate a possible correlation between the data from subsize specimens and the data of standard full size specimens.

For this A533-B steel plate material:

- The USE values derived from full size specimen data were closely predicted by subsize specimen data when the USE was normalized by a factor  $[(B \cdot b^2)/(K_t \cdot K_{\sigma(p)} \cdot L)]$ . This factor includes the specimen volume under the notch, the unsupported span length, and the product of the elastic and the plastic stress concentration factors.
- The predicted USE values were within the typical scatter of CVN data. The predicted values were greater than the measured values; less than 6% greater for the unirradiated cases, and less than 10% greater for the irradiated case.
- The relative shift in the USE due to irradiation to  $1 \times 10^{19}$  n/cm<sup>2</sup> ( $E > 1$  MeV) was nearly the same for each of the three specimen sizes. The ratios of the unirradiated USE to the irradiated USE for both of the subsize specimen data sets were approximately equal to that for the full size specimen data.
- When the absorbed energy data from subsize tests were multiplied by the ratio of the full size to the subsize normalization factors, regression provided a best fit curve to the normalized data which approximated the best fit curve for the actual full size data.
- The radiation induced shift in the DBTT was relatively independent of specimen size, within 15%. The shifts were +76°C, +65°C, and +70°C for full, half, and third size specimen data, respectively.

**APPENDIX A**

**DETAILED PROCEDURE FOR CONDUCTING CVN TESTS WITH**

**THE DROP TOWER**

## EQUIPMENT DESCRIPTION

### **Temperature control equipment (including gas flow control)**

The temperature of interest is achieved by directing heated or chilled gas at the test specimen inside an insulated chamber. The components of the temperature control system are:

- a) Two gas bottle manifolds in 12A supply gas to 11A. Both manifolds are connected to similar two-headed regulators. One gauge reads the current bottle pressure; the other reads the pressure on the lines to the labs. Gas pressure into 11A should be  $\approx 150$  psi to ensure adequate pressure in 11A.

The three bottle manifold against one wall supplies nitrogen or helium. The operator must maintain control of which gas is installed. Nitrogen is used for chilling and helium is used for heating. Helium purity is not relevant for testing; moisture in the nitrogen can result in freeze-up of the gas lines or the specimen becoming stuck by ice.

The five bottle manifold on the opposite wall supplies argon to multiple labs. Argon is inadequate for heating in this system since it does not protect the heating element. Argon in 11A is used only for the in-cell impact testing system.

- b) Tubing from the two manifolds joins at a T to a single line on the north wall of 11A, across from the hot cell window. The lines are labeled "NITROGEN" and "ARGON". The line labelled NITROGEN is also used to supply helium.
- c) The single gas line leads to the south wall of the hot cell where it is labelled "TESTING GAS" and is valved with a needle valve and a pressure regulator valve at about eye level. These are left fully open during testing since neither of them is used to control the gas flow. Below these valves, the line tees to a low pressure cut-off inside the blue Sylvania/GTE temperature control unit (mounted above the computer and oscilloscope), and to the temperature control equipment.

The needle valve is used for positive shut off of the gas system when testing is not ongoing. Closing the valve also activates the low pressure cutoff switch for heater power.

- d) The gas passes through a 3.0 SCFM (air) flow meter that is graduated in percent to another tee, for diverting to either the heater or the chiller or into the hot cell. The knob on the front of the flow meter is used to control flow rate.
- e) The chiller is mounted on the cell wall beside the diverter valves. The lever valves are open when in-line and closed when perpendicular to the line. For chilling, the Dewar is filled with

liquid nitrogen through the hole in the lid. Do not remove the tubing coil from the inside of the Dewar to fill the chiller. Inserting the tubing coil into the filled Dewar results in large quantities of boiling nitrogen and can potentially cause frostbite. The RPTs have agreed that the hand dewars from which the chiller is filled need not be surveyed out of the lab as long as they are not set down in the lab.

**FOR THE IN-CELL SYSTEM:** To direct the gas into the hot cell, disconnect the insulated line leading from the chiller into the cave and connect the insulated line leading into the cell. The direct connections maximize thermal efficiency. This line supplies either chilled nitrogen for sample chilling, or room temperature argon as a protective atmosphere.

The plastic line from the chiller extends to well inside the cave. There is a Swagelok fitting at the junction to a  $\approx 3$  inch long copper elbow and a high temperature plastic union at the junction to a  $\approx 3$  inch length of stainless steel tubing that goes into the chamber. Metal tubing is used close to the furnace to eliminate the possibility of damaging plastic line during tests at elevated temperature. The fittings and metal lines are not visible as they are covered with insulation that is wrapped with copper tape.

- f) For heating, the gas flow is to a flow-through Sylvania Serpentine Type IV heater mounted on the cell wall behind the cave. The heating element plugs into the inlet cap, which is held on by two slot head screws. A  $\frac{1}{4}$  inch stainless line goes from the heater outlet to the chamber inlet. There is a 15 psi pressure gauge and another needle valve in line before the heater. The pressure gauge indicates the gas pressure at the heater inlet. Under normal operating conditions the inlet pressure will read 0 psi because it is less than 1 psi. The maximum value with maximum helium flow will not exceed 3 psi. Do not let the inlet pressure exceed 10 psi, as excessive pressure can lead to overheating of the element and its subsequent failure.
- g) A pneumatic piston loads specimens into the temperature chamber along a track. Full size specimens are placed longitudinally in the center of the track, at the tip of the white ceramic ram tip, and subsize specimens are placed to the left of the center, at the end of the small rod which compensates for the shorter subsize specimens. This rod is attached to the white ceramic ram tip in this left-hand portion of the track.

A small shield attaches to the small rod, which is in place for all specimen sizes. Attachment of the shield is required for testing subsize specimens, but it must be removed for full size specimens. It slides on or off the end of the small rod, and is most easily attached or removed

when the ram is extended through the temperature chamber such that the tip and small rod are exposed. The shield is simply a folded piece of stainless steel sheet. It positions the subsize specimens correctly inside the temperature chamber so that the gas flows onto them properly.

**Wear rubber/vinyl gloves and guard against contamination whenever handling components inside the cave enclosure. An RPT should survey the small parts that must be removed/installed with conversion from full size to subsize specimen testing. Store the parts not currently in use in the container at the front, right hand corner inside the cave.**

#### **Temperature control electronics**

- f) The furnace thermocouple readout (in °C) is mounted in the pneumatics switch/control box that is mounted above the cave, to the right of the tower (OMEGA digicator).
- g) The Sylvania/GTE bench unit, which comprises
  - 1) A gas temperature thermostat in hundreds of °F to measure temperature at the flow-through heater outlet. The gauge above the thermostat indicates the  $\Delta T$  error to within  $\pm 50^\circ\text{F}$  between the thermostat set point and the gas temperature at the heater outlet.
  - 2) A phase angle fired SCR inside the unit on one of the two legs of the single phase 210 volt AC power input. The SCR is simply a solid state switch that controls the power level by opening and closing the circuit several times per second. This SCR is controlled by resistance.

A typical SCR circuit is controlled by a milliamp signal from the thermostat. Some SCRs respond to low voltage DC signals. The SCR circuit incorporated in the Sylvania controller responds to ohmic changes. The thermostat varies resistance with the  $\Delta T$  to control the SCR. The setup seems to be quite unusual. Also, there is a finite minimum current in the circuit due to this configuration. The current is proportional to the resistance of the load. That is, with the  $9\Omega$  heater element as the load, the circuit is essentially open when the SCR is "off". However, placing a pseudo load in the circuit of, say,  $50\text{ k}\Omega$  will result in a significant voltage in the circuit even when the SCR is "off".

- 3) A potentiometer on the back of the unit that adjusts the "full power" or maximum output level.
- 4) Two "ultrafast" semiconductor, cartridge type 25 amp fuses (Buss, FWH-25) located inside the unit, one on each leg of the power. The fuses are "ultrafast" to protect the SCR.

- 5) A pressure detector with a nonfunctional pressure gauge and an unused adjustment knob. The internal pressure sensor and low pressure gauge operate properly despite the fact that the gauge is nonfunctional and that the pressure control is not used.
- 6) An electromagnetic cut-off switch inside the unit, which cuts power when the pressure detector senses low pressure. The detector is not likely to cut power soon enough to prevent damage to the heating element if the gas inadvertently runs out. This condition arises due to the resistance of the lines, since the detector is not close to the heater gas inlet. The gas bottles are supposed to be changed out before they are empty, so theoretically a low pressure situation will not occur.
- 7) Two meter jacks on the middle front of the unit, one each to the power legs. These are very convenient for monitoring power or RMS voltage, but remember to maintain proper safety precautions with live leads. Both jacks are live when the power switch is ON.
- h) The digital gas pressure readout from the manifolds in 12A. The toggle switches the indicator between manifolds. The readout is located on top of the Sylvania unit. It indicates the bottle pressure via transducers located in 12A on the high side of the regulators. When this readout indicates  $\leq 200$  psi, it is time to change out the gas bottles.

#### **Testing equipment**

- 1) Radiation shielding
  - a) The testing area is completely enclosed in a steel walled, four inch thick lead cave, approximately one meter cubed. The lid comprises two horizontally sliding doors on roller bearings. The drop-weight tower extends through a notch in the doors. The drop-weight falls through this notch.
  - b) A small, three compartment storage area constructed of about 20 lead bricks abuts the cave on the left. Access the compartments by lifting off the uppermost bricks, which act as lids for the compartments.

**An RPT should periodically check the interior of the three compartments and the cave, particularly the interior of the temperature chamber, the striker tip, and the anvils. Contact between irradiated specimens and various surfaces has proven to result in permanent contamination only on the high load surfaces, i.e., the anvils and the striker tips. Experience indicates that other surfaces are readily decontaminated. The RPT should also check the specimen handling tools kept in the container affixed to the cave top. The RPT should be kept apprised of work in the lab so he/she can make informed decisions about the frequency**

**of surveys. The RPT should be contacted any time atypical conditions are suspected that may result in contamination.**

2) Drop tower

The experimental apparatus is a twin-rail drop tower, Dynatup model 8200--extended height, rated for 285 J maximum. It is configured with either a 10,000 lbf (44.5 kN) load cell or a 3500 lbf (15.6 kN) load cell. Both are solid state load cells, incorporating semiconductor strain gauges.

- a) The drop weight assembly is a yellow rectangular assembly that contains a number of lead weights. The drop weight assembly should be positioned at least several inches below the positioning stop when not testing to prevent accidental triggering of the release mechanism, thereby allowing specimen placement or retrieval to be performed safely. When reaching into the cave for more extensive activities, such as removing or installing the subsize specimen positioning stop, wrap a safety strap around the weight and the positioning stop, positively tying them together.
- b) An infrared sensor is attached to the tower column just above the closed cave top. It detects and times the passage of a sheet metal flag, called the velocity flag, that is attached to the drop weight assembly.
- c) An adjustable positioning stop is optionally attached to the tower support column with a moveable brace that stabilizes the rails when located at intermediate to high drop heights. It can, however, hold the rails in misalignment. The velocity flag passes through the infrared detector with little clearance. Misaligned rails can result in damage to the flag and sensor or in a missed load trace since the capture signal will fail to trigger the oscilloscope. The flag alignment should be verified after adjusting the positioning stop and after climbing up onto the cave top for any reason. Never pull on the rails - grab the tower column instead. Lower the velocity flag through the sensor using the winch to check the clearance. The pneumatic piston secures the stop to the brace. If the rails become misaligned, loosen the piston, allow the rails to realign themselves, and retighten the piston. Also clean and lubricate the rails periodically.
- d) A pneumatic piston used to trigger the drop weight is affixed to the positioning stop. The air line connects to the pneumatic solenoid bank (solenoid 6-5) attached to the cave door on the right.

- e) An electric winch for lifting the drop weight assembly is located on the tower column. The control lever is mounted on the right of the column, and the take up reel is on the back of the column. Tension must be maintained on the hoist cable to ensure its smooth wind-up. Maintain tension while lowering the hoist latch by pulling down on the cable by hand, particularly as the latch locks into the drop weight assembly. Light tension is sufficient, but if the cable goes slack it will tangle and jam. When hoisting to positions above about five feet, assist the reversal of reel take-up by tapping the cable (from the cell-ward side) toward the column just above the reel as soon as it begins to start another layer of cable winding on itself. Otherwise the cable will tangle or slip off.
  - f) A cable goes from channel A on the digital oscilloscope to the load cell (to the right side of the 10 kip cell and to the back of the 3.5 kip cell). It must be able to traverse the fall zone unimpeded.
  - g) Two segmented aluminum columns inside the cave stop the drop weight after each test, one immediately adjacent to each rail. The height of these stops is adjusted by adding or removing segments. Add one 2" segment to each side when converting from the 3.5 kip load cell/tup to the 10 kip striker/tup. The large striker will impact the anvils if the extra segments are not added. The smaller striker will not impact the specimens if the extra segments are not removed.
- 3) Positioning equipment
- a) The pneumatic ram and the track for loading specimens are located in the cave.
  - b) A computer controlled stepping motor and positioning arm are located in the cave at the base of the drop weight rails near the impact position.
  - c) On top of the pneumatics control box, a COMPUMOTOR stepping motor controller connected to the stepping motor via a power supply by a multiwire cable and to the IBM PC by an RS232 connection.
  - d) Mounted to the cell wall, to the right of the cave, is a dedicated power supply for the stepping motor.

The power supply is not equipped with a switch - it is plugged into a power strip attached to the left side of the computer/oscilloscope table. The power strip has a switch, which is the only means used to turn on and off the power to the stepping motor. The stepping motor will energize whenever there is power to the power supply and the COMPUMOTOR is not on line with the computer (i.e., whenever the ON-LINE light on



the COMPUMOTOR controller is out), in which case the motor will overheat. Keep the power on while conducting normal testing, but turn off the power whenever the system is unattended or there will be a long delay before the next test is run.

- e) A positive specimen stop assembly is adjustable for precise centering of the Charpy impact bars. The assembly is part of the positioning control electrical circuit in the cave. When the specimen contacts the stop, the circuit goes to ground through the positioning arm. When grounded, the pneumatic ram retracts and the positioning arm lowers. The subsize stop assembly is removed for full size testing by removing the two nuts holding the bracket on the bolts.

The stop for full size specimens is the end of a bolt that is tightened or loosened for specimen position adjustment. The full size stop is stable and unlikely to require adjustment, but when it does, fix the end of the bolt and adjust the nut. Adjustment is required periodically due to the compressibility of the Teflon washers used for electrical isolation. The subsize stop is a machined aluminum piece with a positioning screw. It attaches to the permanent piece by two threaded posts and is shimmed with thin foil for improved stability. The subsize stop will require adjustment during installation for subsize testing as well as periodically during testing. Use the aluminum specimens for positioning trials.

- f) The specimens rest on the anvils designed to accommodate both full length and half length specimens. The full size specimens rest across the wider gap (46 mm) centered in the cave between the drop tower rails. The subsize specimens rest across the narrower (20 mm) gap, just left of center between the rails, in nearly the same position as the full size specimens.
- g) A guide attached in front of the furnace to the left of the door guides the subsize specimens onto the positioning arm. It must be removed for full size specimen tests.

#### 4) Pneumatics controls

- a) The air line for the pneumatics parallels the heating/cooling gas line on the hot cell wall. It connects to the solenoid bank attached to the right cave door.
- b) The pneumatics control box consists of four push buttons and the furnace temperature readout on the front and two toggles on the back.

The left most (towards the cell door) toggle switch powers the solenoids; the other toggle switches the electronics. Do not turn off the electronics before the solenoids. Turn off the left most switch first (or only) to prevent a power surge to the solenoids.

Push-button SW1 is labeled "Load Furnace". It closes the temperature chamber door and extends the positioning ram, pushing the specimen into the furnace.

Push-button SW2 is labeled "Position Specimen". It opens the door and extends the ram, pushing the specimen onto the positioning arm, and retracts the ram when the specimen grounds the switch circuit. Note that the ram will retract any time the positioning stop assembly is grounded with tongs, RPT survey equipment, etc.

Push-button SW3 is labeled "Optional Home". It retracts the ram at the operator's discretion.

Push-button SW4 is labeled "Drop Striker". There is a microswitch next to the positioning arm which is closed when the arm is at the bottom of its arc. When the microswitch is not closed, SW4 is disabled. This prevents the striker from being dropped when the positioning arm is in the path of its drop.

### **Testing electronics**

- a) The IBM PC on the table controls only the COMPUMOTOR and serves no other purpose. The monitor should be turned on only when needed since it causes significant extra noise in the oscilloscope trace. Once the computer is booted and the COMPUMOTOR is on line, the monitor should be turned off.
- b) The COMPUMOTOR, located on top of the pneumatics control box, controls the stepping motor via commands from the PC.
- c) A DC precision power supply is on top of the Sylvania/GTE unit. It should be set at 5.000 V before it is turned on. It powers both the load cell and the  $\pm 4$  V DC infrared sensor. This unit should be on for at least an hour before testing to stabilize. Leave it on overnight for ongoing testing.
- d) The passage of the velocity flag through the infrared sensor causes its output change polarity. This change triggers the load trace capture window on the oscilloscope. It connects directly to channel A of the oscilloscope for testing full size specimens. The output of the infrared sensor is passed through a time delay circuit for testing subsize specimens. Regardless of specimen size, the signal tees over to the second oscilloscope where the flag passage is recorded for velocity calculation.
- e) The time delay circuit is in the gray box on top of the Sylvania/GTE unit. The trigger for data acquisition on the oscilloscope is the passage of the bottom of the velocity flag slot. The sensor and flag are positioned such that the top of the slot, i.e., the open portion

in the flag, is just past the center of the sensor when the striker is resting on (i.e., has just contacted) a full size specimen. The full size configuration results in immediate triggering. The time delay circuit delays the trigger signal for tests on subsize specimens such that the oscilloscope captures the load trace after the velocity flag has passed several millimeters further through the detector. This configuration provides maximum accuracy of velocity calculation at impact as well as control of the starting point in the load trace window for both full size and subsize specimens.

The delay timing must be adjusted periodically while testing subsize specimens. The circuit is fairly stable, but it requires periodic checking and adjustment. The delay time is adjusted with the 10 turn potentiometer on the side of the timing circuit box. Adjusting clockwise shortens the delay, shifting the starting point of the data acquisition farther to the left on the oscilloscope screen. Conversely, adjusting counterclockwise lengthens the delay, shifting the starting point of the data acquisition farther to the left on the oscilloscope screen.

It is possible to set the delay timing so that it is appropriate for both half and third size specimens. The scope positions the trigger signal on the cursor as long as the trigger mode is set to "Cursor". If the cursor is positioned to the far right in the screen, the recorded trace will be of the moments preceding the trigger signal. Compensate for the difference between half and third sizes as well as small day-to-day variation by shifting the position of the oscilloscope cursor.

Check and adjust the delay setting by cutting tongue depressors or popsicle sticks with wire cutters into sections  $\approx 23$  mm x 5 mm and taping them together in twos or threes to simulate the thickness of half and third size specimens, respectively. Two sections are  $\approx 3.3$  mm thick, and three sections are  $\approx 5$  mm thick. Test as many of these wooden specimens as needed to ensure that the timing delay is appropriate.

- f) The main Nicolet oscilloscope is located on the table on top of the PC. It captures the test load traces as a function of time and stores the traces on floppy disks. It is connected to the load cell (channel B) and the velocity flag sensor (channel A) as previously indicated. Its set-up is described in a later section of this procedure (see Nicolet Oscilloscope Configuration).
- g) The second Nicolet oscilloscope is in the instrument rack next to the hot cell, near the door to the lab. It captures the passage of the velocity flag on each test. It is also used

recall traces from the floppy disks and to transfer the data to the IBM AT, which is also in the instrument rack. Channel B is connected to the velocity flag sensor. Its range should be set to  $\pm 1V$  and X4, and its time per point setting is generally 500 ns. The DC Level should be about +1.8 V (1800 mV) and the cursor should be positioned near but not all the way over to the left edge of the display screen. Most settings are the same as on the main scope but the Trigger Control Slope is +DC and the Source is (channel) B. All eight Track Protect switches should be in the ON position (see Nicolet Oscilloscope Configuration).

- h) The IBM AT has Quick Basic (QB) installed on it as well as the software related to data acquisition. The Wave Form (WF) Basic programs are similar to "BASICA" and were specifically designed to manipulate the traces captured by the Nicolet scopes. The manual is in the file drawer of the desk. A Wave Form Basic program pulls in the data from the scope, and a Quick Basic program manipulates the data for output and analysis. The combination of programs are run by typing "tall2" at the C:\WFBASIC> prompt followed by [Enter]. Tall2 is a batch file in the WFBASIC directory, where most of the other data acquisition files are also stored, that runs the WF program, then runs the QB program, and then restarts the WF program for analyzing another specimen. Break out of the loop with Ctrl-Break.
- i) A Cole-Palmer multichannel digital thermocouple readout sits on top of the right cave door. It provides the readouts for the thermocouples welded onto the three instrumented specimens for temperature calibrations/correlations. The full size and half size specimens have four TC leads, and the third size specimen has two.

There are two additional TC leads running to the cave top. Both are used to monitor the temperature of the cold gas line during tests at elevated temperature (i.e., when the chamber is being heated by hot gas coming in the other line). One TC is welded to the stainless steel tube leading into the temperature chamber, and it indicates the temperature on the warmer side of the plastic thermal isolation union in the chilling gas line. The other TC is attached to the copper elbow on the cold side of the union. The union can withstand temperatures in excess of 250°C under light load. Check the temperature from these TCs when testing at high temperature for extended periods, but there is little likelihood of approaching temperatures of concern.

## **TESTING PROCEDURE**

The goal of Charpy impact testing is to determine the amount of energy absorbed by the specimens when they are subjected to impact loading. This system accomplishes this by means of an instrumented load cell/striker that records the load as a function of time during the impact. Converting time to an equivalent distance of crosshead travel and integrating the load trace over distance provides the absorbed energy value. The drop height is adjustable, and the resulting variation in impact velocity is between about 2 and 6 m/sec. Impacted samples generally break in two, but some specimens remain intact while undergoing severe deformation.

Eye protection should be worn during testing. Dosimetry pencils and finger rings should be worn when testing radioactive specimens. Be careful to prevent surface contamination. Utilize the same utensils for all radioactive or contaminated specimen handling, and store these utensils in the proper location. Wear gloves whenever handling these utensils, with or without specimens.

- 1) Turn on the power to the following:

IBM PC (reset date and time correctly whenever PC is rebooted)

IBM AT

both oscilloscopes

precision dc power supply

switches on the back of the pneumatics control box

COMPUMOTOR controller

Open the necessary gas lines and the pneumatic air lines

Do not turn on the outlet strip that powers the COMPUMOTOR power supply. It is turned on later.

Do not turn on the GTE/Sylvania heating unit. It is turned on later when testing is to be done at elevated temperatures.

- 2) Hit [Enter] on the IBM PC at the prompt. The ON-LINE LED should illuminate on the COMPUMOTOR.

Turn off the monitor.

Turn on the outlet strip that powers the COMPUMOTOR power supply.

As long as the ON-LINE light on the controller is lit when the outlet strip is on, the stepping motor should not overheat. If the ON-LINE light goes out, the PC will start beeping to indicate that the motor will overheat within several minutes.

In this event, turn off the power to the outlet strip, reboot the PC, and get the ON-LINE light lit before restoring power to the stepping motor.

- 3) When conducting subsize tests, verify the delay timing by testing wooden samples. Test at least one wooden sample every day before starting subsize specimen testing.
- 4) Heat or cool the specimen to the temperature of interest. This is discussed in detail in the next section of the procedure.
- 5) Preparations for each test are completed by following the attached check list. Always fill it in for each specimen with the requested data or initials for each step.

**Check list description:**

- Specimen ID

Use the specimen ID code engraved on the specimen, plus *F*, *H*, or *T* to represent the size, plus *N* or *P* to represent notched-only or precracked, and add an *R* if the specimen is radioactive. Use the same designation for the file name when transferring the data to the AT. For example, a test on a third size specimen engraved as *W101* that is notched only and is unirradiated is given the ID code *W101TN*. The file names generated by the IBM AT during data analysis are *W101TN.DSC* and *W101TN@.WFM*.

- Drop-weight position

Ensure the drop weight assembly is at least several inches below the positioning stop before reaching into the cave. Move the drop weight assembly using the winch.

- Specimen position verification

Mark the surface opposite the notch with a Sharpie pen for easy orientation recognition. Irradiated specimens are marked while in a hot cell, before final shipping to 11A. Any easily identified mark is acceptable. Position full size specimens lengthwise in the center groove of the track and subsize specimens in the left hand groove. Use tongs or tweezers to position all specimens, grabbing each specimen towards the back and with the notch down. The notch should face down and to the left. Verify that the Sharpie pen mark is visible to double check that the specimen is in the track correctly before pressing the "Load Furnace" button on the pneumatic control box.

- Record gas manifold pressure

If the gas pressure gets too low while heating, or the bottle actually runs out, the heater element will burn out. The low pressure side of the manifold in 12A should be set at  $\approx 150$  psi. Do not let the bottle pressure fall this low. Change to another gas bottle when the

high pressure side is down to  $\approx 200$  psi, as indicated by the digital readout in 11A. Ensure that the heater has sufficient time to cool before running completely out of gas. Once the pressure falls below 130 psi, flow will decrease and temperature control will become unstable. However, pressure above about 40 psi will effectively cool the heater as long as the power to the heater is off. Do not attempt to operate the heater with manifold pressure below 100 psi.

**Do the following to switch gas bottles in 12A:** Ensure that the manifold valve for the full bottle in the rack is closed, but open the bottle valve on the full bottle. Close the manifold valve for the near empty bottle, and then open the manifold valve for the full bottle as rapidly as is practical. This procedure does not disturb gas flow to the heater. Bottles can be switched safely while heating specimens.

**Do the following to get new bottles installed in a manifold:** Call facilities (currently Gerry Bruce, the building manager secretary, 376-2653) to order a change out of the empty bottle(s). Notify Bruce Arey, or whomever is keeping track of gas bottle inventory, of the number and gas type of the empty bottles that need to be replaced. Bottle exchange generally takes from one to four hours after you have called in the request. A request placed after 2:30 pm will probably be filled before noon the next day. For the sake of convenience and to be cost effective, try to request that two bottles be exchanged at a time, but try to keep one bottle in reserve to continue testing. Obviously this is not easy with only three bottles to work with.

- Record scope time scale

The scope takes  $4096 (2^{12})$  data points, so a data interval of  $1 \mu\text{s}$  per point, for example, provides 4.1 ms of data acquisition. A typical impact event takes about 3 ms, but if the energy required by the specimen is more than one fourth of the available energy of the striker, the test will take longer. A  $2 \mu\text{s}$  per point interval is recommended for tests on full size specimens and tests on half size notched-only specimens.

The difference in resolution between 1 and  $2 \mu\text{s}$  per point is not significant. When in doubt, use  $2 \mu\text{s}$  to make sure all data are acquired. If the absorbed energy is likely to exceed 175 J, use  $5 \mu\text{s}$  per point. The loss in resolution at this setting is still small. The energy available in the striker is equal to its kinetic energy,  $\frac{1}{2}mv^2$ . The striker mass is 15.353 kg or 14.725 kg when configured with the 10 kip or 3.5 kip tup, respectively. These values are accurate to about five grams. The impact velocity exceeds 6 m/s when the striker

is dropped from the tower's full height. Velocity changes between  $\approx 2$  and 10 m/s should not affect the amount of energy absorbed.

- Record oscilloscope Y-scale setting
  - Use the 100 mV and X1 buttons for third size specimens and 100 mV and X2 for half and full size. Use the X4 button if testing very tough materials.
- Record oscilloscope cursor position
  - Put the oscilloscope in LIVE mode with the trigger control set to AUTO to get the scope to display the current coordinates of the cursor, relative to the left edge of the display. The trigger event is positioned at the cursor, capturing the signal preceding and following the trigger event in proportion to where the cursor is set.
- Record Y-scale cursor position
  - This is the DC LEVEL set point. Assuming that the scope captured the entire test event, the "zero load" will be the average of the first several points, i.e., those preceding the load increase. This average will be the same as the DC LEVEL set point.
- Main scope set to record
  - Depress the LIVE button and then the HOLD NEXT button. When these two LEDs are lit, the scope will record the load signal associated with the next trigger for data acquisition.
- Second scope set to record
  - Depress the LIVE button and then the HOLD NEXT button. When these two LEDs are lit, the scope will record the next trigger signal, i.e., the passage of the velocity flag.
- Cave doors closed
  - This is a safety precaution to prevent specimens from flying out and people from reaching in.
- Drop weight assembly to fully elevated position
  - If the drop weight assembly isn't raised before the specimen is placed on the anvils, it will not be available to fall when the pneumatic plunger actuates, and the heating/cooling will have to be repeated. Lower the drop weight assembly again before reaching back into the cave for ANY reason, and then raise it again.
- COMPUMOTOR "ON-LINE" LED lit



Ensure that the COMPUMOTOR is on line or the specimen positioning arm will not function and the specimen will drop to the bottom of the cave when it is pushed out of the furnace

- Stepping motor power ON

Ensure that the motor power is on or the positioning arm will not function.

- 6) Test the specimen. This is performed after the specimen temperature is stabilized near the desired test temperature.

Stand in front of the pneumatics control box so that you have a clear view of the testing anvils through the closed cave doors. Place one finger each on the "Position Specimen", "Optional Home" and "Drop Striker" buttons so that no time will be required to look for the latter after the specimen is in position.

Press the "Position Specimen" button, and watch the specimen positioning. The positioning ram should retract automatically, but if it does not, press the "Optional Home" button ASAP. Verify that the orientation of the specimen on the anvils is correct by verifying that the Sharpie marks are still visible on the top surface of the specimen. Verify also that the specimen is not skewed with respect to the anvils (i.e., nonperpendicular to the anvils).

Note that third size specimens have been known to "roll" inside the temperature chamber.

Apparently the furnace door occasionally snags on the top corner of the specimen as it is opening and rotates the specimen 90° just before it exits the chamber. Do not drop the striker if the specimen is rotated or skewed. In this case, the test must be restarted.

Press the "Drop Striker" button as rapidly as is practical after verifying that the specimen position is acceptable. The time elapsed between the impact and exiting the temperature chamber should be no more than about two seconds. If the elapsed time exceeds four seconds for any reason, the test should be aborted and restarted.

Complete the last item on the checklist:

- Store load trace on diskette

If the scope is set to SEMIAUTOMATIC, it will record the data on a disk as soon as the trace is captured on the screen. The data will be recorded on the track which was lit prior to the capture, and the LED for the next track will then be the one that is lit. Double check that this has occurred by noting that the next LED is lit. Do NOT try to verify it by recalling the most recently stored track from the disk to the screen - if it is not the current test, recalling the previous track will erase the data on the screen, losing it permanently.

Back up the screen data on another disk. Keep two disks and rotate them such that the 8 most recent traces are kept on the backup disks. Once the data is successfully transferred to the computer, the backup disk is superfluous. One copy of the data on floppy disk should always be kept for back up.

- 7) Measure the time required for the passage of the gap in the velocity flag on the second scope. If a velocity determination is desired, type VEL [ENTER] on the IBM AT and input the information requested. Only the time required for the passage of the gap in the velocity flag is needed for data analysis.

Transfer the load trace to the second scope. Insert one of the floppy disks with the data into the second scope and toggle RECALL.

- 8) Start/continue the TALL2 batch file and input the information requested. Continue with the data analysis and generate at least a data listing, a plot of load vs. distance, and a plot of energy vs. distance.
- 9) Record all pertinent information for each test in the log book. The data listing from step 8 should be taped into the log book. Documentation of the time to heat or cool should be kept in the log book. Any anomalies should be recorded as well.
- 10) Retrieve the specimen and store it appropriately.

### **SHUTDOWN PROCEDURE**

Do the following before leaving the lab for any extended period, whether it is a short break, or the end of the day, or the termination of testing:

- Turn off the power to the stepping motor, i.e., the switch on the power strip attached to the table with the main oscilloscope and the IBM PC.
- Ensure that either the gas flow in the lab is off or that the flow rate and the available quantity of gas remaining will not jeopardize work being conducted across the hall in 6A or other labs. Check with the appropriate technicians about their anticipated usage and needs.

Never turn off the supply of argon to the manifold in 12A. Close the valves on the north wall of 11A, near the door, to reduce line leakage, which for argon and nitrogen is very low. For day to day operations this leakage is insignificant. The helium line leakage losses average over 5% per night. The valve on each helium bottle should therefore be turned off every night.

- Close the cave doors

- Position the drop weight assembly so that it cannot fall by accident by either securing it in a raised position with a strap or lowering it to its lowest point, resting on the shock absorbers.
- Make sure that irradiated specimens are properly stored and covered.

If testing is expected to resume within a day or two, do the following in addition to the steps given above:

- Turn off the power to the computers, the oscilloscopes, the COMPUMOTOR controller, and the pneumatics power.

Leave the pneumatics air line open, and leave the DC power supply turned on.

If testing is to be halted for an extended period, do the following in addition to the steps given above:

- Turn off the DC power supply.

## **TEMPERATURE CONTROL**

### **Chilling**

Chilling specimens to a temperature below ambient entails cooling nitrogen by passing it through a Dewar filled with liquid nitrogen and then passing the cooled gas onto the specimen inside the insulated chamber (i.e, the furnace). The chamber is configured for heating or cooling. Calibration curves developed for each specimen size are used to relate the furnace temperature to the actual specimen temperature.

Since the system chills a specimen by blowing  $-190^{\circ}\text{C}$  gas onto it, "control" per se is not possible at any temperature besides  $-190^{\circ}\text{C}$ . Specimens are chilled to at least  $50^{\circ}\text{C}$  below the test temperature and allowed to warm to the test temperature. Since the temperature chamber is well insulated and the cave provides a relatively isolated and stable environment, heat transfer to a cold specimen is quite constant from one instance to the next and temperature calibration runs are fairly reproducible.

The following steps provide reasonably accurate temperature control between  $-150$  and  $0^{\circ}\text{C}$ . Testing below  $-150^{\circ}\text{C}$  requires dropping the temperature to the lowest temperature achievable,  $\approx -190^{\circ}\text{C}$ , holding for twenty minutes, and allowing the specimen to warm up. The hold time is necessary for the lowest test temperatures to decrease the subsequent heat up rate, since the lower the temperature, the faster the specimen will warm up.

- a) Make sure that the manifold in 12A is set up to deliver nitrogen rather than helium.

The 2000 psi bottles contain standard grade nitrogen, which is 99.5% pure with 0.02 mg of water per liter. Temperatures down to  $-190^{\circ}\text{C}$  can be achieved relatively easily. At very low temperatures, however, the moisture in the nitrogen can cause the gas lines to freeze up, and can cause sticking problems associated with specimen transfer.

Make sure that several portable Dewars filled with liquid nitrogen are available in 11A.

Two portable Dewars are generally sufficient for one cryogenic test, although three or more may be needed for the lowest temperatures or for multiple cryogenic tests. It takes about  $1\frac{1}{2}$  portable Dewars to fill the Dewar in the lab initially.

- b) Turn on the nitrogen gas flow to a fairly low flow rate, about 15% of full scale on the 3 SCFM (air) flow meter. The low flow prevents the lines from freezing closed, as they would if there were no flow when the Dewar is filled with liquid nitrogen.

Fill the Dewar with liquid nitrogen from the portable Dewars. Turn up the nitrogen gas flow rate to about 75-95% of full scale on the meter after filling the Dewar.

To fill the Dewar, pour the liquid nitrogen slowly through the hole in the lid, using a funnel if desired. Do not remove the copper coil to fill the Dewar -- insertion of the warm coil into liquid nitrogen causes a large amount of boiling nitrogen to envelop the operator, potentially resulting in frostbite.

Keep the Dewar full by topping it up every few minutes. Continue to top up the Dewar until the gas flow is shut off as described below.

For consecutive tests at cryogenic tests, turn on the gas flow again and refill the Dewar once per specimen. The furnace will reach  $-100^{\circ}\text{C}$  in about the same amount of time as is required for filling the Dewar.

- c) Watch the readout from the furnace TC, and shut off the gas flow once the readout indicates that the temperature has dropped to the desired furnace start temperature, which must be at least  $50^{\circ}\text{C}$  below the intended test temperature. Use the calibration curve for the appropriate specimen size to determine the actual specimen temperature for a given furnace temperature reading.

Calibration runs are typically made from furnace starting temperatures of  $-190$ ,  $-150$ , and  $-100^{\circ}\text{C}$  for each specimen size. The curves for different starting temperatures do not converge for full size specimens until about  $-20^{\circ}\text{C}$ . Starting temperatures should be as close as possible to those used to develop the calibration curves but a range of  $-6$  to  $+1^{\circ}\text{C}$  should provide high reliability for the test temperature.

Record the starting temperature in the log book. Record the time and temperature at regular intervals as the chamber and specimen warm up until the specimen reaches the desired test temperature.

- d) Perform the impact test when the furnace TC readout reaches the temperature that corresponds to the specimen temperature of interest, as indicated by the appropriate calibration curve.

Prior to the chilling or as the chilling and subsequent heat up are occurring, be sure that all items in the checklist have been prepared for the test so that the test can be performed as soon as the specimen reaches the temperature of interest. When the furnace is within a few degrees of the desired temperature, stand in front of the pneumatics controls and start the test as soon as the readout indicates the proper furnace temperature.

### **Heating**

Heating entails heating helium by passing it through a flow-through heater and then passing it onto the specimen in the insulated chamber. The heater is rated at 1400°F (760°C). The heater control system can control at any gas temperature between ambient and 1400°F. The maximum attainable specimen temperature is significantly lower than the temperature of the heating gas. A temperature calibration curve for each specimen size relates the furnace temperature to the actual specimen temperature.

The desired specimen/furnace temperature is obtained by selecting an appropriate combination of gas temperature and flow rate. The log book contains documentation of previous combinations. The specimen is tested when it is approximately in equilibrium with the flowing gas, where equilibrium is defined as a constant furnace temperature over a three minute period. Given sufficient time to stabilize, the system can maintain a constant temperature for an extended period.

The precision of temperature measurement is approximately  $\pm 2^{\circ}\text{C}$ , although reproducibility for given conditions is limited to about  $\pm 10^{\circ}\text{C}$  due to variations in exact gas temperature set point and gas flow rate set point (i.e., a lack of precision in temperature control). Increasing the gas temperature or the flow rate will result in an increase in the temperature at which the specimen stabilizes. Nominally identical set points can result in a significantly different specimen temperatures. Experience is the best way to determine how to obtain the desired test temperature.

- a) Turn on the helium flow to furnace after verifying that the appropriate valves are open or shut.
- b) Turn on the power to Sylvania unit.
- c) Gradually turn up the set point on the thermostat of the Sylvania unit.

Use increments of about 200°F up to 1000°F. Use 100°F increments to 1200°F, and 50°F increments thereafter. Turn up the thermostat, let it stabilize for one to five minutes, then turn it up again, repeating until reaching the desired set point.

- d) Allow the furnace temperature readout to rise and stabilize.
- e) Complete the specimen testing checklist while the specimen is heating.
- f) Record the time, furnace temperature reading, gas flow rate, and gas set point temperature in the logbook periodically during the heating process.
- g) When the furnace temperature readout has stabilized without a change for three minutes, test the specimen. Log the action and results in the logbook.
- h) Turn off the power to the Sylvania unit, and reset the thermostat to zero.
- i) After the heating element has cooled significantly, turn off the gas flow. Use the thermostat on the Sylvania unit to check the gas temperature. Keep the helium flowing until the gas temperature is below 350°F.

### **Temperature Calibration**

Specimens with 2-4 TCs attached are used for temperature calibration, one of each size. The specimens are loaded into the furnace the normal way taking care to avoid damaging the TCs.

To generate a calibration curve for cryogenic temperatures, chill the specimen/chamber to a predetermined starting temperature allow the specimen/chamber to warm up. Recording the temperature indicated by the specimen TCs as well as that of the furnace TC in the log book every 0.5-2 minutes, depending on how high the heating rate is. Repeat for each anticipated starting temperature. Obtain a best fit curve by regression analysis for each specimen size for the specimen temperature as a function of furnace temperature. Use these curves to determine the specimen temperature for a given furnace temperature while testing. An exponential curve with an R-Squared value very near 1.0 should fit the data reasonably well.

To generate a calibration curve for each specimen size at elevated temperatures, start with gas temperature and flow rate settings that will produce a relatively low temperature. Allow the temperature to stabilize and record the temperature of the specimen TCs as well as that of the furnace TC. Increase the gas temperature and/or flow rate to obtain a higher temperature. The range generated for calibration purposes should be from 50°C to 375°C. High temperatures require rather high flow rates. Once the gas temperature reaches 1400°F, increase the flow rate to obtain a higher

specimen temperatures. Review previous calibration runs from the log books for guidelines on gas temperature and flow rate set points.

Obtain a best fit curve by regression analysis for each specimen size for the specimen temperature as a function of furnace temperature. Use these curves to determine the specimen temperature for a given furnace temperature while testing. A straight line should fit the data reasonably well.

### **RADIOACTIVE SPECIMEN HANDLING**

Shipping and transfers to or from the hot cell require continuous coverage. Handling the specimens in the lab requires only intermittent RPT coverage. The following guidelines should be obeyed:

Always wear safety glasses.

Minimize exposure time.

Maximize the distance between yourself and specimens.

Use shielding to optimal advantage.

Always wear gloves to handle the specimen handling tools or when installing or removing components inside the cave.

Don't reuse gloves, and dispose of them in the low level waste container.

Testing requires transferring one specimen at a time from one of the storage compartments in the lead brick storage adjacent to the cave to the track leading into the insulated chamber. The following techniques should be used for making specimen transfers in to and out of the testing equipment:

- a) While wearing gloves, remove the top lead brick from above the appropriate storage compartment and set it aside. To remove the remaining brick from above the storage compartment, lift only one end and tip the brick up to stand on end. This position allows ready access to the storage compartment, allows the brick to be quickly and easily repositioned, minimizes the risk of contamination associated with the exposed underside of the brick.
- b) Use the long (1 m) plunger type grasping tool to remove the lid from the specimen container and extract one specimen. If the plunger grasper is inappropriate for lid removal, use the scissor type tongs that are stored in the container on top of the cave. Determine the identification code engraved on the specimen as quickly as possible.

- c) Place the specimen in the cave, maximizing the distance between the specimen and yourself at all times. It is difficult to properly position the specimen with this tool. Set the specimen on the track and then replace the lid on the storage compartment. Store the plunger grasping tool in the container on top of the cave. Replace the lead bricks covering any specimens still in the storage compartment.
- d) Use the long tweezers stored in the container on top of the cave to properly position the specimen on the loading track. Close the cave doors as soon as the correct positioning of the specimen has been verified.
- e) Verify that the gloves picked up no contamination. Record the specimen ID code in the log book and proceed with the test.
- f) As soon as possible after the test is completed, open the storage compartment and remove the container lid using the plunger grasper or the tongs. Using the plunger grasper, retrieve the tested specimen (if it didn't break) or its halves (if it fractured completely) and replace them in the specimen container. If there are more untested specimens in the compartment, select one and repeat the procedure.

Most tested specimens will fall into the area directly beneath the anvils that is lined with metal sheet, although occasionally a specimen will come to rest elsewhere on the cave floor. Point out such locations to the RPT the next time the interior of the cave is surveyed.

**NICOLET OSCILLOSCOPE CONFIGURATION** (This portion deleted.)



**APPENDIX B**

**BASIC PROGRAM FOR AUTOMATED CVN TESTING**

'NewChpy2.BAS ; author - Lonnie E. Schubert

' Last modified 22 November 1994

'This program expects to be following a "WaveForm Basic" program. The WFBasic program is to have collected the load trace data off of the o-scope and written an ascii/CSV file of that data. The data in the file is formatted such that the first line consists of the file name in quotes ("TEMP@"), a comma, empty quotes (""), and a comma.

'The second line is the same format with the units ("Seconds ", "Volts ",)

'The following 4096 lines are number, comma, number, comma.

'Note: This program and the WFBasic program should be run from a batch file

'(TALL2.BAT) which runs the WFBasic program and then this one.

'The batch file should have appropriate commands to keep everything running smoothly and looping in a controlled manner.

'This program will write a DOS batch file for making backup copies.

'The controlling DOS batch file should call the "SAFETY.BAT" file.

'This BASIC program is intended for this one purpose only.

'The following is the WFBASIC program currently in use ("SHORT.PGM")

```
' 1 SUB SHORT
'10 TRANSFER(TEMP@,"ALL")
'20 ASTORE TEMP@,"C:\WFBASIC\DATA\TEMP.ASC"
'30 SYSTEM
'40 END
```

'Another general note: In the "SAFETY.BAT" file that the program writes, it expects there to be a compression routine called "LHA" available in the \DOS directory. The LHA program is a copyrighted FREEWARE program. The author grants full public, commercial, and private usage permission. You may wish to upgrade to more current versions as they become available. Or you may wish to utilize a different compression program. If you change something, be sure to change the way the program writes the batch file.

PRINT : PRINT

' ----==\*> 'Real' Variables!!!!!! <\*&====--

'The following variables are 'real' measurements. So, You **\*\*MUST\*\*** check these measurements regularly and change them whenever required.

'The gap in the velocity flag is 'FlagGap#', in meters.

'Check it, but it should not change unless the flag bends or some such.

'It will change, of course, if you use a different flag or one of the 'legs' instead of the gap.

'The distance between the top-inside edge of the velocity flag and the middle of the IR  
'detector sensor is 'HalfExtra#' for the half 'size specimens (in meters) and 'ThirdExtra#' for  
'the one-third size specimens (in meters) and 'MidSubExtra#' for the new 4 mm size (in  
'meters).

'MidSubExtra#' is 0.001 meters greater than 'HalfExtra#'.

'ThirdExtra#' is 0.0017 meters greater than 'HalfExtra#'.

'PROCEDURE: accurately position a 'dummy' Half size specimen, lower the striker  
'assembly, gently, by hand, to rest on the specimen, check with a hand mirror that the  
'specimen is still properly positioned, and measure the distance from the top of the gap of  
'the velocity flag to the center of the IR detector.

'Double check the measurement.

'Check the value every time you switch to sub-size testing from the full size configuration  
'and any time you adjust (or bump) the velocity flag or the IR sensor mount.

'Further, note that the flag and sensor should have already been adjusted such that when  
'the striker [configured for full-size specimens] rests on a properly positioned full size  
'specimen that the top-inside edge of the velocity flag is just below the center of the IR  
'detector. It should be noticeable with the unaided eye, but it should be within 0.5 mm of  
'the center.

'The acceleration due to gravity is 'g#' in meters per second per second.

'g#' is, of course, constant.

'The value  $9.81 \text{ m/s}^2$  is very close for the Hanford site. [this latitude and elevation.]

'The calibration factor for the full size (10 kip) load cell is

' 'FullCalib#' in kilonewtons per volt. (06 October 1991) The cell SN# is 8496-2256

'The calibration factor for the sub-size (3.5 kip) load cell is

' 'SubCalib#' in kilonewtons per volt. (07 July 1992) The cell SN# is 8902-10-6782

'The mass of the striker assembly in the full size configuration

'is 'FullMass#' (in kilograms).

'The mass of the striker assembly in the sub-size configuration

'is 'SubMass#' (in kilograms).

'A note on the masses. Both mass values were calculated as the sum of all of the  
'individual components. All of the components were measured to within 1/10th gram,  
'except the drop weight housing -- the component affixed to the guide rails. It was  
'measured with an accuracy of about  $\pm 7$  grams.

FlagGap# = .00418#

HalfExtra# = .051#

MidSubExtra# = HalfExtra# + .001#

ThirdExtra# = HalfExtra# + .0017#

g# = 9.81#

FullCalib# = 98.676#

SubCalib# = 31.203#

FullMass# = 15.353#

SubMass# = 14.725#

' ----==\*\*> End of 'Real' variables!!! <\*\*\*====----

100

PRINT : PRINT "The file name is expected to be formatted such that the first"

PRINT "3 or 4 characters are the specimen ID#, followed by an initial"

PRINT "for the size designation (F, H, M, or T), followed by an initial for"

PRINT " 'precracked' or 'notch only' (P or N), and followed by an 'R'"

PRINT "IF the material is radioactive (irradiated).": PRINT

INPUT "Enter the file name, 7 characters max., no extension: ", FileName\$

IF FileName\$ = "" OR LEN(FileName\$) > 7 THEN 100

DscFileName\$ = FileName\$ + ".dsc"

CsvFileName\$ = "c:\csv\" + FileName\$ + "1.csv"

120

Mo\$ = LEFT\$(DATE\$, 2)

IF Mo\$ = "01" THEN Month\$ = " January "

IF Mo\$ = "02" THEN Month\$ = " February "

IF Mo\$ = "03" THEN Month\$ = " March "

```

IF Mo$ = "04" THEN Month$ = " April "
IF Mo$ = "05" THEN Month$ = " May "
IF Mo$ = "06" THEN Month$ = " June "
IF Mo$ = "07" THEN Month$ = " July "
IF Mo$ = "08" THEN Month$ = " August "
IF Mo$ = "09" THEN Month$ = " September "
IF Mo$ = "10" THEN Month$ = " October "
IF Mo$ = "11" THEN Month$ = " November "
IF Mo$ = "12" THEN Month$ = " December "

```

```

Day$ = MID$(DATE$, 4, 2)
Year$ = RIGHT$(DATE$, 4): Check% = VAL(Year$)
  IF Check% < 1994 THEN
    BEEP: PRINT "The cumputer's date setting is invalid."
    INPUT "Enter the test date (dd Month yyyy):", TestDate$
    GOTO 200
  END IF
  Today$ = Day$ + Month$ + Year$

```

150

```

PRINT : PRINT : PRINT
PRINT " Today is "; Today$
PRINT " If this is the test date, tap Enter."
PRINT
INPUT " Otherwise, enter the correct date (dd Month yyyy): ", TestDate$
  IF TestDate$ <> "" THEN 200
TestDate$ = Today$

```

200

```

  IF LEN(TestDate$) < 9 THEN 120

```

210

'This section writes a DOS batch file which can and will (must) be  
'CALL'ed from the DOS batch file controlling this program.  
'The batch file will copy a duplicate of the descriptive file

'to the 'a:' drive. It will also create a compressed rendition  
 'of the '.CSV' data file and copy a duplicate of it to 'a:'.  
 'You should regularly clear all of the non-compressed '.CSV'  
 'data files from the hard drive.

```

OPEN "c:\wfbasic\safety.bat" FOR OUTPUT AS #1
PRINT #1, "rem This file was written by 'NewChpy2.bas(exe)'"
PRINT #1, "rem It is called by the batch file 'Tall2.bat' and"
PRINT #1, "rem should not need to be run otherwise."
PRINT #1, "rem This file was written on "; Today$; " at "; TIME$
PRINT #1, ":retry"
PRINT #1, "copy c:\wfbasic\data\"; DscFileName$; " a: /v"
PRINT #1, "if exist a:\"; DscFileName$; " goto mark"
PRINT #1, "@echo off"
PRINT #1, "echo."
PRINT #1, "echo "; CHR$(7); " File copy error!"
PRINT #1, "echo Most likely the disk is full."
PRINT #1, "echo Please replace the disk in drive A: and tap a key."
PRINT #1, "pause"
PRINT #1, "goto retry"
PRINT #1, ":mark"
PRINT #1, "c:\dos\lha a c:\wfbasic\data\"; FileName$; "1 "; CsvFileName$
PRINT #1, "if errorlevel 2 goto mark"
PRINT #1, "if errorlevel 1 goto problem"
PRINT #1, "goto continue"
PRINT #1, ":problem"
PRINT #1, "@echo off"
PRINT #1, "echo."
PRINT #1, "echo "; CHR$(7); " File creation error!"
PRINT #1, "echo Either the hard-drive is full or the FileName has been used before."
PRINT #1, "echo I can't logically handle either problem. You'll have to fix it yourself."
PRINT #1, "echo."
PRINT #1, "echo If the hard-drive is full, the solution should be obvious to you. ;->"

```

```
PRINT #1, "echo If you've used the file name before, you can either restart this process"
PRINT #1, "echo by tapping 'Ctrl-Break' to halt and exit the batch file, or you can let"
    PRINT #1, "echo the process continue and fix things later."
    PRINT #1, "echo I suggest the former (halting w/ Ctrl-Break and restarting w/ a"
    PRINT #1, "echo new/different filename), but what do I know, I'm just a computer."
    PRINT #1, "echo."
PRINT #1, "echo If the hard-drive is full, you have to halt. Nothing else will work."
    PRINT #1, "echo."
PRINT #1, "echo If you continue, the file 'FileName.CSV' will be the current load trace."
PRINT #1, "echo Also, the other/old file will still be on the disk as 'FileName.LZH'."
PRINT #1, "echo You will have to rename either or both. After renaming, compress the"
PRINT #1, "echo '.CSV' file with the 'LHA' command, and also copy the resulting '.LZH'"
    PRINT #1, "echo file to the A: drive as a backup."
    PRINT #1, "echo."
PRINT #1, "echo If you don't know how to use 'LHA' figure it out. It will be good for you!"
PRINT #1, "echo At the DOS prompt, type 'lha' and tap 'Enter' for a syntax summary."
    PRINT #1, "pause"
    PRINT #1, "echo."
    PRINT #1, "echo "; CHR$(7); " ----=*> DON'T forget!!!! <*=----"
    PRINT #1, "goto end"
    PRINT #1, ":continue"
    PRINT #1, "copy c:\wfbasic\data\"; FileName$; ".lzh a: /v"
    PRINT #1, "if exist a:"; FileName$; ".lzh goto end"
    PRINT #1, "@echo off"
    PRINT #1, "echo."
    PRINT #1, "echo "; CHR$(7); " File copy error!"
    PRINT #1, "echo Most likely the disk is full."
    PRINT #1, "echo Please replace the disk in drive A: and tap a key."
    PRINT #1, "pause"
    PRINT #1, "copy c:\wfbasic\data\"; DscFileName$; " a: /v"
    PRINT #1, "goto continue"
    PRINT #1, ":end"
```

```

CLOSE
220
PRINT : PRINT "Enter the Specimen ID and descriptive information. **Use NO commas.**"
INPUT "Limit entry to about 30 characters or so. ", SpID$
IF SpID$ = "" THEN 220
230 PRINT : PRINT
INPUT "Enter the test temperature (in degrees C) ", TestTempC#
IF TestTempC# = 0 THEN
PRINT : PRINT " Was the Specimen Test Temperature 0°C?": BEEP
INPUT " 'y' continues, else reprompts for temperature. ", y$
IF UCASE$(y$) = "Y" THEN 240 ELSE 230
END IF
IF TestTempC# < -273 OR TestTempC# > 500 THEN 230
240
PRINT : PRINT "For the velocity calculation, you should have measured"
PRINT "the time of passage of the gap in the velocity flag through"
PRINT "the IR sensor with the second o-scope."
PRINT "If not, enter an average time value from recent tests."
PRINT "(Of course the tests must have been from the same drop height.)"
PRINT : PRINT " To enter the velocity directly, enter '1'.": PRINT
INPUT "Enter the time of passage for the flag gap, in microseconds: ", MuSec#
IF MuSec# <> 1 THEN 245
INPUT "Enter the known velocity for this test: ", Velocity#
IF Velocity# < .5 THEN 240
GOTO 260
245
IF MuSec# < 500 THEN 240
Sec# = MuSec# / 1000000#
250
'NOTE!!! See the end of this file for a discussion of the <<*==--
' velocity calculation equations. <<*==--
VelocityFull# = FlagGap# / Sec#

```



260

PRINT : PRINT

PRINT "Enter the specimen size designation ('Case' is insignificant)"

INPUT "'Full', 'Half', 'Mid', or 'Third': ", Size\$

'The nested 'IF' statements within this BLOCK IF are to  
'keep the routine from resetting a manually entered velocity.

IF UCASE\$(Size\$) = "FULL" THEN

IF Velocity# &gt;= .5 THEN 262

Velocity# = VelocityFull#

262

Mass# = FullMass#

CalibFactor# = FullCalib#

ELSEIF UCASE\$(Size\$) = "HALF" THEN

IF Velocity# &gt;= .5 THEN 264

Velocity# = SQR((VelocityFull# ^ 2) + (2 \* g# \* HalfExtra#))

264

Mass# = SubMass#

CalibFactor# = SubCalib#

ELSEIF UCASE\$(Size\$) = "MID" THEN

IF Velocity# &gt;= .5 THEN 266

Velocity# = SQR((VelocityFull# ^ 2) + (2 \* g# \* MidSubExtra#))

266

Mass# = SubMass#

CalibFactor# = SubCalib#

ELSEIF UCASE\$(Size\$) = "THIRD" THEN

IF Velocity# &gt;= .5 THEN 268

Velocity# = SQR((VelocityFull# ^ 2) + (2 \* g# \* ThirdExtra#))

268

Mass# = SubMass#

CalibFactor# = SubCalib#

ELSE

BEEP: PRINT " Spell it correctly."

GOTO 260

END IF

'A note on impact velocity calculation.

'(The "IF-THEN-ELSE Block" of the preceding section.)

'With a full size specimen, the impact should begin an instant after

'the passage of the top edge of the gap in the velocity flag, less

'than one millimeter more fall. Accordingly, the velocity is simply

'the gap dimension divided by the time.

'For sub-size specimens, the striker is shorter, and the drop-weight

'assembly will fall significantly farther (measured by 'HalfExtra#').

'Neglecting friction, the velocity change due to the acceleration of

'gravity is equal to the square root of (2gh) where g is 9.81 m/sec<sup>2</sup>

'and h is the fall distance in meters. Also note that the final

'impact velocity equals the square root of the sum of the square of the

'velocity measured for full size and 2gh.

'--==\*>> SEE THE END OF THIS FILE FOR DETAILS!!! <<\*==--

300

'Writes the descriptive info. file.

OPEN "c:\wfbasic\data\" + DscFileName\$ FOR OUTPUT AS #1

PRINT #1, "This file is, "; DscFileName\$

PRINT #1, "The load trace '.CSV' file is, "; CsvFileName\$

PRINT #1, "The Test date was, "; TestDate\$

PRINT #1, "The Specimen ID# & info. is:, "; SpID\$

PRINT #1, USING "The specimen test temperature (degrees C) was, +###.#"; TestTempC#

PRINT #1, "The specimen tested was size, "; Size\$

PRINT #1, USING "The striker velocity (m/sec) at impact was, #.#####"; Velocity#

PRINT #1, USING "The time measured for the passing of the timing flag was ####.# microsec."; MuSec#

CLOSE

'Note: I've inserted the commas and formatting to ensure that, if

'ever the need arises, it will be a simple matter to write a BASIC

'program which can retrieve the info. in the file.

'The rules for the INPUT #1 statement should make it obvious

'how one would read the info. from the file.

1000

'The following routine will collect data from a comma separated variable (CSV)

'file and massage it into a "standard" x-y file, still CSV format.

'The program is for time vs. voltage data from the CVN system. ('Raw' data  
'from the o-scope.)

'It assumes the first two lines will be preliminary string values.

'(Namely: "Temp@", "", and "Seconds ", "Volts ", )

'It assumes there will be 4096 x-y data pairs, one per line (##,##,##).

'It will set the last 4000 points to be the "Excel" plottable trace,

'and average out the zero-point load.

'The program "CSVM.BAS" is specialized for this purpose, and this routine

'is modified from it.

PRINT : PRINT " Reading in x-y data.": PRINT

' ---\*\*> The next line is a metacommand, not a comment. <\*\*---

'\$DYNAMIC

DIM mm(4096), kN(4096), dJ(4096), SumJ(4096), Dummy(4096) AS DOUBLE

' Sets an array for 'Nicolet' Charpy files

' "mm()" is the first number read from the file, "kN()" is the second

' number (or, the odd entries and the even entries, respectively).

' These two variables are read from the .CSV file and subsequently

' converted to mm and kN values.

' "dJ()" is the differential energy, and "SumJ()" is the

' cumulative energy. These two values and "Dummy()" are calculated

' in this program.

' (As noted: The Nicolet data will consist of 4096 numeric pairs.

' The values represent time versus volts.)

1020

'The output file will be written as "FileName\$1.csv and placed in

'the \CSV directory on "this" AT's hard drive.

```
inname$ = "c:\wfbasic\data\temp.asc"
```

'Reads the values from the file into the "mm(), kN()" array, and  
'counts the exact number of entries.

'(Since the WFBasic program adds a comma to the end of each line,  
' the "Nothing\$" variable is actually nothing -- except a  
' place holder.)

1040

```
OPEN inname$ FOR INPUT AS #2
    INPUT #2, XUnits$, YUnits$, Nothing$
    INPUT #2, XUnits$, YUnits$, Nothing$
    n% = -1
    DO
        n% = n% + 1
        INPUT #2, mm(n%), kN(n%), Nothing$
    LOOP UNTIL EOF(2)
CLOSE 2
```

1200

'This section calculates the displacement during the fracture event  
'by assuming that the velocity calculated at impact ('Velocity#') is  
'constant throughout the event. (Since the assumption is not correct,  
'the program corrects for it later.)

```
FOR j% = 0 TO n%
    mm(j%) = mm(j%) * Velocity# * 1000#
NEXT
```

'The mm() array variables are now in units of millimeters.

1250

'The following SET line and FOR-NEXT loop adjusts the distance to be zero  
'at the "97th" value; the first value in a 4000 point chart (Excel max.).  
'This merely shifts the curve horizontally.

```
mm96# = mm(96)
```

```

FOR j% = 0 TO n%
    mm(j%) = mm(j%) - mm96#
NEXT

```

1500

'This section assumes the first 12 points are representative of "zero" load. This assumption allows conversion to load from volts with the first few points beginning near zero load.

'The assumption should be valid for all valid load traces. If not, the rest of the program is probably not going to give valid calculations, but everything should still work. However, you will need to utilize Excel to get the final energy values.

```

VoltSum# = 0#
FOR j% = 0 TO 11
    VoltSum# = VoltSum# + kN(j%)
NEXT

```

```

VoltAvg# = VoltSum# / 12#

```

'This FOR-NEXT loop shifts the volt values up to 'zero'.

```

FOR j% = 0 TO n%
    kN(j%) = kN(j%) - VoltAvg#
NEXT

```

'This FOR-NEXT loop converts the volts to kilonewtons.

```

FOR j% = 0 TO n%
    kN(j%) = kN(j%) * CalibFactor#
NEXT

```

2000

'The following pair of DO-LOOPS finds the beginning of the load/fracture event.

'The following DO-LOOP finds where the load actually rises

'above background noise.

m% = 0

DO

    m% = m% + 1

LOOP UNTIL kN(m%) > .16

'The following DO-LOOP backs up to the beginning of the event.

DO WHILE kN(m%) > 0#

    m% = m% - 1

LOOP

3000

'The following pair of FOR-NEXT loops vertically shift the load

'trace to a "true" zero. As long as the load trace was processed

'properly off of the o-scope, the value of "ZeroAvg#" should be

'a small number, and the sum of the energy at the distance "mm(m%)"

'should be very close to zero.

SumAvg# = 0#

FOR j% = 0 TO m%

    SumAvg# = SumAvg# + kN(j%)

NEXT

    ZeroAvg# = SumAvg# / m%

FOR j% = 0 TO n%

    kN(j%) = kN(j%) - ZeroAvg#

NEXT

4000

'The next FOR-NEXT loop calculates the differential energies and

'sums them in a running total. The loop fills the dJ() and SumJ()

'array variables.

dJ(0) = 0#: SumJ(0) = 0#

FOR j% = 1 TO n%

    dJ(j%) = (mm(j%) - mm(j% - 1)) \* kN(j%)

```

SumJ(j%) = SumJ(j% - 1) + dJ(j%)
NEXT
PRINT : PRINT : PRINT "*****"
PRINT "The following line should have two words, 'Seconds' & 'Volts'"
PRINT XUnits$; YUnits$: PRINT
PRINT "If not, the units are off, and the calculations will be wrong."
PRINT : PRINT
    'Thus, the file is printed as the adjusted x,y data with
    'the calculated running total of the energy.

OPEN CsvFileName$ FOR OUTPUT AS #2
    FOR j% = 0 TO n%
PRINT #2, USING "#.#####^,#.#####^,#.#####^"; mm(j%); kN(j%); SumJ(j%)
        'The "PRINT" line formats the values in scientific notation
        'to retain max. precision.
    NEXT
CLOSE 2

PRINT : PRINT "The descriptive file and the data file have been written."
PRINT "The data file is ready to be imported into Excel.": SLEEP 1
PRINT : PRINT "The rest of these calculations may take awhile."

CLOSE

5000

'This next section will not always work right, so the 'velocity corrected' energy may not be
'accurate. The objective is to find where the load zero's out at the end and cut it off there.
'I'm putting in the averaging routine to increase confidence in the 'end' find, but the 'true' load
'trace is still used for the energy calculation. Again, the 'finder' will not always be correct!

i% = 0: l% = n% - 4
DO
    Dummy(1) = (kN(1) + kN(2)) / 3
    Dummy(2) = (kN(1) + kN(2) + kN(3) + kN(4)) / 5
    Dummy(3) = (kN(1) + kN(2) + 2 * kN(3) + kN(4) + kN(5) + kN(6)) / 8
    FOR j% = 4 TO l%

```

```
Dummy(j%) = (kN(j% - 4) + kN(j% - 3) + kN(j% - 2) + 2 * kN(j% - 1) + 5 * kN(j%) + 2 * kN(j% + 1) + kN(j% + 2) + kN(j% + 3) + kN(j% + 4)) / 15
```

```
    NEXT
```

```
Dummy(n% - 3) = (kN(n% - 6) + kN(n% - 5) + kN(n%) + 2 * kN(n% - 3) + kN(n% - 2) + kN(n% - 1) + kN(n%)) / 8
```

```
    Dummy(n% - 2) = (kN(n% - 3) + kN(n% - 1) + kN(n%)) / 3
```

```
    Dummy(n% - 1) = (kN(n% - 2) + kN(n% - 1) + kN(n%)) / 3
```

```
    Dummy(n%) = kN(n% - 1) / 2
```

```
FOR j% = 0 TO n%
```

```
    kN(j%) = Dummy(j%)
```

```
    NEXT
```

```
PRINT " Still working!": PRINT
```

```
    i% = i% + 1
```

```
    LOOP UNTIL i% = 5
```

'Note that i% determines how many times the waveform is averaged.

'Increase or decrease the value of i%

'following the "LOOP UNTIL" statement to control the

'number of averaging passes conducted.

```
e% = 950
```

```
DO
```

```
    e% = e% + 1
```

```
    IF e% = 4095 THEN EXIT DO
```

```
LOOP UNTIL kN(e%) < -.015
```

```
    IF e% = 4095 THEN
```

```
        BEEP: BEEP: BEEP: PRINT : PRINT : BEEP
```

```
        PRINT " The load trace may not be complete!"
```

```
        PRINT " Using entire load trace for energy.": PRINT
```

```
        SLEEP 4
```

```
    END IF
```

'This section calculates the "true" energy from the just established



'best guess energy ("apparent" energy).

'Mass# is the striker assembly mass.

$$\text{TotalKineticE\#} = .5 * \text{Mass\#} * (\text{Velocity\#} ^ 2)$$

$$\text{Factor\#} = 1 - (\text{SumJ(e\%)} / (4 * \text{TotalKineticE\#}))$$

$$\text{VelCorrect\#} = \text{SumJ(e\%)} * \text{Factor\#}$$

'\*\*\*\*\* Comment/Uncomment the following line to On/Off printer output. \*\*\*\*\*

' GOTO 9999

'The next section prints output on the printer.

LPRINT : LPRINT

LPRINT " Descriptive file is "; DscFileName\$

LPRINT " Test Date was "; TestDate\$

LPRINT " Specimen Description: "; SpID\$

LPRINT " Specimen Test Temp. (in degrees C): "; TestTempC#

LPRINT " Size is "; Size\$

LPRINT USING " The flag-gap measurement was ####.# microseconds."; MuSec#

LPRINT USING " The test velocity was #.##### m/sec."; Velocity#

LPRINT USING " Total 'Raw' energy for load trace ##.### J"; SumJ(n%)

LPRINT USING " Computer 'guess' of 'apparent' energy ##.### J"; SumJ(e%)

LPRINT USING " Velocity corrected energy of the 'guess' ##.### J"; VelCorrect#

LPRINT USING " Full curve length (Max. Displ.): ##.### mm"; mm(n%)

LPRINT USING " 'Start' = ##.### mm, 'End' = ##.### mm"; mm(m%); mm(e%)

9999

'This section is only remark information. The program has ended.

'This section discusses the velocity calculations.

'Followed by a discussion of the energy correction calculation.

'The following applies to any particle undergoing uniform (constant)  
'acceleration [rectilinear]

'(a = v / t ; and v = a\*t ; and s / t = v , in general--by definition.)

't = time (the full time interval being examined).

' [t begins at the moment of weight release from rest.]

'  $\tau$  = the time interval between the velocity measurement and impact for  
' a subsize specimen test.

' s = displacement/distance (one-dimensional Space passed through,  
' from rest to impact).

' h = displacement/distance corresponding to time  $\tau$ .  
' (The distance from the velocity measurement position to the  
' [subsize] impact position.)

' a = the acceleration (equals g for free-fall and is constant).

' v1 = the initial velocity (the measured velocity).  
' (The velocity measured for a full size specimen at impact.)

'  $v1 = a \cdot (t - \tau) = (s - h) / (t - \tau)$

' v2 = the velocity after time interval t  
' (the velocity at impact for a subsize specimen)

'  $v2 = v1 + a \cdot \tau = v1 + \delta v = v1 + (h / \tau) = s / t$

'  $\delta v = v2 - v1 = a \cdot \tau = h / \tau$

'  $h = v1 \cdot \tau + \frac{1}{2} \cdot a \cdot \tau^2$   
' (this equation is evident by definition, but it also follows  
' from the equation,  $v2 = v1 + a \cdot \tau$ , by integration w/rspcto.  $\tau$ .)

'  $v2 = v1 + \delta v$   
'  $v2^2 = (v1 + \delta v)^2$   
'  $= v1^2 + 2 \cdot v1 \cdot \delta v + \delta v^2$

' Substituting  $a \cdot \tau$  for  $\delta v$

'  $v2^2 = v1^2 + 2 \cdot v1 \cdot a \cdot \tau + a^2 \cdot \tau^2$   
'  $= v1^2 + 2a \cdot (v1 \cdot \tau + \frac{1}{2} \cdot a \cdot \tau^2)$

' Substituting h for the '()' enclosed term.

'  $v2^2 = v1^2 + 2ah$

' and  $v2 = \sqrt{v1^2 + 2ah}$

' and thus  $v2 = \sqrt{v1^2 + 2gh}$

'and this equation is the one utilized in this program as:

"velocity# = SQR((VelocityFull# ^ 2) + (2 \* g# \* HalfExtra#))"

' (of course "ThirdExtra#" is substituted as appropriate.)

'One can verify these equations from various reference books.

'The most likely source is a college physics course text book.

'Most technical reference books should have the equations also,

'but you may have to look up several variants of possible labels.

'(Such as Uniform acceleration, Free fall, constant velocity, etc.)

'Note that for an initial velocity of zero, i.e., starting from rest,

'the equation reduces to:

'

$$v = \sqrt{2gh}$$

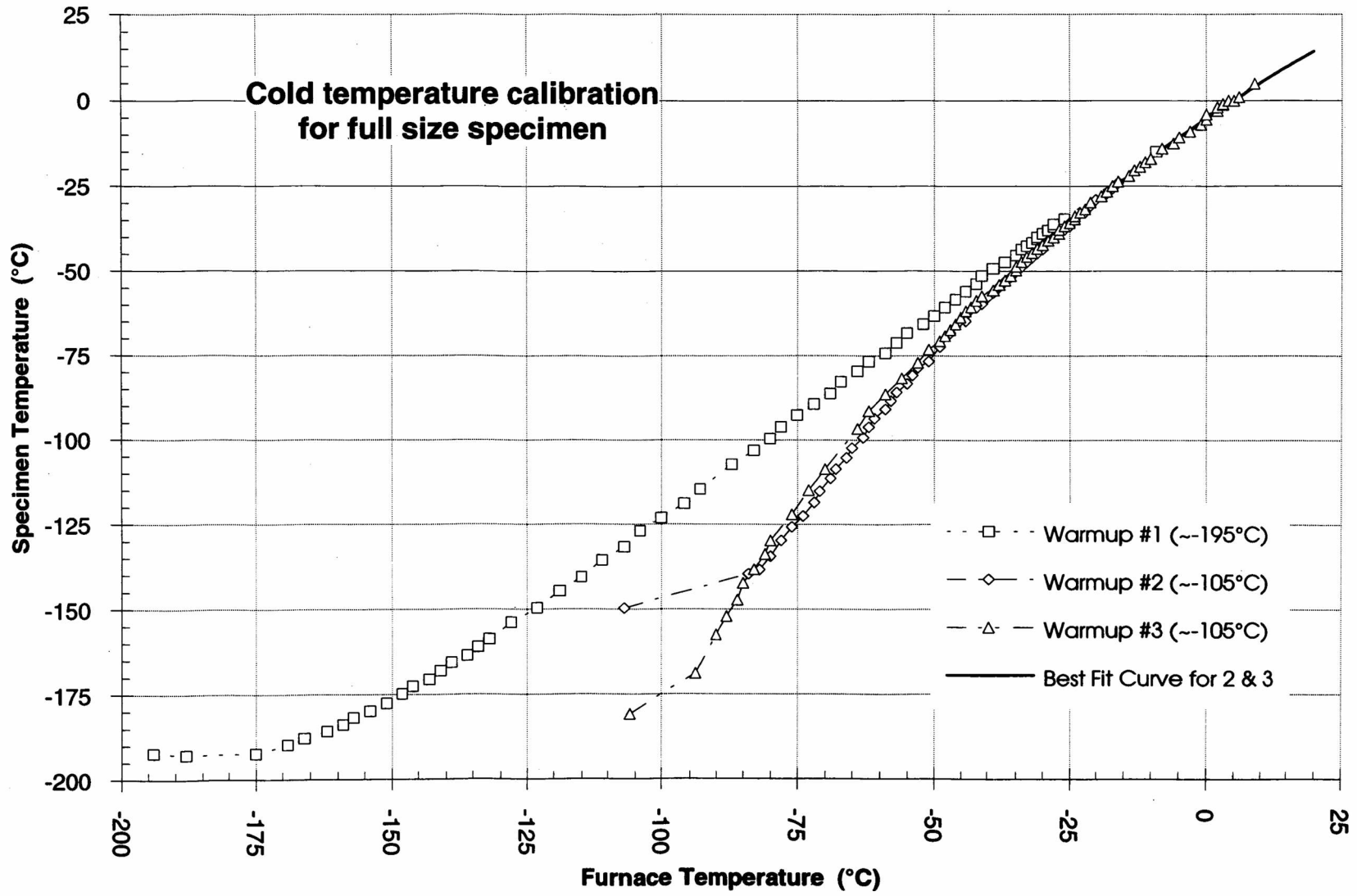
'This equation should be generally recognized as the equation of

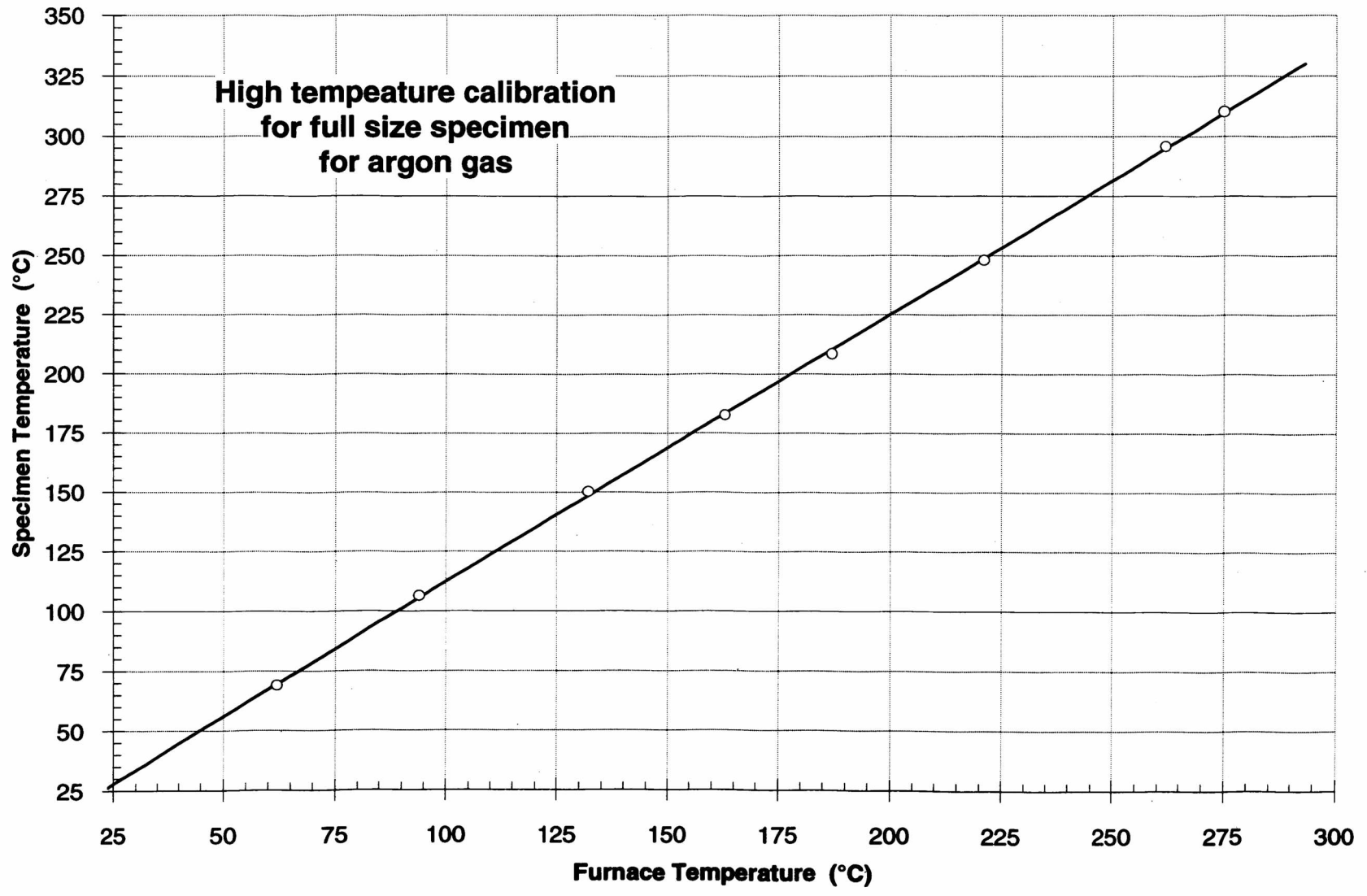
'velocity after free fall from rest and a specific height (in vacuum).

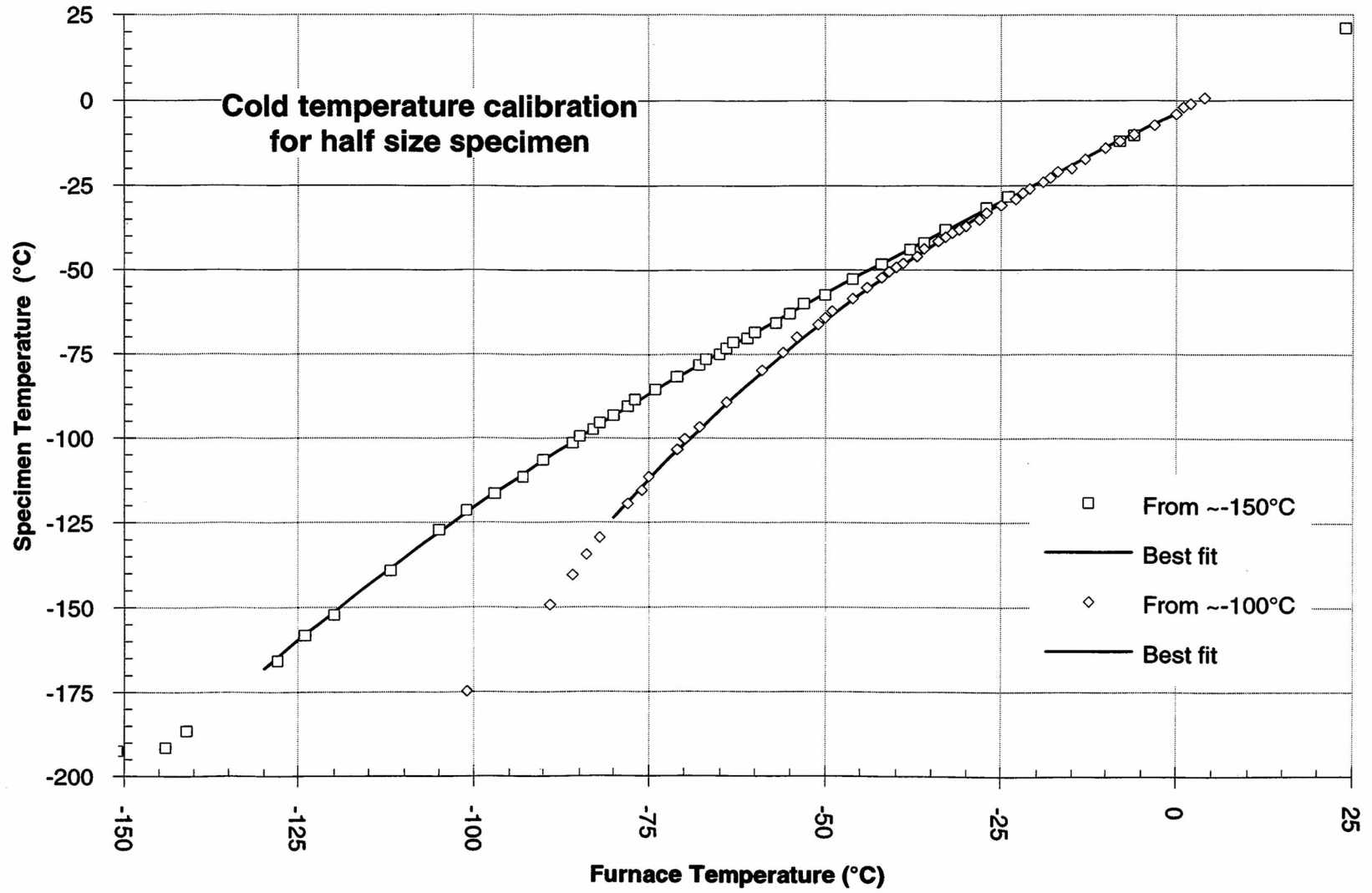
END

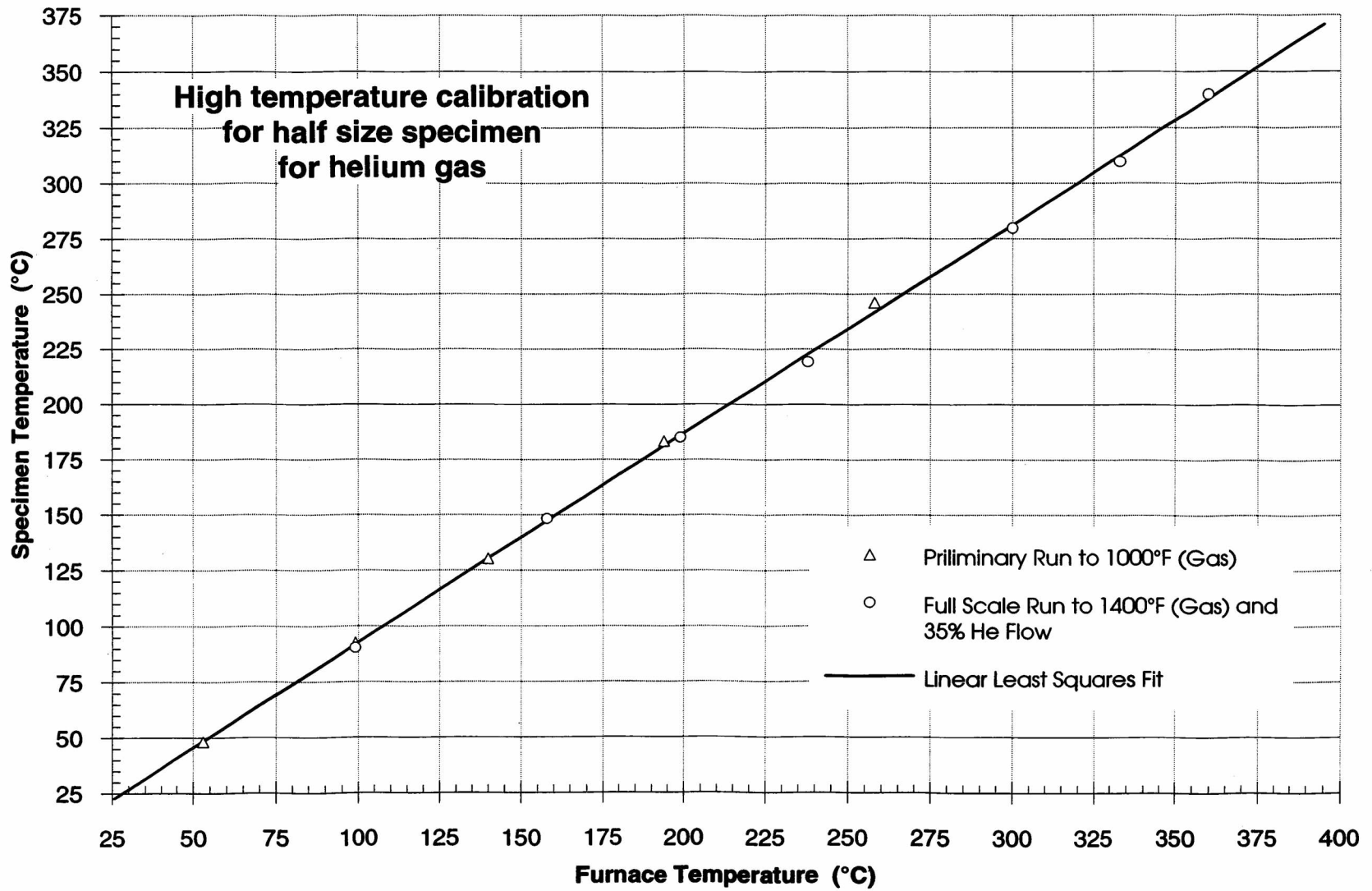
**APPENDIX C**

**TEMPERATURE CALIBRATION CHARTS**

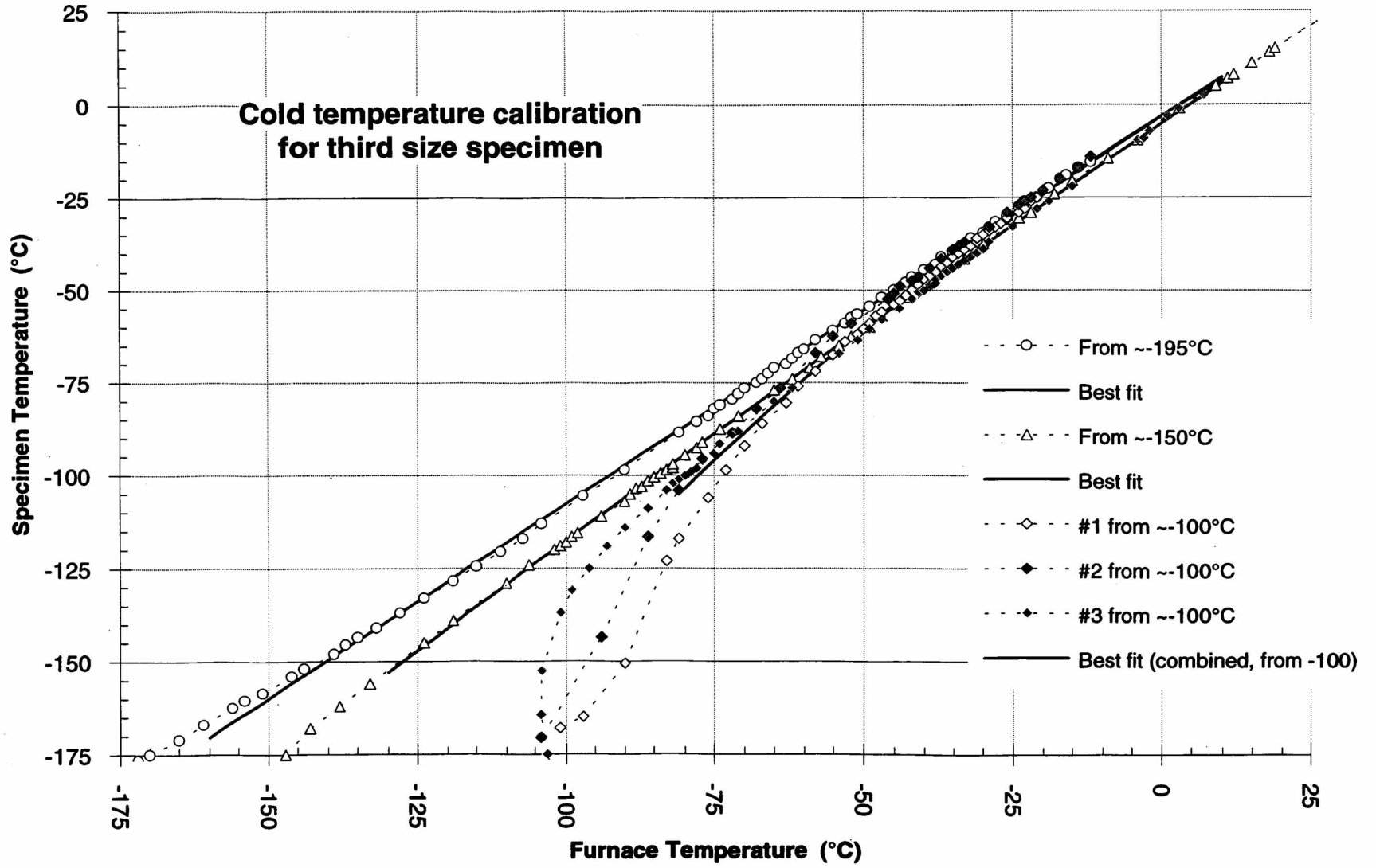


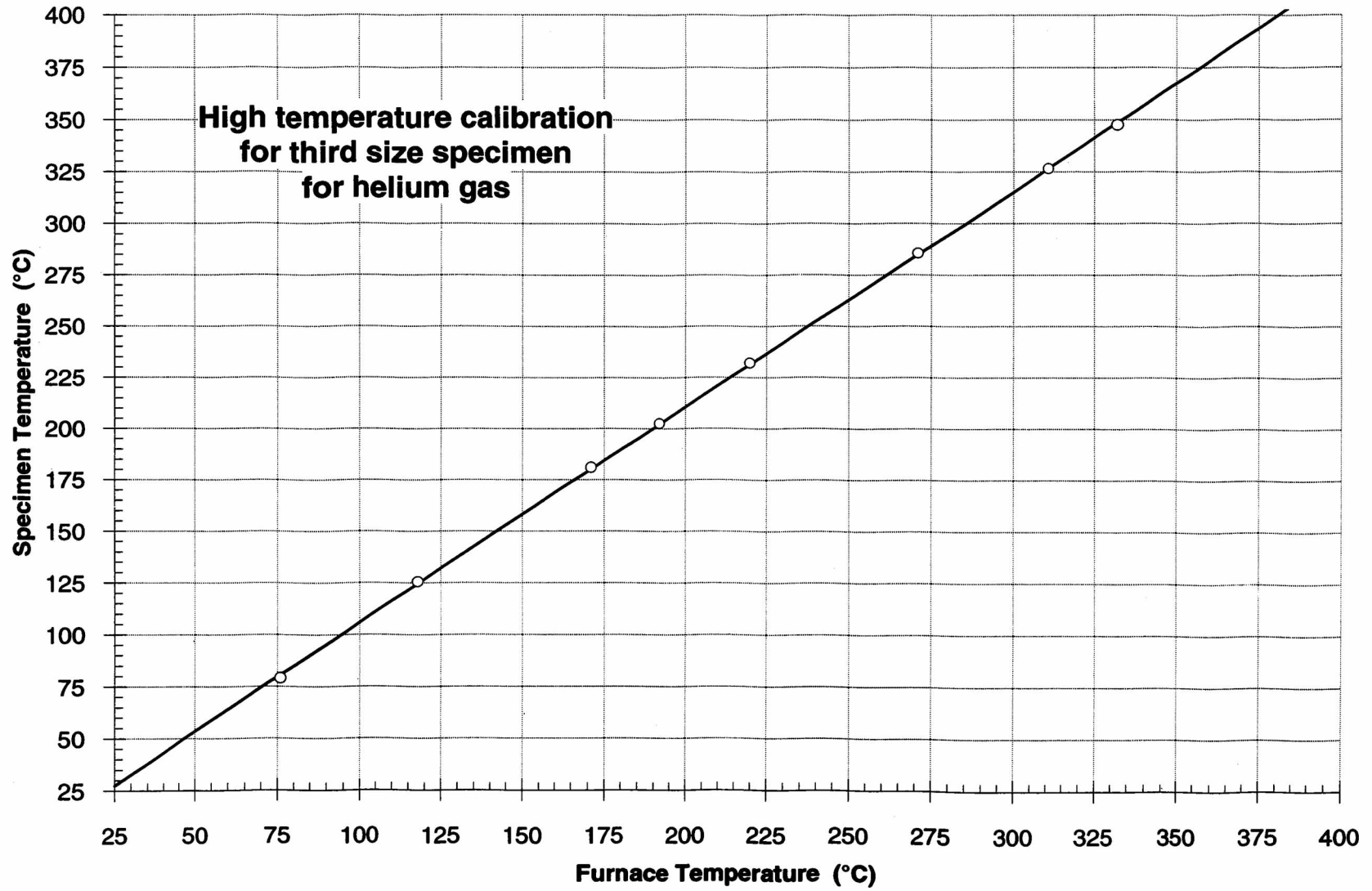












**APPENDIX D**  
**CURVE FIT STATISTICS**

Full size, unirradiated

$$Y = \#A + \#B * \text{TANH}(\#C * (X - \#D))$$

r <sup>2</sup> Coef Det	DF Adj r <sup>2</sup>	Fit Std Err	F-value
0.9380149688	0.8966916146	6.8669077478	35.310163598

Parm	Value	Std Error	t-value	95% Confidence Limits	
a	32.11719836	4.178131512	7.686976407	22.19857830	42.03581842
b	31.27491194	6.209218630	5.036851462	16.53461947	46.01520441
c	0.011285332	0.004751226	2.375246289	6.22178e-06	0.022564442
d	87.88760375	19.15529002	4.588163565	42.41415629	133.3610512

---

Full size, irradiated

$$Y = (\#A + .9) + \#A * \text{TANH}(\#B * (X - \#C))$$

r <sup>2</sup> Coef Det	DF Adj r <sup>2</sup>	Fit Std Err	F-value
0.8345113846	0.7517670770	7.3959274196	17.649491115

Parm	Value	Std Error	t-value	95% Confidence Limits	
a	25.56881934	3.270958331	7.816919922	17.80377106	33.33386762
b	0.013156528	0.007755248	1.696467801	-0.00525394	0.031566996
c	163.4659994	17.79751690	9.184764389	121.2158195	205.7161793

---

Half size, unirradiated

$$Y=(\#A+1.25)+\#A*\text{TANH}(\#B*(X-\#C))$$

r <sup>2</sup> Coef Det	DF Adj r <sup>2</sup>	Fit Std Err	F-value
0.9997914049	0.9995828097	0.0860786406	9585.9514851

Parm	Value	Std Error	t-value	99% Confidence Limits	
a	5.968016005	0.048117765	124.0293673	5.746565913	6.189466097
b	0.014208079	0.000339599	41.83783958	0.012645160	0.015770999
c	122.4216457	1.119124747	109.3905269	117.2711514	127.5721400

---

Half size, irradiated

$$Y=(\#A+.5)+\#A*\text{TANH}(\#B*(X-\#C))$$

r <sup>2</sup> Coef Det	DF Adj r <sup>2</sup>	Fit Std Err	F-value
0.9635098356	0.9478711937	0.9086295722	105.61857972

Parm	Value	Std Error	t-value	95% Confidence Limits	
a	5.292781314	0.350445160	15.10302299	4.481831933	6.103730695
b	0.015716611	0.003985409	3.943537778	0.006494155	0.024939066
c	187.1087867	8.507544080	21.99327854	167.4218616	206.7957117

---

Third size, unirradiated

$$Y=\#A+\#B*\text{TANH}(\#C*(X-\#D))$$

r <sup>2</sup> Coef Det	DF Adj r <sup>2</sup>	Fit Std Err	F-value
0.9718664274	0.9437328547	0.3836574306	57.574535570

Parm	Value	Std Error	t-value	95% Confidence Limits	
a	2.430051339	0.229803474	10.57447610	1.837136356	3.022966323
b	2.271613693	0.345112441	6.582242253	1.381190524	3.162036862
c	0.011489814	0.004061795	2.828752974	0.001009994	0.021969634
d	99.70245294	15.83622554	6.295846994	58.84347355	140.5614323

---

Third size, irradiated

$$Y=2.05+1.95*\text{TANH}(\#A*(X-\#B))$$

r <sup>2</sup> Coef Det	DF Adj r <sup>2</sup>	Fit Std Err	F-value
0.9687728588	0.9618334941	0.2704270629	310.23424565

Parm	Value	Std Error	t-value	99% Confidence Limits	
a	0.010116501	0.001282569	7.887685836	0.006051580	0.014181423
b	170.1728380	6.572239864	25.89267001	149.3430501	191.0026259

---

## BIBLIOGRAPHY

- [1] Nanstad, R. K., McCabe, D. E., Menke, B. H., Iskander, S. K., and Haggag, F. M., "Effects of Radiation on  $K_{Ic}$  Curves for High Copper Welds," *Effects of Radiation on Materials: 14th International Symposium (Vol. II)*, ASTM STP 1046, N. H. Packan, R. E. Stoller, and A. S. Kumar, Eds. American Society for Testing and Materials, Philadelphia, PA, 1990, pp. 214-233.
- [2] ASTM A 370 - 92, "Standard Test Methods and Definitions for Mechanical Testing of Steel Products," *Annual Book of ASTM Standards*, Volume 03.01, American Society for Testing and Materials, Philadelphia, PA, 1993, pp. 9-19.
- [3] ASTM E 23 - 93a, "Standard Test Methods for Notched Bar Impact Testing of Metallic Materials," *Annual Book of ASTM Standards*, Volume 03.01, American Society for Testing and Materials, Philadelphia, PA, 1993, pp. 206-224.
- [4] "Title 10," *Code of Federal Regulations*, Parts 0 to 199, U.S. Government Printing Office, Washington, DC, January 1987 (10CFR50, Appendix G).
- [5] *ASME Boiler and Pressure Vessel Code, An American National Standard*, Sections III and XI, American Society of Mechanical Engineers, New York, 1986.
- [6] "Radiation Embrittlement of Reactor Vessel Materials," *Regulatory Guide 1.99* (Revision 2), U. S. Nuclear Regulatory Commission, Washington, DC, May 1988.
- [7] ASTM A 533/A 533M - 90, "Standard Specification for Pressure Vessel Plates, Alloy Steel, Quenched and Tempered, Manganese-Molybdenum and Manganese-Molybdenum-Nickel," *Annual Book of ASTM Standards*, Volume 01.04, American Society for Testing and Materials, Philadelphia, PA, 1993, pp. 327-329.
- [8] ASTM A 20/A 20M - 92, "Standard Specification for General Requirements for Steel Plates for Pressure Vessels," *Annual Book of ASTM Standards*, Volume 01.04, American Society for Testing and Materials, Philadelphia, PA, 1993, pp. 64-88.
- [9] Grounes, M., "Review of Swedish Work on Irradiation Effects in Pressure Vessel Steels and Significance of Data Obtained," *Effects of Radiation on Structural Metals*, ASTM STP 426, American Society for Testing and Materials, Philadelphia, PA, 1967, pp. 224-259.
- [10] McConnell, P., Sheckherd, J. W., Perrin, J. S., and Wullaert, R. A., "Experience in Subsize Specimen Testing," *The Use of Small-Scale Specimens for Testing Irradiated Materials*, ASTM STP 888, W. R. Corwin and G. E. Lucas, Eds., American Society for Testing and Materials, Philadelphia, PA, 1986, pp. 353-368.
- [11] Lucas, G. E., Odette, G. R., Sheckherd, J. W., McConnell, P., and Perrin, J., "Subsize Bend and Charpy V-Notch Specimens for Irradiated Testing," *The Use of Small-Scale Specimens for Testing Irradiated Materials*, ASTM STP 888, W. R. Corwin and G.

E. Lucas, Eds., American Society for Testing and Materials, Philadelphia, PA, 1986, pp. 305-324.

[12] Wullaert, R. A., "Applications of the Instrumented Charpy Impact Test," *Impact Testing of Metals, ASTM STP 466*, American Society for Testing and Materials, Philadelphia, PA, 1970, pp. 148-164.

[13] Wullaert, R. A., Ireland, D. R., and Tetelman, A. S., "Radiation Effects on the Metallurgical Fracture Parameters and Fracture Toughness of Pressure Vessel Steels," *Irradiation Effects on Structural Alloys for Nuclear Reactor Applications, ASTM STP 484*, American Society for Testing and Materials, Philadelphia, PA, 1970, pp. 20-41.

[14] Wilshaw, T. R. and Pratt, P. O., "The Effect of Temperature and Strain Rate on the Deformation and Fracture of Mild-Steel Charpy Specimens," *Proceedings of the First International Conference on Fracture*, Volume 2, Sendai, Japan, September 1965, p. 973.

[15] Knott, J. F., *Fundamentals of Fracture Mechanics*, Halsted Press, John Wiley and Sons, Inc., New York, 1973, pp. 38 & 179.

[16] Hill, R., *Mathematical Theory of Plasticity*, Oxford, London, 1950, pp. 247 ff.

[17] Neuber, H., U. S. Atomic Energy Commission translation of *Theory of Notch Stresses, Principles for Exact Calculation of Strength with Reference to Structural Form and Material*, Second Edition, Springer, Berlin, 1958, pp. 60, 62, & 71

[18] Tetelman, A. S. and McEvily, A. J. R., *Fracture of Structural Materials*, Wiley, New York, 1967.

[19] Green, A. P. and Hundy, R. B., "Initial Plastic Yielding in Notch Bend Tests," *Journal of the Iron and Steel Institute, JISIA*, Volume 4, 1965, p. 128.

[20] Ewing, D. J. F. *Journal of Mechanics and Physics of Solids*, Volume 16, 1968, p. 205.

[21] Server, W. L., "Impact Three-Point Bend Testing for Notched and Precracked Specimens," *Journal of Testing and Evaluation, JTEVA*, Volume 6, Number 1, January 1978, pp. 29-34.

[22] Lucas, G. E., Odette, G. R., Sheckherd, J. W., and Krishnadev, M. R., "Recent Progress in Subsize Charpy Impact Specimen Testing for Fusion Reactor Materials Development," *Fusion Technology*, Volume 10, November 1986, pp. 728-733.

[23] Corwin, W. R. and Hougland, A. M., "Effects of Specimen Size and Material Condition on the Charpy Impact Properties of 9Cr-1Mo-V-Nb Steel," *The Use of Small-Scale Specimens for Testing Irradiated Materials, ASTM STP 888*, W. R. Corwin and G. E. Lucas, Eds., American Society for Testing and Materials, Philadelphia, PA, 1986, pp. 325-338.



- [24] Ritchie, R. O., "On the Relationship between Fracture Toughness and Charpy V-notch Energy in Ultrahigh Strength Steel," *What does the Charpy Test Really Tell Us?* American Society for Metals, Metals Park, Ohio, 1978, pp. 54-73.
- [25] Kurishita, H., Kayano, H., Narui, M., Yamazaki, M., Kano, Y., and Shibahara, I., "Effects of V-Notch Dimensions on Charpy Impact Test Results for Differently Sized Miniature Specimens of Ferritic Steel," *Materials Transactions, JIM*, Volume 34, Number 11, 1993, pp. 1042-1052.
- [26] Kurishita, H., Kayano, H., Narui, M., Yamazaki, M., "Current Status of Small Specimen Technology in Charpy Impact Testing," *Journal of Nuclear Materials*, Volumes 212-215, 1994, pp. 1682-1687.
- [27] Hu, W. L. and Gelles, D. S., "Miniature Charpy Impact Test Results for the Irradiated Ferritic Alloys HT-9 and Modified 9Cr-1Mo," *Proceedings of: Topical Conference on Ferritic Alloys for use in Nuclear Energy Technologies*, J. W. Davis and D. J. Michel, Eds., Snowbird, UT, June 1983, pp. 631-645.
- [28] Loudon, B. S., Kumar, A. S., Garner, F. A., Hamilton, M. L., and Hu, W. L., "The Influence of Specimen Size on Charpy Impact Testing of Unirradiated HT-9," *Journal of Nuclear Materials*, Volumes 155-157, 1988, Part B, pp. 662-667.
- [29] Kumar, A. S., Garner, F. A., Hamilton, M. L., "Effect of Specimen Size on the Upper Shelf Energy of Ferritic Steels," *Effects of Radiation on Materials: 14th International Symposium (Volume II)*, ASTM STP 1046, N. H. Packan, R. E. Stoller, and A. S. Kumar, Eds., American Society for Testing and Materials, Philadelphia, PA, 1990, pp. 487-495.
- [30] Kumar, A. S., Loudon, B. S., Garner, F. A., and Hamilton, M. L., "Recent Improvements in Size Effects Correlations for DBTT and Upper Shelf Energy of Ferritic Steels," *Small Specimen Test Techniques Applied to Nuclear Reactor Vessel Thermal Annealing and Plant Life Extension*, ASTM STP 1204, W. R. Corwin, F. M. Haggag, and W. L. Server, Eds., American Society for Testing and Materials, Philadelphia, PA, 1993, pp. 47-61.
- [31] Rosinski, S. T., Kumar, A. S., Cannon, N. S., and Hamilton, M. L., "Application of Subsize Specimens in Nuclear Plant Life Extension," *Small Specimen Test Techniques Applied to Nuclear Reactor Vessel Thermal Annealing and Plant Life Extension*, ASTM STP 1204, W. R. Corwin, F. M. Haggag, and W. L. Server, Eds., American Society for Testing and Materials, Philadelphia, PA, 1993, pp. 405-416.
- [32] Kumar, A. S., Rosinski, S. T., Cannon, N. S., Hamilton, M. L., "Subsize Specimen Testing of a Nuclear Reactor Pressure Vessel Material," *Effect of Radiation on Materials: 16th International Symposium*, ASTM STP 1175, A. S. Kumar, D. S. Gelles, R. K. Nanstad, and E. A. Little, Eds., American Society for Testing and Materials, Philadelphia, PA, 1993, pp. 147-155.

- [33] Kumar, A. S., Cannon, N. S., Hamilton, M. L., "Effect of Specimen Size on the Impact Properties of a Pressure Vessel Weld Material," *Effect of Radiation on Materials: 16th International Symposium, ASTM STP 1175*, A. S. Kumar, D. S. Gelles, R. K. Nanstad, and E. A. Little, Eds., American Society for Testing and Materials, Philadelphia, PA, 1993, pp. 283-291.
- [34] Turner, C. E., "Measurement of Fracture Toughness by Instrumented Impact Test," *Impact Testing of Metals, ASTM STP 466*, American Society for Testing and Materials, Philadelphia, PA, 1970, pp. 93-114.
- [35] Yamada, R., "On the Relation Between Stress and Strain in the Impact Test," *Japan Society of Mechanical Engineers*, Volume 31, 1928, p. 420.
- [36] Watanabe, S., "Study on Impact Test by Means of Piezo-Electricity and Cathode-Ray Oscillograph," *Scientific Papers of the Institute of Physical and Chemical Research*, Tokyo, Volume 213, 1929, p. 99.
- [37] Augland, B., "Fracture Toughness and the Charpy V-Notch Test," *British Welding Journal*, Volume 9, 1962, p. 434.
- [38] Grumbach, M., Prudhomme, M., and Sanz, G., *Revue de Metallurgie*, April 1969, p. 271.
- [39] Cheresh, M. C. and McMichael, S., "Instrumented Impact Test Data Interpretation," *Instrumented Impact Testing of Plastics and Composite Materials, ASTM STP 936*, S. L. Kessler, G. C. Adams, S. B. Driscoll, and D. R. Ireland, Eds., American Society for Testing and Materials, Philadelphia, PA, 1987, pp. 9-23.
- [40] Ireland, D. R., "Procedures and Problems Associated with Reliable Control of the Instrumented Impact Test," *Instrumented Impact Testing ASTM STP 563*, American Society for Testing and Materials, Philadelphia, PA, 1974, pp. 3-29.
- [41] Server, W. L., and Ireland, D. R., "Nonstandard Test Techniques Utilizing the Instrumented Charpy and Izod Tests," *Instrumented Impact Testing ASTM STP 563*, American Society for Testing and Materials, Philadelphia, PA, 1974, pp. 74-91.
- [42] Venzi, S., Priest, A. H., and May, M. J., "Influences of Inertial Load in Instrumented Impact Tests," *Impact Testing of Metals, ASTM STP 466*, American Society for Testing and Materials, Philadelphia, PA, 1970, pp. 165-180.
- [43] Saxton, H. J., Ireland, D. R., and Server, W. L., "Analysis and Control of Inertial Effects During Instrumented Impact Testing," *Instrumented Impact Testing ASTM STP 563*, American Society for Testing and Materials, Philadelphia, PA, 1974, pp. 50-73.
- [44] Rintamaa, R., Rahka, K., Wallin, K., Ikonen, K., Talja, H., Kotilainen, H., and Sirkkola, E., Research Report 290, Technical Research Centre of Finland (VTT), Espoo, Finland, 1984, p. 44.

- [45] Rintamaa, R., Wallin, K., and Valo, M., "Improved Instrumented Impact Testing Facility for Irradiation Damage Assessment," *Innovative Approaches to Irradiation Damage and Fracture Analysis*, PCP - Volume 170, D. L. Marriot, T. R. Mager, and W. H. Bamford, Eds., American Society of Mechanical Engineers (ASME), New York, 1989, pp. 115-120.
- [46] Ahlstrand, R., Törrönen, K., Valo, M., and Bärs, B., "Surveillance Programs and Irradiation Embrittlement Research of the Loviisa Nuclear Power Plant," *Radiation, Embrittlement of Nuclear Reactor Pressure Vessel Steels: An International Review (Second Edition)*, ASTM STP 909, American Society for Testing and Materials, Philadelphia, PA, 1986, pp. 55-69.
- [47] Server, W. L., Norris, D. M., Jr., and Prado, M. E., "Ductile Crack Initiation in the Charpy V-Notch Test," *What does the Charpy Test Really Tell Us?* American Society for Metals, Metals Park, Ohio, 1978, pp. 187-200.
- [48] Marquardt, Donald, W., "An Algorithm for Least-Squares Estimation of Nonlinear Parameters," *Journal of the Society for Industrial and Applied Mathematics*, Volume 11, Number 2, June 1963, pp. 431-441.
- [49] Bevington, Philip R., "Data Reduction and Error Analysis for the Physical Sciences," McGraw-Hill Book Company, 1969, pp. 297-300.

## VITA

Lonnie Eugene Schubert was born 29 June 1964 in Parsons, Kansas. He attended the Parsons public schools for his primary and secondary education, but he completed his last two years of high school at Parsons Christian Academy, a small private school. He studied at Labette Community College in Parsons, Kansas for one semester, after which he completed training with the United States Army Reserve. Upon completion of this training, Mr. Schubert attended Labette Community College for another semester. He worked regularly in the employ of his parents throughout these years at the restaurant which the family has owned for more than 20 years.

From 1984 to 1986 Lonnie attended and completed studies at Rhema Bible Training Center in Broken Arrow, Oklahoma. In November of 1986 Mr. Schubert was wed to Mary Elizabeth Pursell, a native of Rolla, Missouri. The following year the couple moved to Rolla, Missouri and Lonnie enrolled at the University of Missouri in Rolla. He graduated cum laude in May of 1991 with a bachelors degree in Metallurgical Engineering.

Mr. Schubert had joined the United States Army Reserve Officer Training Corps while completing his college work, and he completed several months of training for the Army beginning in the summer of 1991. First Lieutenant Schubert is currently a member of the United States Army Reserve, inactive.

Subsequently, he was accepted into the graduate program of the University of Missouri-Rolla, Nuclear Engineering Department as a masters candidate. His program of study concentrated on the physical aspects of radiation effects in materials.

Much of the research Lonnie conducted toward his masters thesis was completed at the Pacific Northwest Laboratory (PNL) in Richland, Washington, which is operated by the Battelle Memorial Institute for the Department of Energy. His time at PNL was sponsored by the Associated Western Universities, a DOE sponsored program.